Asymmetric LPM morphogenesis: the *heart and soul* of organ laterality in zebrafish

by

Sally Horne

DISSERTATION

Submitted in partial satisfaction of the requirements for the degree of

DOCTOR OF PHILOSOPHY

in

Genetics

in the

GRADUATE DIVISION

of the

UNIVERSITY OF CALIFORNIA, SAN FRANCISCO

For Nick

Preface

My time in graduate school has been one of the most challenging and joyful periods in my life. Neither this rich experience nor the work in this text would have been possible without the invaluable contributions of many people at UCSF. My thesis advisor, Didier Stainier, has provided expert guidance in every aspect of my graduate training. Through his constant encouragement and by his personal example he has inspired me to find my own passion for science - I cannot thank him enough. I am grateful to the rest of my thesis committee: Gail Martin, Ira Herskowitz, and Sharon Amacher for their insights, guidance and hard work on my behalf; and to Kathleen Yamamoto, Felix Aburto, Sue Adams and Danny Dam, all of whom work magic behind the scenes.

The members of the Stainier lab, both past and present, have been amazing colleagues and friends. I am particularly grateful to Debbie Yelon, Erik Kupperman, Wayne Liao and Jon Alexander, who all provided excellent mentoring during my early years in the lab, to Holly Field, Elke Ober, Heather Verkade and Duc Dong, my intellectual partners in the study of endodermal organ morphogenesis; and to Steve Waldron and Alex Navarro for outstanding fish care.

I am also deeply indebted to my husband, Nick Badovinac, and to my entire family, who have lovingly supported me in every aspect of my life.

Figure 2.2 represents data that I contributed to:

> Restricted expression of cardiac myosin genes reveals regulated aspects of heart tube assembly in zebrafish, *Dev Biol* 1999; 214: 23-37.
>
> By Deborah Yelon, Sally Horne and Didier Y. R. Stainier.

The remainder of Chapter 2, as well as Chapters 3 and 4 represent data from:

> Positional cloning of *heart and soul* reveals multiple roles for PKC lambda in zebrafish organogenesis. *Curr Biol* 2001; 11: 1492-1502.
>
> By Sally Horne-Badovinac, Dan Lin, Steve Waldron, Monica Schwartz, Geraldine Mbamalu, Tony Pawson, Yuh-Nung Jan, Didier Y. R. Stainier and Salim Abdelilah-Seyfried.
>
> Dan Lin, Geraldine Mbamalu and Tony Pawson contributed biochemical data on the effects of the two *has* lesions on aPKCλ function (Figure 3.2). Salim Abdelilah-Seyfried and Yuh-Nung Jan contributed data on epithelial defects in the retina of *has* mutants (Figure 4.4). Steve Waldron assisted as a technician under my supervision in the positional cloning of *has*. As a rotation student under my supervision, Monica Schwartz designed the *has* morpholino and performed the initial injection experiments with this reagent.

The text of Chapter 5 has been submitted for publication:

> Asymmetric migration of the lateral plate mesoderm drives gut looping in zebrafish. *Science* (submitted) 2003.
>
> By Sally Horne-Badovinac, Michael Rebagliati and Didier Y. R. Stainier
>
> Mike Rebagliati contributed the *spaw*-MO prior to publication

Abstract

Asymmetric LPM morphogenesis: the *heart and soul* of organ laterality in zebrafish

Sally Horne

Many vertebrate organs display morphological asymmetry with respect to the midline, yet little is known about the mechanisms used to translate the left-right (L-R) positional information provided by asymmetrically expressed genes into organ laterality. In this dissertation, I show that the zebrafish *heart and soul* (*has*) mutation causes striking defects in the L-R morphogenesis of the heart and digestive organs. Importantly, asymmetric gene expression appears to be unaffected in *has* mutants, indicating that *has* disrupts the transfer of L-R positional information from the lateral plate mesoderm (LPM) to the developing organs. Through positional cloning of the gene, I show that *has* encodes atypical protein kinase C λ, a gene known to be required for the establishment of apico-basal polarity in epithelial cells. This finding led to the investigation of a number of epithelial defects in *has* mutants and suggested that a defect in epithelial integrity could be responsible for the defects in asymmetric organ morphogenesis. In fact, I go on to show that a defect in the epithelial integrity of the LPM appears to be responsible for the L-R morphogenetic defects observed in the digestive organs of *has* mutants.

By combining my initial work on *has* mutants with studies of other mutant and wild-type embryos, I show that zebrafish employ at least two mechanisms to transfer L-R positional information from the LPM to the endoderm during asymmetric organ morphogenesis. Genes expressed asymmetrically within the LPM first act cell non-autonomously to provide a signal for the initial leftward budding of the liver and then act

autonomously within the LPM to drive asymmetric morphogenesis within this tissue. I further show that the LPM undergoes a dynamic asymmetric migration that appears to provide the motive force to displace the endoderm to the left during gut looping and to reinforce the leftward position of the liver. These data provide new insights into the cellular mechanisms that drive asymmetric morphogenesis downstream of L-R gene expression.

Table of Contents

List of Tables

List of Figures

Introduction

When viewed externally, the left and right sides of the vertebrate body plan appear to be symmetric. However, vertebrate internal organs often display morphological asymmetries with respect to the left-right (L-R) axis. The development of the L-R axis has been described as a three-step process: (1) initial break in symmetry; (2) establishment of asymmetric gene expression; and (3) transfer of positional information to developing organs [1]. The majority of what we understand about L-R asymmetry falls under the first two steps. The initial break in symmetry appears to involve the rotation of localized monocilia, which leads to asymmetric gene expression in the lateral plate mesoderm (LPM) [2, 3]. Little is known, however, about the mechanisms that underlie the transfer of positional information from the LPM to the developing organs.

Genetics should provide the tools necessary to investigate the molecular and cellular mechanisms that drive L-R organ morphogenesis. To date, however, no mutations have been described that specifically disrupt this third step in the development of the L-R axis. Many mutations have been described that disrupt either the first or second step [1, 4]. These types of mutations also affect all subsequent steps in the cascade. For instance, the mouse *iv* mutation disrupts a dynein gene [5] required for proper function of the node monocilia [6]. Consequently, *iv* mutants also display defects in asymmetric gene expression and organ laterality [7, 8]. However, a mutation that

specifically disrupts the transfer of L-R positional information to the developing organs should show defects in asymmetric organ morphogenesis in the presence of normal L-R gene expression.

The zebrafish *heart and soul* (*has*) mutation causes striking defects in the L-R morphogenesis of the heart and digestive organs, yet asymmetric gene expression appears to be normal. This mutation has formed the foundation of my thesis work and has provided invaluable information on the mechanisms used to translate L-R positional information into organ asymmetry. In this chapter, I will first review the types of asymmetric morphogenesis that occur in the zebrafish heart and digestive organs up to 48 hours post fertilization (hpf). I will next review our current knowledge of asymmetric gene expression in zebrafish and relate the observed patterns, where possible, to L-R morphogenetic events.

Heart morphogenesis

Morphological changes in the developing heart tube provide the first obvious instance of L-R asymmetry in the vertebrate embryo. In all vertebrates, the heart tube undergoes dextral looping, a morphogenetic process in which the linear tube bends into an S-like structure with the ventricle to the right of the atrium. In some vertebrates there is also an earlier asymmetry, in which the atrial end of the linear heart tube is positioned to the left of the midline prior to looping. This phenomenon has been described in mice [9], but has been predominantly studied in zebrafish, where it has been termed cardiac jogging [10]. In this section I will detail our current understanding of the early stages of L-R morphogenesis in the zebrafish heart.

The first major event in cardiac morphogenesis occurs during mid-somitogenesis stages when the cardiac precursors migrate toward the midline. The cardiac precursors arise as bilateral cell populations in the anterior LPM (Figure 1.1a). As components of the LPM, the pre-cardiac cells undergo differentiation and migrate as part of the LPM epithelia. The cardiac precursors give rise to two major cell populations: the myocardium, which makes up the outer muscular layer of the heart tube and the endocardium, which forms the endothelial lining of the tube. The myocardial precursors migrate with the rest of the anterior LPM toward the midline, while the endocardial precursors appear to exit the LPM and undergo their medial migration independent of the LPM epithelium (Le Trinh personal communication). During the medial migration of the anterior LPM, the myocardial precursors further differentiate into ventricular precursors, which lie at the medial edges of the heart field and atrial precursors, which are situated laterally [11].

When the myocardial precursors meet at the midline, between 18 and 20 somites, they begin to form the heart tube. The sheets of myocardial cells fuse at their anterior and posterior ends, but leave a central lumen, such that the myocardium looks like a ring when viewed dorsally. However, this ring is actually a three-dimensional structure known as the cardiac cone [12] (Figure 1.1b). The apex of the cone points dorsally and corresponds to the ventricular end of the heart tube, while the wide base of the cone rests ventrally upon the yolk. In order for the heart tube to elongate, the cone tilts by approximately 90°, shifting its lumenal axis from a dorsal-ventral orientation to an anterior-posterior orientation [11] (Figure 1.1c). Tilting occurs around 22 somites and it is at this point that L-R symmetry is first broken in the zebrafish heart. The cone tilts

such that the apex points toward the right posterior, causing the heart tube to elongate toward the left anterior. It is the diagonal position of the heart tube with respect to the midline that inspired the term cardiac jogging [10, 11, 13] (Figure 1.1d).

The next occurrence of asymmetric morphogenesis in the heart is dextral looping. During heart tube elongation, the ventricular end of the tube stays near the midline, while the atrial end elongates toward the left. Once the tube is formed, the atrial end gradually migrates back toward the midline, such that the organ once again becomes symmetrical with respect to the L-R axis. Looping occurs between 30 and 48 hpf when the midline heart tube bends to place the ventricle to the right of the atrium.

Digestive organ morphogenesis

Some of the most dramatic examples of asymmetric organ morphogenesis in response to left-right (L-R) positional cues occur in the digestive system, where the liver and pancreas occupy asymmetric positions with respect to the midline, and the intestine bends and folds in a complex pattern for proper packing into the abdominal cavity [14]. However, the relatively late stage at which the digestive organs form and their depth within the embryo have made L-R morphogenesis of these endodermal organs highly understudied when compared to the heart. Zebrafish provide an ideal system for the study of endodermal organ laterality. In zebrafish the asymmetric positioning of the intestine, liver and pancreas occur between 24 and 30 hpf [15, 16], even earlier than heart looping. Furthermore, the recent development of a transgenic line expressing GFP throughout the endodermal organs, the gut GFP line, has greatly enhanced the visibility of digestive organs in both live and fixed embryos [15].

One of the most interesting aspects of endodermal organ morphogenesis in vertebrates is that all of the digestive organs arise from a common intestinal primordium. In most vertebrates the intestinal primordium takes the form of an epithelial tube of endodermal cells and organs such as the liver and pancreas bud as evaginations of the endodermal epithelium. In zebrafish, the intestinal primordium is a solid rod of endodermal cells and accessory organs bud as solid protrusions from this rod [15, 16]. Intestinal lumen formation in zebrafish occurs subsequent to most of the budding events through a process of cavitation [17].

At 48 hpf, approximately one day after the intestinal rod assembles at the ventral midline, the endodermal organs display striking asymmetry with the liver on the left, a portion of the intestine looped to the left, and the pancreas on the right (Figure 1.2c). How does this pattern emerge? In the case of the intestine and liver, asymmetric morphogenesis occurs in close spatial and temporal proximity. Within the midline endodermal rod, the region that will loop lies between the caudal border of the pharyngeal endoderm and the pancreatic islet (Figure 1.2a). Concurrent with gut looping, the anterior two-thirds of the looping region becomes thickened as the liver buds from the ventral side of the looping endoderm toward the left side of the embryo (Figure 1.2b) [15]. Subsequent morphogenesis of the surrounding LPM eventually separates the liver from the intestinal endoderm, leaving a small connection at the hepatic duct (Figure 1.2c) [15]. The pancreas arises from two buds, one from the anterior edge and one from the posterior edge of the looping region. The posterior bud, which corresponds to the pancreatic islet, moves from the dorsal aspect of the developing intestine to its right side immediately following looping (Figure 1.2b). When the anterior bud emerges four hours

later, the posterior bud loses its attachment to the future intestine and the two buds fuse on the right side of the looped gut. The single pancreas maintains its attachment to the gut at the origin of the anterior bud (Figure 1.2c) [16].

L-R positional information in zebrafish

L-R positional information is supplied to individual organs by genes whose expression is restricted to one side of the midline. In zebrafish asymmetric gene expression has been observed in the LPM and the brain. However, it is the LPM expression that is believed to regulate L-R morphogenesis in the heart and digestive organs; as such we will focus exclusively on asymmetric expression in this tissue. In mouse and chick, asymmetric gene expression has been described for both the left and right LPM. To date, however, all genes that show asymmetric expression in zebrafish are located on the left.

Nodal is a TGFβ signaling molecules that is believed to sit at the top of the L-R gene expression hierarchy in all vertebrates. *cyclops* (*cyc*) was the first *nodal*–related gene described in zebrafish that showed asymmetric LPM expression [18, 19]. The role of *cyc* within the LPM appears to be minor, however, as *cyc* point mutants have no clear defects in visceral organ laterality [10]. Recently a second *nodal*-related gene, *southpaw* (*spaw*), has emerged as the predominant *nodal* family member affecting L-R asymmetry in the zebrafish LPM [20]. Asymmetric *spaw* expression begins in the left LPM between the 10 and 12 somite stage, making it the earliest molecular marker of L-R asymmetry in zebrafish. Importantly, reducing *spaw* function using morpholino-knockdown eliminates all L-R gene expression from the LPM (including *spaw* itself) and disrupts the asymmetric morphogenesis of the heart and digestive organs ([20], Chapter 5).

During most of the period when *spaw* shows left-sided LPM expression, its transcripts are found throughout the A-P extent of this tissue. However, other genes that show asymmetric expression downstream of *spaw* show A-P restriction within the LPM to regions of L-R organ morphogenesis. *spaw* induces the asymmetric expression of its downstream antagonist, *lefty2*, only in the heart forming region [21]. In the case of *pitx2*, a downstream effector of Nodal signaling, *spaw* induces two domains of asymmetric expression: one in the heart forming region [22] and one in the gut looping region [22, 23].

Several genes show asymmetric expression in the heart cone just prior to cardiac tilting/jogging. Like *lefty2* and *pitx2* (mentioned above), *bmp4* [10] and *nkx2.5* [25] also show asymmetric expression in the cardiac cone, although their relationship to the *Nodal* pathway is less clear. The asymmetric localization of these genes within the myocardium just prior to the onset of L-R morphogenesis is highly suggestive of a direct role for these genes in regulating tilting/jogging. However, it is unclear whether this localized expression also regulates cardiac looping. Most asymmetric gene expression disappears from the heart concurrent with the tilting of the cone and several mutants have been identified that genetically uncouple the direction of jogging from the direction of looping [13]. These data suggest that there must be a second source of positional information regulating looping morphogenesis that acts either independently of or in addition to asymmetric gene expression in the myocardium.

The pattern of asymmetric gene expression in the gut looping region appears to be much simpler. To date, *pitx2* is the only gene that shows A-P restriction to the left LPM adjacent to the looping endoderm. This domain of *pitx2* expression is present during the

time when the intestinal primordium is still in the midline [22, 23], however, it may persist as late as 30 hpf, through the early stages of L-R morphogenesis in the endoderm (Brent Bisgrove, personal communication). In the heart, it is likely that asymmetrically expressed genes act autonomously within the myocardium to regulate L-R morphogenesis. However, the mechanism used to transmit positional information from the LPM to the endoderm is unclear.

Overview

This dissertation addresses several aspects of asymmetric organ morphogenesis in zebrafish. Chapter 2 shows that the *heart and soul* (*has*) mutation causes novel defects in the L-R morphogenesis of the heart and digestive organs. To further investigate the role of *has* in organ laterality, Chapter 3 details the positional cloning of the *has* gene and shows that it encodes atypical protein kinase C λ (aPKCλ). aPKCs had previously been shown to be required for the establishment of apico-basal polarity in epithelial cells. Consistent with this role for aPKCs, Chapter 4 demonstrates that *has* mutants display defects in the formation and maintenance of a number of embryonic epithelia. This finding raised the intriguing possibility that a defect in epithelial integrity was responsible for the L-R morphogenetic defects in *has* mutants. Chapter 5 shows that, for the gut looping defect in *has* mutants, the defective epithelium appears to be the LPM. This observation and others led to a model for gut looping in which a dynamic asymmetric migration of the LPM provides the motive force to displace the gut endoderm to the left. Chapter 6 then expands on the role of the LPM in endodermal organ asymmetry by showing that leftward liver budding occurs in two steps: one that appears to depend on signal from the LPM and one that depends on the asymmetric morphogenesis of the

Figure 1.1 Early heart tube morphogenesis in zebrafish

(a) The cardiac precursors arise as bilateral populations in the LPM. **(b)** The bilateral fields migrate toward the midline and fuse to form a three-dimensional structure called the cardiac cone. **(c)** In order for the heart tube to elongate, the cardiac cone tilts by approximately 90°, shifting its lumenal axis from a dorsal-ventral orientation to an anterior-posterior orientation. It is during tilting morphogenesis that L-R symmetry is first broken in the zebrafish heart. The cone tilts such that the apex points toward the right posterior, causing the heart tube to elongate toward the left anterior. **(d)** The diagonal position of the heart tube with respect to the midline is called cardiac jogging.

Figure 1.1

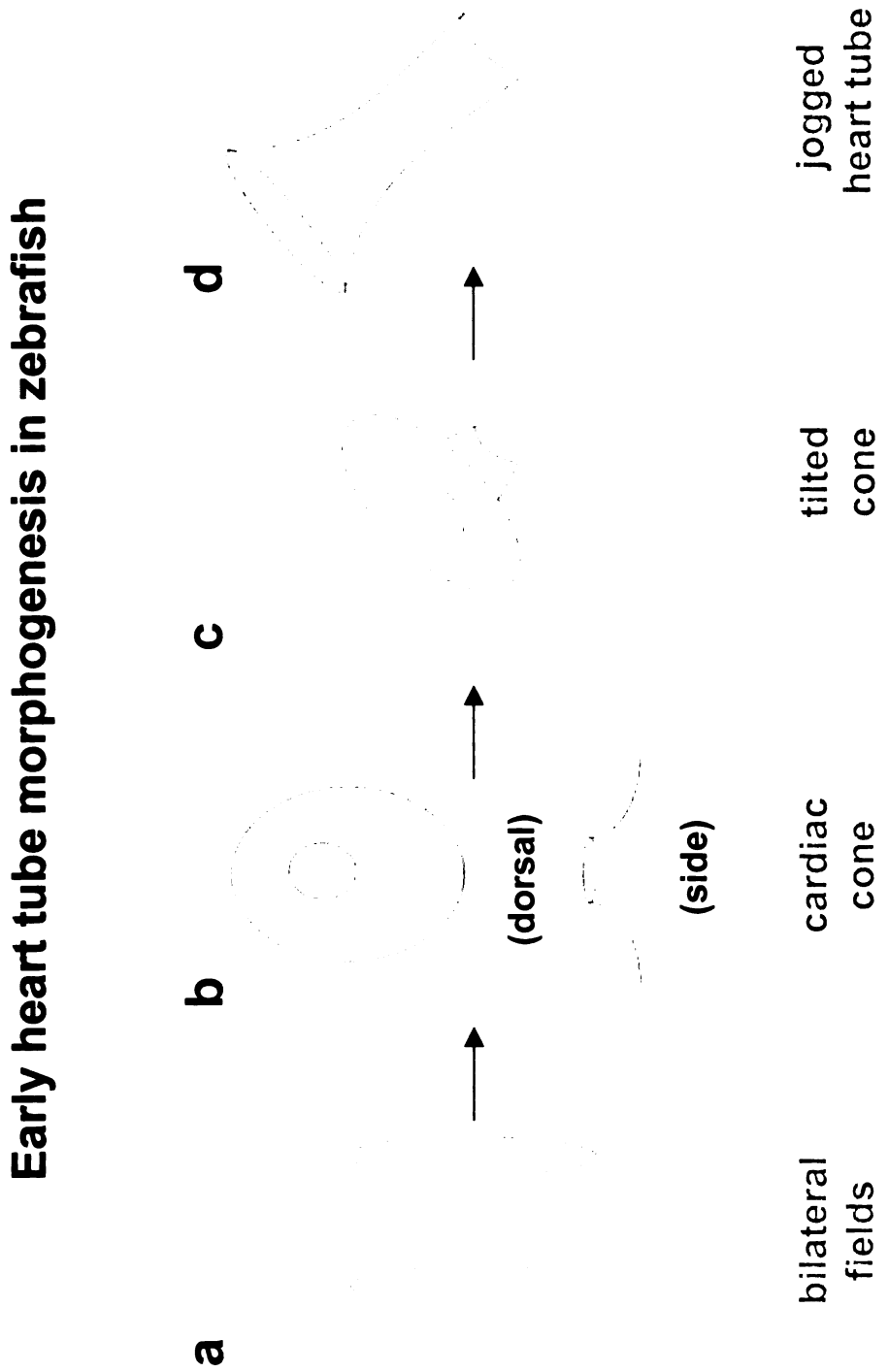
Early heart tube morphogenesis in zebrafish
a
b
c
d
(dorsal)
(side)
bilateral fields
cardiac cone
tilted cone
jogged heart tube

Figure 1.2 L-R morphogenesis of the digestive organs in zebrafish

(a) At 24 hpf the intestinal primordium is in the midline. The gray bracket marks the gut looping region between the caudal border of the pharyngeal endoderm and the posterior pancreatic bud (pancreatic islet; red bracket). **(b)** By 30 hpf the gut has looped, the liver is budding to the left (blue bracket) and the pancreatic islet has moved from the dorsal aspect of the developing intestine to the right (red bracket). **(c)** By 48 hpf the asymmetric pattern has become much more elaborate. The liver is on the left (L) the intestinal bulb is looped to the left (I) and the two pancreatic buds have fused to create a single pancreas on the right (P). In all images anterior is to the top and left is to the left.

Figure 1.2


L-R morphogenesis of the digestive organs in zebrafish
a
b
c
liver bud
islet
islet
24 hpf
30 hpf
48 hpf
A
P
V
R
L
D

References

1. Burdine, R.D., and Schier, A.F. (2000). Conserved and divergent mechanisms in left-right axis formation. Genes Dev *14*, 763-776.

2. Hamada, H., Meno, C., Watanabe, D., and Saijoh, Y. (2002). Establishment of vertebrate left-right asymmetry. Nat Rev Genet *3*, 103-113.

3. Tabin, C.J., and Vogan, K.J. (2003). A two-cilia model for vertebrate left-right axis specification. Genes Dev *17*, 1-6.

4. Bisgrove, B.W., Morelli, S.H., and Yost, H.J. (2003). Genetics of Human Laterality Disorders: Insights from Vertebrate Model Systems. Annu Rev Genomics Hum Genet.

5. Supp, D.M., Witte, D.P., Potter, S.S., and Brueckner, M. (1997). Mutation of an axonemal dynein affects left-right asymmetry in inversus viscerum mice. Nature *389*, 963-966.

6. Okada, Y., Nonaka, S., Tanaka, Y., Saijoh, Y., Hamada, H., and Hirokawa, N. (1999). Abnormal nodal flow precedes situs inversus in iv and inv mice. Mol Cell *4*, 459-468.

7. Lowe, L.A., Supp, D.M., Sampath, K., Yokoyama, T., Wright, C.V., Potter, S.S., Overbeek, P., and Kuehn, M.R. (1996). Conserved left-right asymmetry of nodal expression and alterations in murine situs inversus. Nature *381*, 158-161.

8. Meno, C., Ito, Y., Saijoh, Y., Matsuda, Y., Tashiro, K., Kuhara, S., and Hamada, H. (1997). Two closely-related left-right asymmetrically expressed genes, lefty-1 and lefty-2: their distinct expression domains, chromosomal linkage and direct neuralizing activity in Xenopus embryos. Genes Cells *2*, 513-524.

9. Biben, C., and Harvey, R.P. (1997). Homeodomain factor Nkx2-5 controls left/right asymmetric expression of bHLH gene eHand during murine heart development. Genes Dev *11*, 1357-1369.

10. Chen, J.N., van Eeden, F.J., Warren, K.S., Chin, A., Nusslein-Volhard, C., Haffter, P., and Fishman, M.C. (1997). Left-right pattern of cardiac BMP4 may drive asymmetry of the heart in zebrafish. Development *124*, 4373-4382.

11. Yelon, D., Horne, S.A., and Stainier, D.Y. (1999). Restricted expression of cardiac myosin genes reveals regulated aspects of heart tube assembly in zebrafish. Dev Biol *214*, 23-37.

12. Stainier, D.Y., Lee, R.K., and Fishman, M.C. (1993). Cardiovascular development in the zebrafish. I. Myocardial fate map and heart tube formation. Development *119*, 31-40.

13. Chin, A.J., Tsang, M., and Weinberg, E.S. (2000). Heart and gut chiralities are controlled independently from initial heart position in the developing zebrafish. Dev Biol *227*, 403-421.

14. Moore, K.L., and Persaud, T.V.N. (1998). The Developing Human. W. B. Saunders Company, Philadelphia, London, New York, St. Louis, Sydney, Toronto.

15. Field, H., Ober, E.A., Roeser, T., and Stainier, D.Y. (2003). Formation of the digestive system in zebrafish: I. Liver morphogenesis. Dev Biol *253*, 279-290.

16. Field, H.A., Si Dong, P.D., Beis, D., and Stainier, D.Y. (2003). Formation of the digestive system in zebrafish: II. Pancreas morphogenesis. Dev Biol *261*, 197-208.

17. Horne-Badovinac, S., Lin, D., Waldron, S., Schwarz, M., Mbamalu, G., Pawson, T., Jan, Y., Stainier, D.Y., and Abdelilah-Seyfried, S. (2001). Positional cloning of *heart and soul* reveals multiple roles for PKC lambda in zebrafish organogenesis. Curr Biol *11*, 1492-1502.

18. Rebagliati, M.R., Toyama, R., Haffter, P., and Dawid, I.B. (1998). cyclops encodes a nodal-related factor involved in midline signaling. Proc Natl Acad Sci U S A *95*, 9932-9937.

19. Sampath, K., Rubinstein, A.L., Cheng, A.M., Liang, J.O., Fekany, K., Solnica-Krezel, L., Korzh, V., Halpern, M.E., and Wright, C.V. (1998). Induction of the zebrafish ventral brain and floorplate requires cyclops/nodal signalling. Nature *395*, 185-189.

20. Long, S., Ahmad, N., and Rebagliati, M. (2003). The zebrafish nodal-related gene *southpaw* is required for visceral and diencephalic left-right asymmetry. Development *130*, 2303-2316.

21. Bisgrove, B.W., Essner, J.J., and Yost, H.J. (1999). Regulation of midline development by antagonism of lefty and nodal signaling. Development *126*, 3253-3262.

22. Essner, J.J., Branford, W.W., Zhang, J., and Yost, H.J. (2000). Mesendoderm and left-right brain, heart and gut development are differentially regulated by pitx2 isoforms. Development *127*, 1081-1093.

23. Campione, M., Steinbeisser, H., Schweickert, A., Deissler, K., van Bebber, F., Lowe, L.A., Nowotschin, S., Viebahn, C., Haffter, P., Kuehn, M.R., and Blum,

M. (1999). The homeobox gene Pitx2: mediator of asymmetric left-right signaling in vertebrate heart and gut looping. Development *126*, 1225-1234.

24. Bisgrove, B.W., Essner, J.J., and Yost, H.J. (2000). Multiple pathways in the midline regulate concordant brain, heart and gut left-right asymmetry. Development *127*, 3567-3579.

25. Schilling, T.F., Concordet, J.P., and Ingham, P.W. (1999). Regulation of left-right asymmetries in the zebrafish by Shh and BMP4. Dev Biol *210*, 277-287.

Organ morphogenesis defects in *heart and soul* mutants

In recent years the zebrafish has emerged as a premier model organism for the study of vertebrate organogenesis. External fertilization combined with the optical clarity of the embryo facilitates easy visualization of deep tissues in both living and fixed embryos. One of the greatest strength of zebrafish is the ability to do forward genetics. Two large-scale screens for embryonic lethal mutations have identified many mutants with discrete and novel defects in organ formation [1, 2].

The *heart and soul* (*has*) mutation was isolated in one of these large-scale screens [1] based on a number of morphological defects that are easily visualized in live embryos. These include: a small heart, patchy retinal pigmented epithelium, retinal degeneration, failure of the brain ventricles to inflate and general body curvature (Figure 2.1b) [3-5]. My initial interest in the *has* mutant was in understanding the small heart phenotype. Visual inspection of the heart in live *has* mutant embryos 1 day post fertilization revealed that, unlike wild-type embryos that have a contractile heart tube extending out over the yolk, *has* mutants have only a small dense lump of beating tissue tucked beneath the head [5].

In this chapter we report that the small heart phenotype observed in *has* mutants is due to a gross malformation of the heart tube. The atrium, which lies posterior to the ventricle in wild-type embryos, surrounds the ventricle in *has* mutants. This morphology

arises when the cardiac cone fails to tilt from a dorsal-ventral (D-V) to anterior-posterior (A-P) orientation. The tilting of the cardiac cone produces the first morphological L-R asymmetry in the zebrafish heart, therefore, we further examined *has* mutants for defects in L-R morphogenesis in the digestive organs. In *has* mutants, the gut fails to loop and the liver and pancreas are both symmetrical with respect to the midline. Our data indicate that Has is required by several organs for the execution of proper L-R morphogenesis.

Results

Malformation of the heart tube in *has* mutants

Given the small appearance of the heart in live *has* mutants [5], we initially investigated whether a defect in myocardial differentiation was responsible this phenotype. We used wholemount in situ hybridization and immunohistochemistry to examine a number of myocardial markers in *has* mutants at various stages (data not shown). This analysis revealed that the small, dense nature of the *has* heart is not due to a reduced amount of myocardium, but rather to a gross malformation of the heart tube. Staining with the myosin heavy chain markers MF20 and S46 revealed that, the atrium, which lies posterior to the ventricle in the wild-type heart (Figure 2.2a), surrounds the ventricle in the *has* heart (Figure 2.2b, c).

The *has* mutation blocks heart tube assembly at an intermediate stage

In zebrafish, the ventricular precursors initially lie medial to the atrial precursors in the bilateral cardiac fields [6]. Therefore, the aberrant orientation of the atrium with respect to the ventricle that we observe in *has* mutants could be the result of an early disruption of the medial-lateral (M-L) patterning of the myocardial precursors. Alternatively, initial M-L patterning could be normal and the mutation might instead disrupt a morphogenetic process independent of the proper specification of ventricular and atrial lineages. To distinguish between these two possibilities and identify the point at which heart tube morphogenesis goes awry in *has* mutants, we followed the expression of *cardiac myosin light chain 2* (*cmlc2*) and *ventricular myosin heavy chain* (*vmhc*) during heart tube assembly.

In *has* mutants, the myocardial precursors migrate toward the midline in a normal manner and fuse to from the cardiac cone (Figure 2.2d-f). At the 23 somite stage, however, when the apex of the cone normally tilts to allow for the elongation of the heart tube (Figure 2.2g), the *has* cone remains stationary (Figures 2.2h, i). The mutant heart remains a cone-like structure, but becomes increasingly dysmorphic throughout the time that the more lateral regions of the cone are coalescing into a tube in wild-type siblings (Figures 2.2j-l). In time, the atrial precursors that make up the wide base of the *has* cone fold back over the ventricular precursors in the apex, resulting in the atrium being inside out over the ventricle (Figures 2.2b, c).

These data suggest that the abnormal chamber orientation in *has* mutants is unlikely to be caused by improper specification of ventricular and atrial lineages, as *cmlc2* and *vmhc* expression are normal though the formation of the cardiac cone (Figures 2.2d-f; and data not shown). Instead, the *has* mutation blocks heart tube assembly at an intermediate stage. Has function appears to be required for the tilting of the cone that normally facilitates the conversion of the M-L pattern of myocardial precursors into the A-P pattern of the heart tube.

Defects in L-R morphogenesis of the digestive organs in *has* mutants

The tilting of the cardiac cone marks the point in heart morphogenesis when the M-L arrangement of the ventricular and atrial precursors is converted to an A-P orientation, but it also corresponds to the first occurrence of morphological L-R asymmetry in the zebrafish heart. To investigate whether other organs in *has* mutants display defects in L-R morphogenesis, we used wholemount in situ hybridization with *foxa3* to examine the digestive organs in *has* mutants.

By 30 hours post fertilization (hpf) in wild-type, the gut tube primordium loops to the left [7]. In *has* mutants, the gut primordium fails to loop and remains in the midline (data not shown). At 48 hpf in wild-type, the intestine remains on the left and now the primordia of three organs are present. The liver is on the left; the swimbladder is dorsal and lies roughly in the midline and the pancreas projects to the right (Figure 2.3a). In *has* mutants, the swimbladder is small and the liver and pancreas adopt symmetrical positions (Figure 2.3b). In the case of the pancreas, the two pancreatic buds have not fused; the anterior bud is symmetrical across the midline (or perhaps duplicated) and the posterior bud (pancreatic islet) is small and remains associated with the dorsal side of the gut tube (Figure 2.3b). These data indicate that the developing digestive organs in *has* mutants display striking morphogenetic defects with respect to the L-R axis.

Discussion

We have shown that the small appearance of the heart in *has* mutants is caused by a malformation of the heart tube in which the atrium folds inside out over the ventricle. This observation was also made independently by Jau-Nian Chen and Mark Fishman [8]. The aberrant chamber orientation arises from a failure of the cardiac cone to tilt from a D-V to A-P position. The tilting of the cardiac cone marks the first occurrence of morphological L-R asymmetry in the zebrafish heart. Concurrent with the D-V to A-P transition, the ventricular apex of the cone points toward the right posterior, which allows the heart tube to elongate toward the left anterior. This early leftward outgrowth of the heart tube has been termed cardiac jogging [9]. Over the course of several hours the heart tube moves back to the midline where it undergoes looping morphogenesis, which places the ventricle to the right of the atrium.

Many zebrafish mutations have been identified that affect the leftward jogging of the heart tube [7, 9, 10]. In all cases described to date, however, the D-V to A-P tilting of the cone occurs but with randomized orientation. In these mutants, the heart can jog to the left, to the right, or grow out in the midline. *has* represents a new class of heart L-R asymmetry mutant, as it is the only mutant currently described in which tilting/jogging morphogenesis is blocked as opposed to randomized. Mutants that show randomization in jogging often show defects in the midline or D-V patterning that result in disrupted L-R gene expression. We have not observed any obvious midline or D-V patterning defects in *has* mutants (data not shown). Asymmetric gene expression will need to be analyzed to better determine the extent of the laterality defect in *has* mutants (See Chapter 5).

We have further shown that *has* mutants display striking morphogenetic defects in the digestive system. L-R morphogenesis of the digestive organs has been far less studied in zebrafish than heart morphogenesis. Studies that have examined digestive organ asymmetry in L-R mutants have typically examined only one organ per study, such as the liver or pancreas, and the position of that organ is typically randomized [7, 10]. Using *foxA3*, a marker that labels most of the digestive tract endoderm, we have shown that the liver, pancreas and gut are all symmetrical in *has* mutants, further supporting our hypothesis that *has* represents a new class of L-R asymmetry mutant.

Materials and Methods

Zebrafish strains

The *has*^{m129} and *has*^{m567} alleles were used interchangeably, as these alleles are phenotypically indistinguishable.

Immunofluorescence

Wholemount immunofluorescence was performed as previously described [11], using the monoclonal antibodies MF20 [12] and S46 (generous gift of Dr. Frank Stockdale). The secondary reagents, goat anti-mouse IgG1-FITC and goat anti-mouse IgG2b-TRITC (Southern Biotechnology Associates) recognize S46 and MF20, respectively. Double-exposure photographs were taken using Fujichrome 1600 ASA film and a Zeiss Axioplan microscope; images were processed using Adobe Photoshop 4.0.

In situ hybridizations

In situ hybridizations were performed as previously described [6]. Embryos older than 24hpf were raised in 0.003% 1-phenyl-2-thiourea (PTU, Sigma) in egg water to inhibit production of pigment. Probes used include: *cmlc2* [6], *vmhc* [6], and *foxA3* (*forkhead* 2) [13].

Figure 2.1 Comparison of wild-type and *has* mutant embryos at 33 hpf.

(a) wild-type. **(b)** *has*. *has* mutants were first identified based on clearly visible defects in the heart (red arrowhead), a patchy retinal pigmented epithelium (black arrowhead), degeneration of the neural retina, failure of the brain ventricles to inflate (blue arrowhead) and a general body curvature.

Figure 2.1

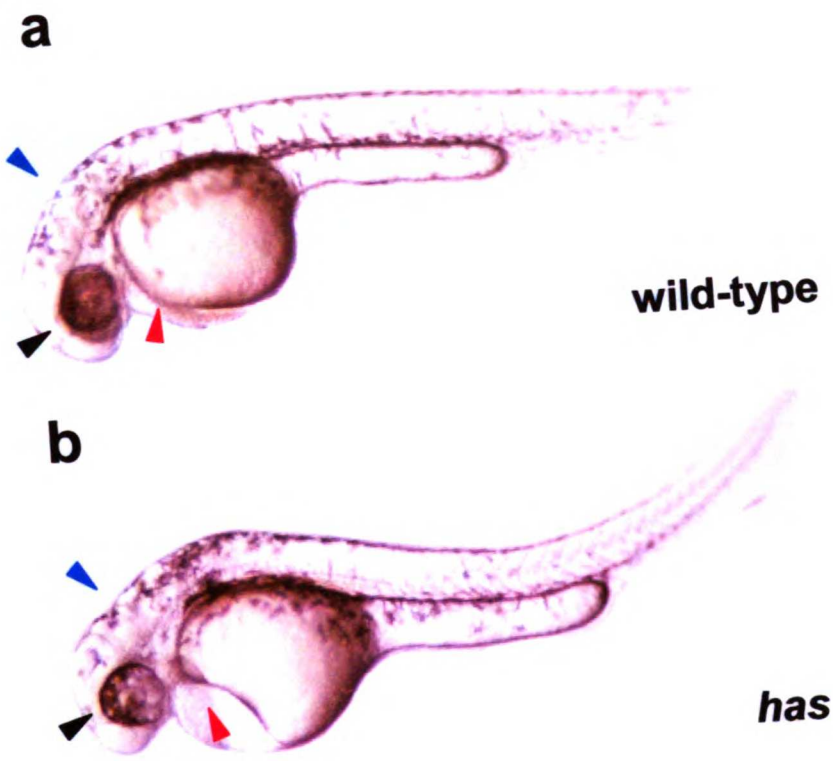

Figure 2.2 *has* disrupts heart tube assembly at an intermediate stage.

(a-c) 27 hpf embryos stained with MF20 (TRITC) and S46 (FITC), anterior to the left. Red fluorescence indicates MF20 staining of ventricular tissue, while yellow fluorescence indicates the overlap of S46 and MF20 staining in atrial tissue. (a) Lateral view of a wild-type embryo. The atrium (yellow) lies posterior to the ventricle (red). (b) Lateral view of a *has* mutant. (c) Ventral view of a *has* mutant. The atrium (yellow) surrounds the ventricle (red). **(d-l)** Dorsal views, anterior at the top. (d, g, j) Expression of *cmlc2* in wild-type embryos. (e, h, k) Expression of *cmlc2* in *has* mutants. (f, i, l) Expression of *vmhc* in *has* mutants. (d-f) 21-somite stage; the cardiac cone has formed and *has* mutants are indistinguishable from their wild-type siblings. (g-i) 23-somite stage; while the apex of the cone has tilted in wild-type embryos (g), the cone in *has* mutants remains stationary (h, i). (j-l) 24 hpf; the *has* heart still retains a cone-like structure (k, l), even as formation of the wild-type heart tube is nearly complete (j).

Figure 2.2

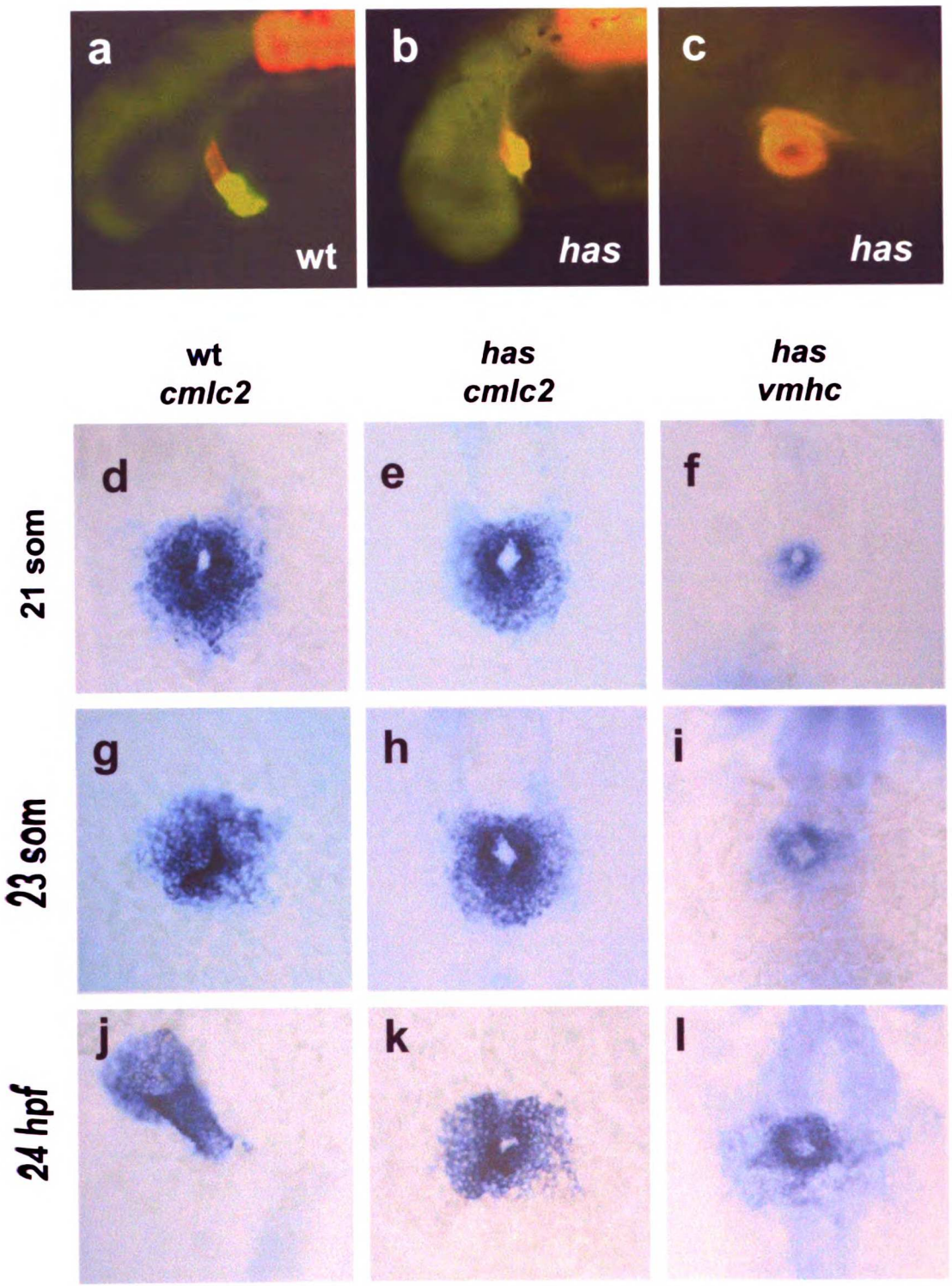
a
wt
b
has
c
has
wt
cmlc2
has
cmlc2
has
vmhc
21 som
d
e
f
23 som
g
h
i
24 hpf
j
k
l

Figure 2.3. Morphological defects in the digestive organs of *has* mutants.

(a,b) Dorsal views, anterior to the top. Wholemount *in situ* hybridization with *foxA3* reveals the general shape of the digestive tract. **(a)** In wild-type embryos the intestinal primordium (I) and liver (L) are on the left, the swimbladder (S) is in the midline and the pancreas (P) on the right. **(b)** In *has* mutants, the intestinal primordium and a small swimbladder are in the midline and the liver and pancreas adopt symmetrical positions. The two pancreatic buds have not fused; the anterior bud (aP) is symmetrical across the midline (or perhaps duplicated) and the posterior bud (pP) is small and remains associated with the dorsal side of the gut tube

Figure 2.3

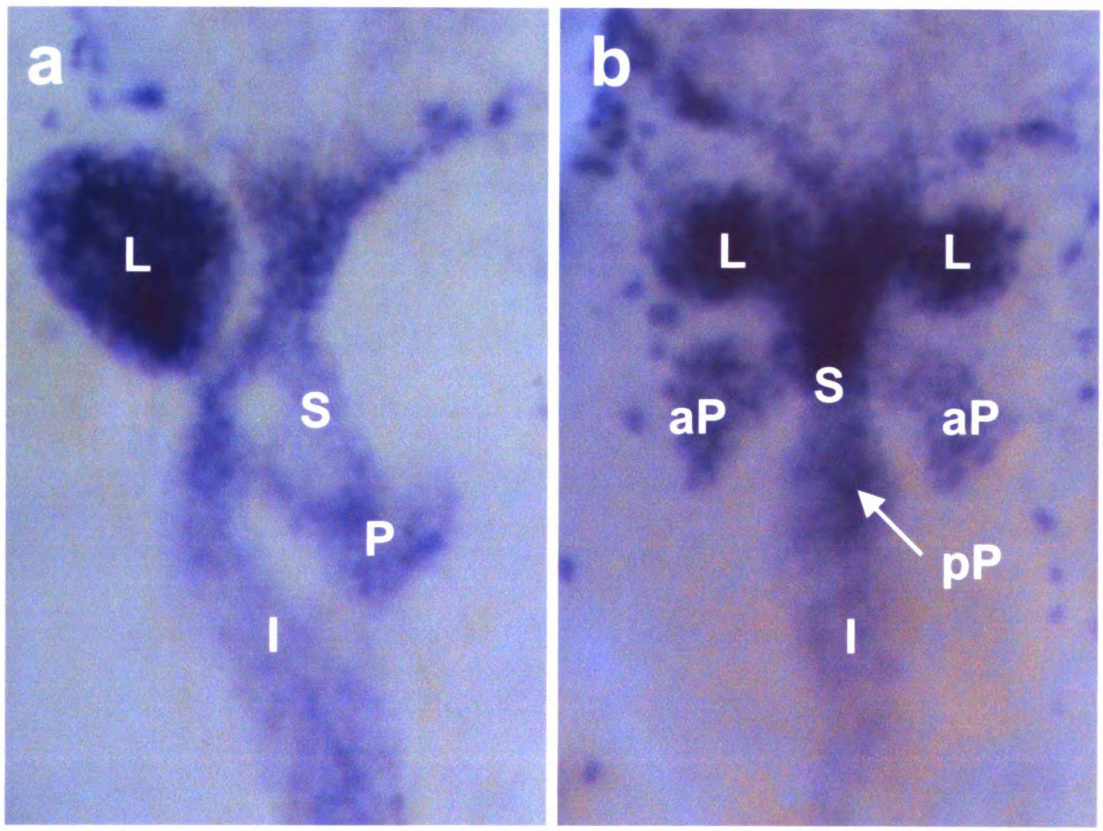

References

1. Driever W, Solnica-Krezel L, Schier AF, Neuhauss SC, Malicki J, Stemple DL, Stainier DY, Zwartkruis F, Abdelilah S, Rangini Z, Belak J, Boggs C: A genetic screen for mutations affecting embryogenesis in zebrafish. *Development* 1996; 123:37-46.

2. Haffter P, Granato M, Brand M, Mullins MC, Hammerschmidt M, Kane DA, Odenthal J, van Eeden FJ, Jiang YJ, Heisenberg CP, Kelsh RN, Furutani-Seiki M, Vogelsang E, Beuchle D, Schach U, Fabian C, Nusslein-Volhard C: The identification of genes with unique and essential functions in the development of the zebrafish, Danio rerio. *Development* 1996; 123:1-36.

3. Schier AF, Neuhauss SC, Harvey M, Malicki J, Solnica-Krezel L, Stainier DY, Zwartkruis F, Abdelilah S, Stemple DL, Rangini Z, Yang H, Driever W: Mutations affecting the development of the embryonic zebrafish brain. *Development* 1996; 123:165-178.

4. Malicki J, Driever W: *oko meduzy* mutations affect neuronal patterning in the zebrafish retina and reveal cell-cell interactions of the retinal neuroepithelial sheet. *Development* 1999; 126:1235-1246.

5. Stainier DY, Fouquet B, Chen JN, Warren KS, Weinstein BM, Meiler SE, Mohideen MA, Neuhauss SC, Solnica-Krezel L, Schier AF, Zwartkruis F, Stemple DL, Malicki J, Driever W, Fishman MC: Mutations affecting the formation and function of the cardiovascular system in the zebrafish embryo. *Development* 1996; 123:285-292.

6. Yelon D, Horne SA, Stainier DY: Restricted expression of cardiac myosin genes reveals regulated aspects of heart tube assembly in zebrafish. *Dev Biol* 1999; 214:23-37.

7. Chin AJ, Tsang M, Weinberg ES: Heart and gut chiralities are controlled independently from initial heart position in the developing zebrafish. *Dev Biol* 2000; 227:403-421.

8. Fishman MC, Chien KR: Fashioning the vertebrate heart: earliest embryonic decisions. *Development* 1997; 124:2099-2117.

9. Chen JN, van Eeden FJ, Warren KS, Chin A, Nusslein-Volhard C, Haffter P, Fishman MC: Left-right pattern of cardiac BMP4 may drive asymmetry of the heart in zebrafish. *Development* 1997; 124:4373-4382.

10. Bisgrove BW, Essner JJ, Yost HJ: Multiple pathways in the midline regulate concordant brain, heart and gut left-right asymmetry. *Development* 2000; 127:3567-3579.

11. Stainier DY, Gilbert W: Pioneer neurons in the mouse trigeminal sensory system. *Proc Natl Acad Sci U S A* 1990; 87:923-927.

12. Bader D, Masaki T, Fischman DA: Immunochemical analysis of myosin heavy chain during avian myogenesis in vivo and in vitro. *J Cell Biol* 1982; 95:763-770.

13. Odenthal J, Nusslein-Volhard C: fork head domain genes in zebrafish. *Dev Genes Evol* 1998; 208:245-258.

heart and soul encodes atypical protein kinase C λ

In the previous chapter, we showed that the *has* mutation represents a new class of L-R asymmetry mutant, in which L-R morphogenesis of the heart and digestive organs is blocked as opposed to randomized. In order to further investigate the role of *has* in L-R morphogenesis, we must identify the gene disrupted by the mutation. In this chapter we describe the positional cloning of the *has* gene and show that it encodes atypical Protein Kinase C λ (aPKCλ). In collaboration with Dan Lin, Geraldine Mbamalu and Tony Pawson, we use biochemical studies to show that the truncated proteins encoded by the has^{m129} and has^{m567} alleles are kinase inactive. We further show that injection of wild-type aPKCλ is sufficient to rescue *has* mutants and that injection of a morpholino antisense oligo against aPKCλ can phenocopy *has*. Finally we describe the dynamic pattern of aPKCλ mRNA expression during development. *has* represents the first mutation identified in a gene from the highly conserved Par-3/Par-6/aPKC complex in a vertebrate organism and it is therefore likely to be an important tool for the study of cell polarity, epithelial formation, and L-R organ morphogenesis in vertebrates.

Results

Positional cloning of *has*

The *has* mutation was mapped to LG2 by half tetrad analysis [1], through linkage to the centromeric marker Z4300. Fine mapping on 2940 meioses placed *has* 0.2 cM proximal to *elrA*. A contiguous stretch of genomic DNA was constructed across the *has* region and further fine mapping localized *has* to two overlapping PACs, 70N12 and 238M4 (Figure 3.1a). To identify individual genes within this region, we radiolabelled each PAC insert and probed a normalized cDNA library prepared from 24 hpf embryos. 31 positive clones were chosen for analysis, of which nine mapped to one or both of the PACs by PCR analysis. Sequencing revealed that the nine clones corresponded to three different genes. Two of these genes mapped exclusively to the 238M4 PAC and showed no obvious homology to other genes in the database. The third gene mapped to both the 70N12 and 238M4 PACs and showed high homology to *aPKCλ*.

Genetic lesions in aPKCλ

To test whether the *has* phenotype is due to a mutation in *aPKCλ*, cDNA sequences from the wild-type and mutant alleles were compared. This analysis revealed that both alleles encode truncated proteins. The *m129* allele contains a base change from C → T at position 1519 that creates a premature stop codon, removing 73 amino acids from the C-terminus of the protein. Likewise, a G → A mutation at position 1532 in the *m567* allele results in a premature stop codon that truncates the protein by 69 amino acids (Figure 3.1b). The striking proximity and similarity of these two lesions corresponds well with the observation that these two alleles are phenotypically indistinguishable.

The *m129* and *m567* truncations render murine aPKCλ kinase-inactive

Although the catalytic domain of aPKCλ is left intact in these alleles, we wished to determine whether the kinase activity of the truncated proteins is affected. To test this, site-directed mutagenesis was employed to introduce the corresponding *m129* and *m567* mutations in the murine *Pkcλ* cDNA. To assay catalytic activity, an *in vitro* kinase reaction was performed. Specifically, exogenously expressed Flag-tagged aPKCλ proteins were immunoprecipitated and incubated with Myelin Basic Protein (MBP) as a substrate. Figure 3.2a shows that, in contrast to the wild-type Flag-aPKCλ, both the *m129* and *m567* truncated proteins exhibit little to no kinase activity toward MBP. In fact, the kinase activity of the mutant proteins is indistinguishable from a form of the protein rendered kinase-inactive by a K273E mutation. The kinase assay gave similar results using Enolase as a substrate (data not shown).

One explanation for the loss of catalytic activity in the corresponding *m129* and *m567* mutations in murine aPKCλ is that both truncated proteins lack a highly conserved 3-Phosphoinositide-dependent Protein Kinase-1 (PDK1) binding site that is located in the C-terminus of aPKCλ [2]. Presence of this critical docking site is required for an activating phosphorylation of aPKCs on a conserved threonine residue in the T-loop of the kinase domain by PDK1 [3]. To test this hypothesis, we employed an antibody that specifically recognizes the phosphorylated state of Thr-402 within the T-loop of the protein. Comparison of the exogenously expressed wild-type protein with the truncated mutant gene products on a western blot revealed that only the wild-type protein was phosphorylated on Thr-402 by endogenous PDK1 in transiently transfected 293T cells

(Figure 3.2b). Together, these data strongly suggest that the gene products of the *m129* and *m567* alleles are catalytically inactive.

Injection of *aPKCλ* mRNA rescues *has*

To gain final confirmation that *has* corresponds to *aPKCλ*, we microinjected *aPKCλ* mRNA into zebrafish embryos at the 1-4 cell stage and showed that this was sufficient to rescue the *has* mutant phenotype. 64% of injected mutant embryos showed partial rescue, in which wild-type character was restored to either the heart or the RPE. For example, many partially rescued embryos had a wild-type heart tube and a disrupted RPE. Subsequent PCR genotyping of all injected embryos revealed that 13% of homozygous mutants had been scored as wild-type with respect to the heart and RPE phenotypes. In total, > 75% of *has* embryos injected with *aPKCλ* mRNA showed at least partial rescue of the mutant phenotype (Figure 3.3a, b).

Morpholino knockdown of aPKCλ phenocopies *has*

To complement the rescue experiments we also injected a morpholino antisense oligonucleotide [4] against *aPKCλ*. Injection of 4 ng of the morpholino oligo phenocopied the *has* mutation in > 95% of embryos injected (n > 1000). Interestingly, the phenotype produced by the morpholino appeared to be somewhat stronger than has^{m129} and has^{m567} (Figure 3.3a). To address this difference in phenotypic strength, we compared protein levels of wild-type, *has* mutant, and morpholino-injected embryos at 32 hpf on a western blot. We used a monoclonal antibody that specifically recognizes the C-terminal end of wild-type aPKCλ, which fails to detect the truncated alleles. Figure 3.3c shows that some full-length protein is present in *m567* (-/-) embryos. Similar

observations were made for the *m129* allele (data not shown). The full-length protein observed in these mutants could be due to maternal contribution or may result from readthrough of the premature stop codon. In the morpholino-injected embryos, however, levels of full-length protein are further reduced, which likely accounts for the more severe phenotype. Together with the genetic linkage and biochemical evidence, these data strongly argue that *has* encodes aPKCλ.

Dynamic expression of aPKCλ mRNA during embryogenesis

To gain an understanding of the pattern of *aPKCλ* gene expression, we performed wholemount *in situ* hybridization on both wild-type and mutant embryos between the stages of 8 cells and 50 hpf. No difference in mRNA levels was observed between wild-type and mutant embryos at any stage. There is strong maternal expression of *aPKCλ* (Figure 3.4a) and early zygotic expression is present throughout the axial and paraxial regions of the embryo (Figure 3.4b). Starting from about the 12 somite stage, expression is down-regulated in the tail and dorsal trunk, but remains high in the brain, eyes and a ventral region of the axis (Figure 3.4c). Over time, the ventral staining in the posterior of the embryo declines and expression becomes restricted to the anterior 1/3 of the embryo (Figure 3.4d). Also starting from about the 12 somite stage, expression is observed close to the yolk and lateral to the head, which may represent expression in the lateral plate mesoderm (Figure 3.4e). By the 28 somite stage, expression begins in the fin buds (Figure 3.4f, h). Then at 28 hpf, increased expression can be seen in the ventral midline at the level of the fin buds (Figure 3.4f). This domain of expression is likely to represent endodermally derived organs in this region, as it is absent in *casanova* mutant embryos (data not shown), which lack all endoderm [5]. Finally, between 40 and 50 hpf,

uniformity of staining within the head and eyes is lost and staining appears to be split into a dorsal and ventral domain in the brain (Fig 3.4g). Expression in the pharyngeal region also begins at this time (Figure 3.4g).

Discussion

We have positionally cloned *has* and shown that it encodes aPKCλ. During development, aPKCs are thought to participate in a highly conserved complex with Par3 and Par6 to regulate cell polarity [6]. Examples include: the establishment of early anterior-posterior polarity in the *C. elegans* zygote, and regulation of apico-basal polarity in polarized epithelial cells [6]. *has* represents the first mutation in this complex to be described in a vertebrate.

We were quite surprised to find that the *has* mutation, which appears to cause discrete defects in L-R organ morphogenesis, disrupts a gene required for a basic cell biological process such as the establishment of apico-basal polarity in epithelia. The apparent late onset of phenotypes in *has* mutants is unlikely to be due to a hypomorphic mutation, as our biochemical data suggest that has^{m129} and has^{m567} encode null alleles. We have observed, however, a strong maternal contribution of the aPKCλ transcript (Figure 3.4a) and most vertebrates have two aPKCs, λ and ζ. It is likely, therefore, that aPKCζ and maternal aPKCλ show some functional overlap with zygotic aPKCλ to produce the relatively late phenotypes we observe in *has* mutants.

The patchy appearance of the retinal pigmented epithelium (RPE), is the only phenotype in *has* mutants, that on the surface, appears to be consistent with a defect in epithelial integrity. Intriguingly, five zebrafish mutations have been identifed that show a similar RPE defect to that of *has* [7, 8]. Two of these, *oko meduzy* (*ome*) [9] and *mosaic eyes* (*moe*), [8] have been shown to have polarity defects in the retinal neuroepithelium. To date, *has* is the only patchy RPE mutant to have been cloned, but it appears likely that this phenotype is a hallmark for genes involved in the formation of polarized epithelia.

Further investigation will be required to determine if the defects in organ morphogenesis in *has* mutants are due to an underlying defect in epithelial polarity or to some previously unknown function of aPKCλ. It will also be interesting to investigate whether mutations like *ome* and *moe* cause defects in L-R organ morphogenesis similar to those seen in *has* mutants.

Materials and Methods

Genetic mapping and positional cloning

A mapping strain was created by crossing a *has*^{m129} AB male to a wild-type WIK female. Early pressure (EP) embryos were used to initially place *has* on LG2 and subsequent linkage analysis was performed on a combination of haploid and homozygous mutant diploid embryos. PCR primers within the 3' UTR of *elrA* were used to initiate a chromosome walk to *has* using YAC (Research Genetics) and PAC clones [10]. Sequences from the recovered ends of each genomic clone were then used to identify additional clones and determine clone overlap. Further fine mapping with single-strand conformational polymorphisms localized the *has* gene to two overlapping PACs, 70N12 and 238M4. To identify cDNAs encoded on the 70N12 and 238M4 PACs, the inserts were excised with NotI and purified by pulse field gel electrophoresis. Radiolabeled probes were prepared as described [11] and used to screen a 24 hpf normalized cDNA filter (RZPD). Sequences from several partial cDNA clones and one full-length cDNA clone (ICRFp524H18162Q8) were used to assemble the full-length sequence for zebrafish *aPKCλ*. To identify the mutant lesions, cDNA was prepared from pools of 60 *has*^{m129} and *has*^{m567} mutant embryos. Three overlapping fragments from the coding sequence of *aPKCλ* were PCR amplified from both cDNA pools and cloned into the pGemT vector (Promega) for sequencing.

DNA constructs and mutagenesis

Murine aPKCλ pCMV5 Flag and kinase-inactive aPKCλ pCMV5 Flag were obtained from Christopher L. Carpenter (Division of Signal Transduction, Beth Israel Deaconess Medical Center). To engineer the *m129* and *m567* truncations it was necessary to

generate aPKCλ with an amino-terminal Flag epitope tag. To accomplish this, the carboxy-terminal Flag epitope was removed by restoring the natural stop codon using PCR mutagenesis and the cDNA was then subcloned into pFlag CMV2 (Kodak). The R → stop mutation at position 513 (corresponding to the *m129* allele) and the W → stop mutation at position 517 (corresponding to the *m567* allele) were made using the QuikChange site-directed mutagenesis kit (Stratagene). All constructs and mutations were confirmed by sequencing.

Immunoprecipitation and westerns

293T cells were cultured in DMEM supplemented with 10% FBS. Transient transfections were performed using Lipofectin and Opti-MEM medium (Life Technologies) as described in the manufacturer's instructions. Transfected cells were rinsed once in phosphate buffered saline (PBS) and lysed in phospholipase C (PLC) lysis buffer with 10 μg mL^{-1} aprotonin, 10 μg mL^{-1} leupeptin, 1 mM sodium vanadate ($NaVO_3$) and 1 mM PMSF [12]. For immunoprecipitations, lysates were incubated with goat anti-mouse sepharose and with anti-Flag antibodies at a concentration of 1 μg mL^{-1} for 2h at 4 °C. Beads were washed three times in PLC lysis buffer. Proteins were separated by SDS-PAGE, transferred to Immobilon-P membrane (Millipore), and immunoblotted with the appropriate antibody. The antibodies were the mouse monoclonal anti-Flag M2 antibody (Kodak) and the Sheep polyclonal anti-phospho-PRK2 that recognizes PDK1 phosphorylation sites in a variety of enzymes including pThr-402 of aPKCλ (Upstate Biotechnology). Blots were developed by enhanced chemiluminescence (Pierce).

Protein kinase assay

Immunoprecipitates were washed twice in PLC lysis buffer, twice in kinase reaction buffer (50 mM Hepes pH 7.5, 25 mM $MgCl_2$, 4 mM $MnCl_2$) containing 0.1 mM $NaVO_3$ and resuspended in 25 μL kinase reaction buffer containing 5μCi [γ-^{32}P] ATP and 2.5 μg myelin basic protein (MBP) as a substrate. Reactions were incubated at room temperature for 30 min and halted by the addition of 25 μL 2x SDS-PAGE sample buffer. Samples were resolved by SDS-PAGE on a 12% gel and incorporation of ^{32}P was detected by autoradiography.

Injections

For rescue experiments, capped mRNA was synthesized from the ICRFp524H18162Q8 EST plasmid using the T7 promoter and the mMessage mMachine Kit (Ambion) and 50 pg of capped RNA was microinjected into *has* mutants at the 1 to 4 cell stage. Phenotypic analysis was performed between 30 and 48 hpf, with special attention paid to the heart and RPE defects, as they are fully penetrant and easily visible under a dissecting microscope. The *aPKCλ* morpholino (5' TGTCCCGCAGCGTGGGCATTATGGA-3') was designed by and purchased from Gene Tools. 4 ng of the morpholino oligo was injected into embryos at the 1 to 4 cell stage.

PCR genotyping of *has*^{m567}

To detect *has*^{m567}, we designed a co-dominant marker using the dCAPs system (5'-GGCCCATCCTTTTTTCCCAAATGTAGAC -3', 5'-TTCAGGCTCCAGGTAAGTCC -3') to amplify a 170 bp PCR fragment. We digested the PCR products with XcmI

(NEB) to selectively remove 24 bp from the wild-type allele and resolved the bands on a 3.5% agarose gel.

Morpholino western

To examine the effectiveness of *has* morpholino knockdown, zebrafish embryos were manually dechorionated, pooled, de-yolked and lysed in a solution of 10mM Tris-HCl (pH 7.5), 1mM EDTA, 50mM KCL, 1% SDS, 1mM leupeptin and 1mM PMSF. Total protein concentration was determined using a Coomassie Protein Assay kit (Pierce). 10 μg of total protein was loaded in each lane and separated by SDS-PAGE. Protein was transferred onto Hybond ECL Nitrocellulose membrane (Amersham Pharmacia Biotech) and immunoblotted with the mouse monoclonal anti-PKCλ antibody (Transduction Labs). Blots were developed using ECL (Amersham Pharmacia Biotech).

In situ hybridizations

In situ hybridizations were performed as previously described [13]. Embryos older than 24 hpf were raised in 0.003% 1-phenyl-2-thiourea (PTU, Sigma) in egg water to inhibit production of pigment. To produce the *aPKCλ* antisense probe, a 580 bp fragment was amplified from the 3' UTR of the gene (5'-TCCTTTAGTTTGCAGAGTCCG-3', 5'-GGTCCTGCATTGAAGAAAGC-3') and TA cloned into the pGemT vector (Promega). The plasmid was linearized with NotI and transcribed using T7.

Figure 3.1 Positional cloning reveals that *has* encodes aPKCλ

(a) Positional cloning of the *has* gene. PCR primers to the *elrA* gene were used to initiate a chromosome walk and a contiguous stretch of genomic DNA was constructed across the *has* region using YAC and PAC clones. The numbers between each genetic marker represent the number of recombinational breakpoints between the markers examined. Markers proximal to *has* were tested on 2569 meioses and markers distal to *has* were tested on 2940 meioses. The 70N12 and 238M4 PACs were subsequently used to screen cDNA filters and both PACs contain the *aPKCλ* gene. **(b)** Sequence alignment of *aPKCλ* from human, mouse and zebrafish and *DaPKC* from *Drosophila*. Dark shading indicates conserved residues and light shading marks similar residues. has^{m129} and has^{m567} encode truncated proteins; the positions of the premature stop codons are marked with red arrows. *m129* is R → stop and *m567* is W → stop. The conserved PDK1 docking site is underlined in blue and the conserved threonine, which is phosphorylated by PDK1 is marked with a blue arrowhead.

Figure 3.1

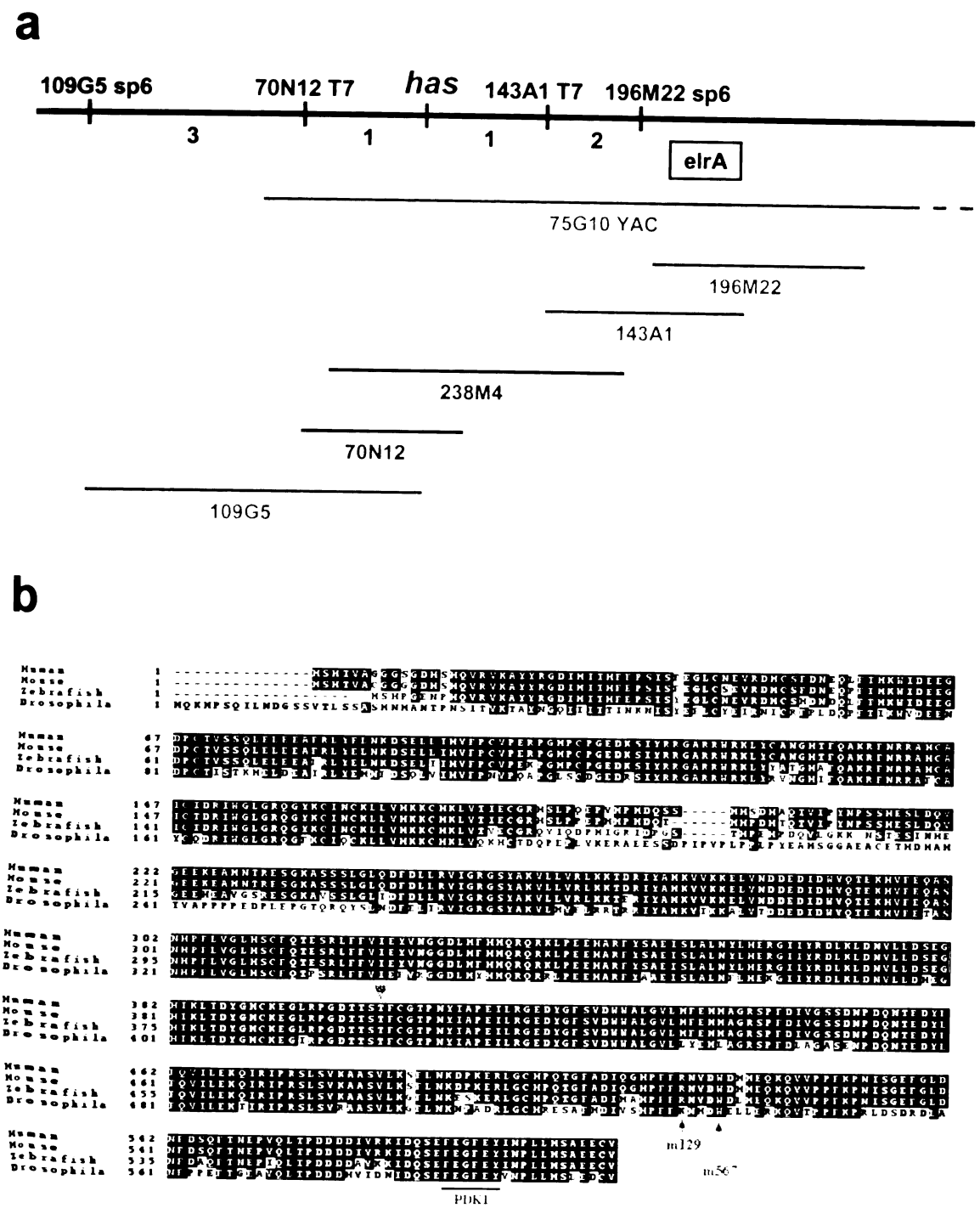
a
109G5 sp6
70N12 T7
has
143A1 T7
196M22 sp6
3
1
1
2
elrA
75G10 YAC
196M22
143A1
238M4
70N12
109G5
b
m129
PDK1

Figure 3.2 The *m129* and *m567* truncations render murine aPKCλ kinase-inactive

(a) Kinase assay to examine the effect of the *m129* and *m567* truncations on aPKCλ activity. Site-directed mutagenesis was used to recreate the *m129* and *m567* mutations in mouse *aPKCλ* in order to compare the kinase activity of the resulting truncated proteins with wild-type and kinase-inactive (K273E) versions of the enzyme. Constructs were Flag-tagged and transfected into 293T cells. Proteins were immunoprecipitated from cell lysates and relative protein levels were examined on a western blot using an antibody against the Flag epitope (lower panel). In the kinase-inactive lane of the western blot, the band appears as a triplet likely due to the use of two alternate methionine start sites in this construct. Kinase activity was assessed *in vitro* using myelin basic protein (MBP) as a substrate. The activity of the *m129* and *m567* truncations is indistinguishable from the kinase-inactive version of the protein (upper panel). **(b)** Western blot to examine the phosphorylation state of Thr-402 in the T-loop of aPKCλ. Transfections and immunoprecipitations were carried out as described above. The upper panel shows that only the wild-type protein is phosphorylated on Thr-402. In the lower panel, the upper bands in lanes 2-4 demonstrate that protein levels from the immunoprecipitation are roughly equivalent, while the lower band present in all lanes is the immunoglobulin heavy chain from the FLAG antibody. unt., untransfected.

Figure 3.2

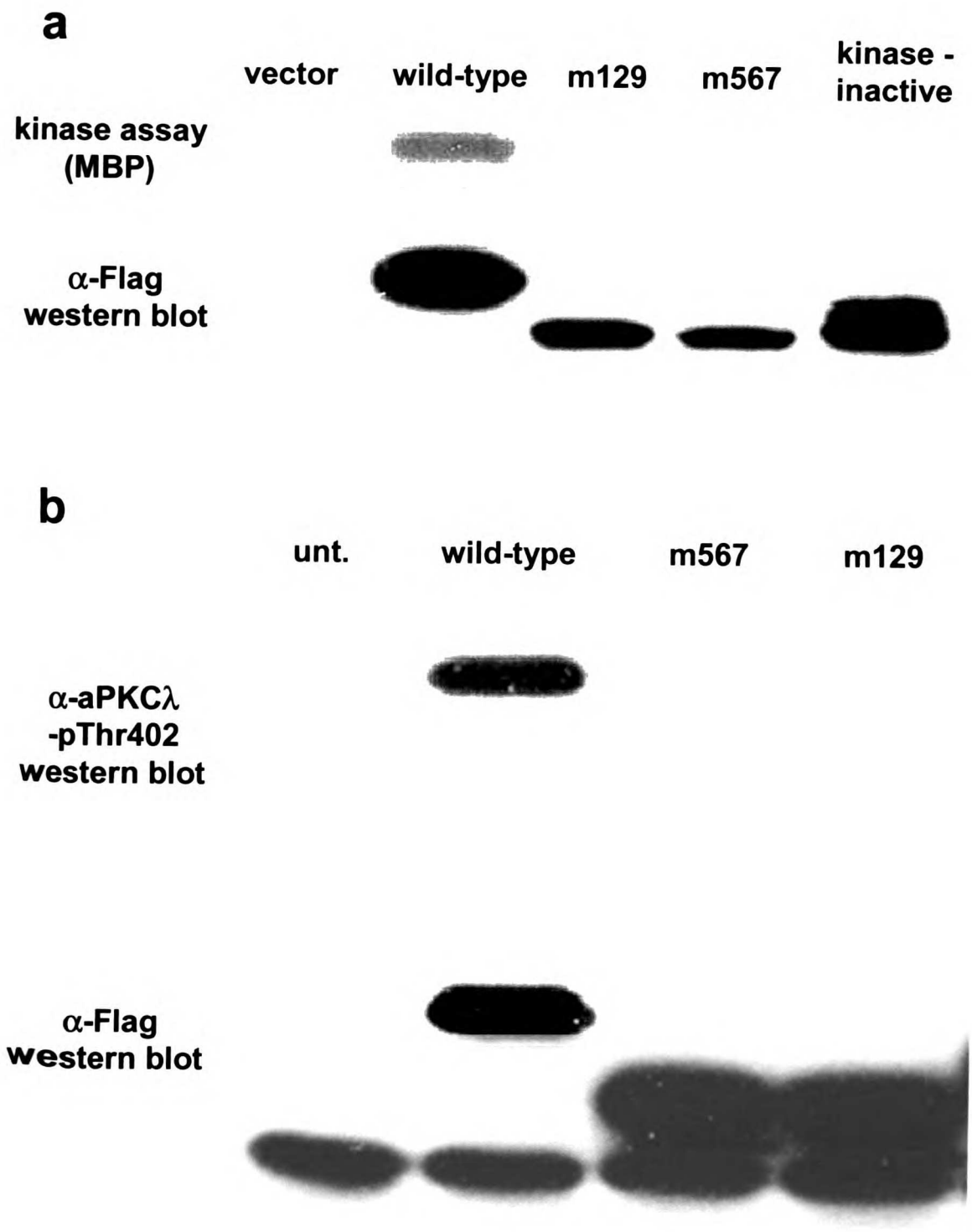
a
vector
wild-type
m129
m567
kinase - inactive
kinase assay (MBP)
α-Flag western blot
b
unt.
wild-type
m567
m129
α-aPKCλ -pThr402 western blot
α-Flag western blot

Figure 3.3 Injection of wild-type mRNA and morpholino oligos for *aPKCλ*.

(a) Phenotypic comparison of wild-type, *has*, *aPKCλ* injected, and morpholino (MO) injected embryos. The top row shows live embryos with arrowheads marking the RPE. The bottom row shows wholemount *in situ* hybridization for *cardiac myosin light chain 2* and arrows mark the position of the heart. The *has* mutants shown with partial rescue have wild-type heart morphology and a disorganized RPE. Injection of an *aPKCλ* MO into wild-type embryos essentially phenocopies the *has* mutation. Anterior is to the left and dorsal to the top. **(b)** Table showing percentages of full and partial rescue among *has* mutants injected with *aPKCλ* mRNA. The genotype of all embryos was determined by PCR (see methods). **(c)** Western blot using an antibody that specifically recognizes the C-terminus of aPKCλ to detect levels of full-length aPKCλ protein in extracts from 32 hpf embryos. In has^{m567} mutants, there is still a detectable amount of full-length protein as compared to embryos injected with *aPKCλ* MO. This full-length protein may be due to maternal contribution and/or occasional readthrough of the premature stop codon.

Figure 3.3

a
wild-type
has
partial rescue
MO
live
cmcl2
b
mutants injected
full rescue
partial rescue
no rescue
44
6 (13%)
26 (64%)
10 (23%)
c
rat brain
wild-type
has
MO

Figure 3.4 Dynamic expression of *aPKCλ* mRNA

(a) 8-cell stage; animal pole to the top. *aPKCλ* shows strong maternal expression. **(b)** 10 somites (14 hpf) lateral view. Expression is uniform throughout the axial and paraxial regions of the embryo. **(c)** 20 somites (19 hpf); lateral view. *aPKCλ* expression becomes more restricted to anterior and ventral regions of the embryo. **(d-f)** 28 hpf. **(d)** Lateral view. Expression becomes further restricted to the anterior of the embryo. **(e)** Dorso-anterior view. *aPKCλ* is expressed heavily throughout the brain and eyes. There is also expression ventral and lateral to the head, which may correspond to the anterior lateral plate mesoderm (arrows). **(f)** Dorso-posterior view. The arrow denotes expression in the fin buds and the arrowhead marks expression in digestive organs. **(g,h)** 50 hpf. **(g)** Lateral view. Expression in the brain is less uniform and there is now strong expression in the pharyngeal region (arrow). **(h)** Dorsal view. Anterior is to the left in all panels except (a).

Figure 3.4

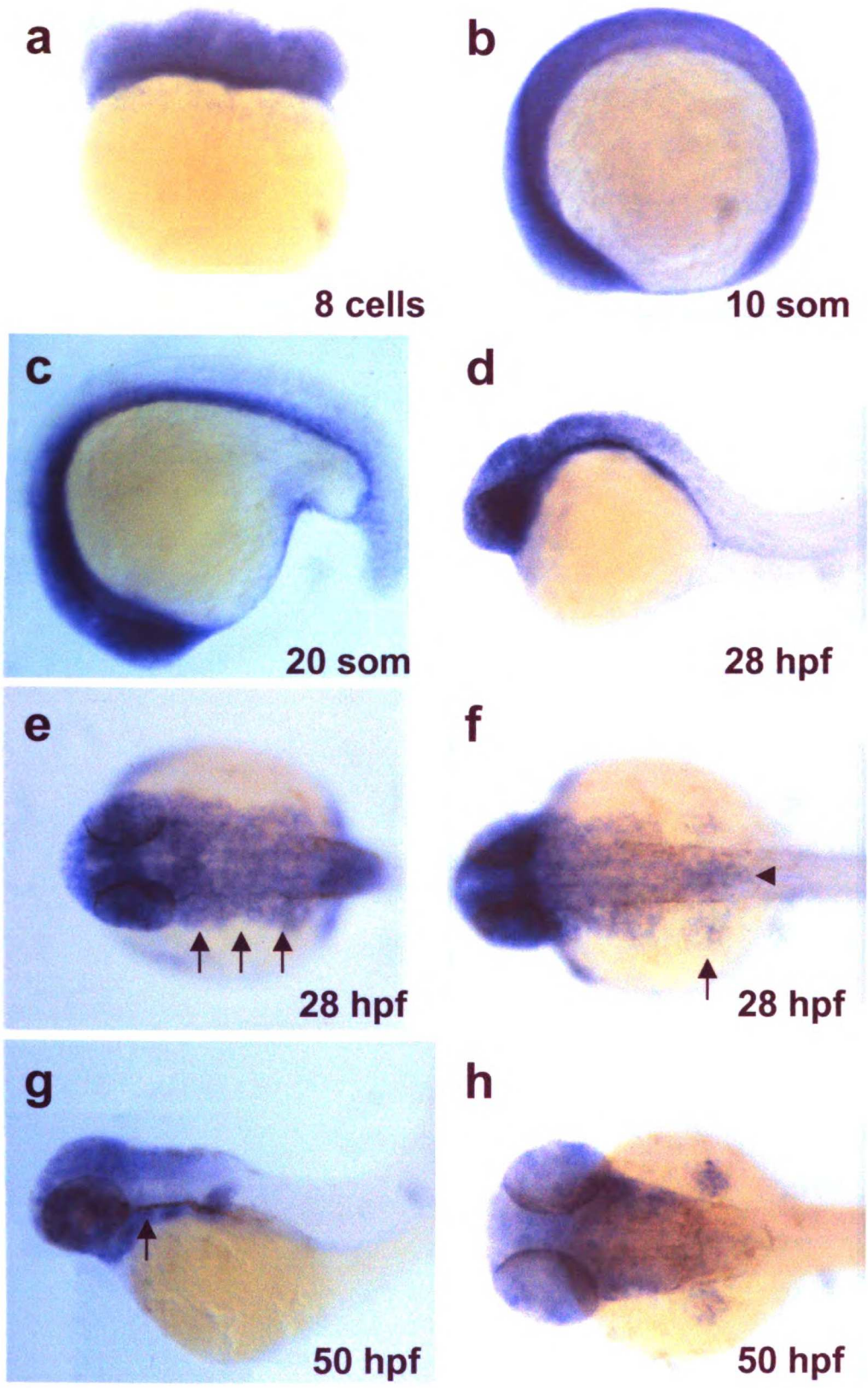

References

1. Johnson, S.L., Africa, D., Horne, S., and Postlethwait, J.H. (1995). Half-tetrad analysis in zebrafish: mapping the *ros* mutation and the centromere of linkage group I. Genetics *139*, 1727-1735.

2. Balendran, A., Biondi, R.M., Cheung, P.C., Casamayor, A., Deak, M., and Alessi, D.R. (2000). A 3-phosphoinositide-dependent protein kinase-1 (PDK1) docking site is required for the phosphorylation of protein kinase C zeta (PKC zeta) and PKC-related kinase 2 by PDK1. J Biol Chem *275*, 20806-20813.

3. Belham, C., Wu, S., and Avruch, J. (1999). Intracellular signalling: PDK1--a kinase at the hub of things. Curr Biol *9*, R93-96.

4. Nasevicius, A., and Ekker, S.C. (2000). Effective targeted gene 'knockdown' in zebrafish. Nat Genet *26*, 216-220.

5. Alexander, J., Rothenberg, M., Henry, G.L., and Stainier, D.Y. (1999). *casanova* plays an early and essential role in endoderm formation in zebrafish. Dev Biol *215*, 343-357.

6. Ohno, S. (2001). Intercellular junctions and cellular polarity: the PAR-aPKC complex, a conserved core cassette playing fundamental roles in cell polarity. Curr Opin Cell Biol *13*, 641-648.

7. Malicki, J., Neuhauss, S.C., Schier, A.F., Solnica-Krezel, L., Stemple, D.L., Stainier, D.Y., Abdelilah, S., Zwartkruis, F., Rangini, Z., and Driever, W. (1996). Mutations affecting development of the zebrafish retina. Development *123*, 263-273.

8. Jensen, A.M., Walker, C., and Westerfield, M. (2001). *mosaic eyes*: a zebrafish gene required in pigmented epithelium for apical localization of retinal cell division and lamination. Development *128*, 95-105.

9. Malicki, J., and Driever, W. (1999). *oko meduzy* mutations affect neuronal patterning in the zebrafish retina and reveal cell-cell interactions of the retinal neuroepithelial sheet. Development *126*, 1235-1246.

10. Amemiya, C.T., and Zon, L.I. (1999). Generation of a zebrafish P1 artificial chromosome library. Genomics *58*, 211-213.

11. Brownlie, A., Donovan, A., Pratt, S.J., Paw, B.H., Oates, A.C., Brugnara, C., Witkowska, H.E., Sassa, S., and Zon, L.I. (1998). Positional cloning of the zebrafish *sauternes* gene: a model for congenital sideroblastic anaemia. Nat Genet *20*, 244-250.

12. Henkemeyer, M., Orioli, D., Henderson, J.T., Saxton, T.M., Roder, J., Pawson, T., and Klein, R. (1996). Nuk controls pathfinding of commissural axons in the mammalian central nervous system. Cell *86*, 35-46.

13. Yelon, D., Horne, S.A., and Stainier, D.Y. (1999). Restricted expression of cardiac myosin genes reveals regulated aspects of heart tube assembly in zebrafish. Dev Biol *214*, 23-37.

Epithelial defects in *heart and soul* mutants

The formation, maintenance and movement of epithelial sheets are critical processes during development. Mature epithelial cells have a polarized configuration with separate apical and basolateral membrane domains. These domains have distinct complements of lipids and proteins that are separated by a large junctional complex at the apical side of the lateral membrane. In vertebrates, this apical junctional complex consists of the zonula adherens and the zonula occludens. The zonula adherens is comprised of cadherin/catenin-based adherens junctions, which provide cell-cell adhesion and facilitate apical constriction of cells [1]. The zonula occludens is located just apical to the zonula adherens and consists of tight junctions. These provide a regulated barrier to paracellular diffusion and prevent the mixing of lipids and proteins between the apical and basolateral membrane compartments [2].

In recent years, a highly conserved protein complex has been identified that regulates cell polarity in a wide range of cell types and organisms. The core of this complex consists of the PDZ-containing proteins, Par-3 and Par-6, and an atypical Protein Kinase C (aPKC). The role of these proteins in the formation of polarized epithelia is best understood from work in *Drosophila*. Bazooka (*Drosophila* Par-3) [3, 4], DmPar-6 [5] and DaPKC [6] localize to the apico-lateral membrane in a number of

embryonic epithelia. Immunohistochemical analysis has shown that this complex partially overlaps with and extends just apical to Armadillo (β-catenin) localization at the zonula adherens. Loss of function of any one of these genes in *Drosophila* results in a number of epithelial defects including loss of apical adherens junctions, changes in cell shape, and mislocalization of proteins in the plasma membrane.

Less is understood about the role of the Par-3/Par-6/aPKC complex in vertebrate epithelia. In MDCK II cells, Par-3 (ASIP), Par-6 and the two vertebrate aPKCs, λ and ζ, co-localize with the tight junction protein, ZO-1, indicating that this complex localizes to the zonula occludens in mature, polarized epithelia [7, 8]. This conclusion is further supported by immunogold electron microscopy, which places Par-3 at the tight junction in the rat intestinal epithelium [7]. Further studies have shown that a dominant negative form of aPKCλ can disrupt the deployment of tight junction proteins including Claudin and Occludin when MDCK II cells are depolarized and then repolarized using a calcium switch [8]. aPKCλ and Par-3 have also been observed to co-localize with ZO-1 at adherens junctions in NIH 3T3 cells [7], suggesting that these proteins may localize to other cell junctions in the absence of tight junctions.

In order to gain a firm understanding of the role of this complex in the formation and maintenance of polarized epithelia in vertebrates, loss of function mutations need to be identified and analyzed. In the previous chapter we reported that the zebrafish *heart and soul* (*has*) mutation disrupts aPKCλ. In this chapter we extend the phenotypic characterization of *has* mutants by investigating epithelial defects in mutant embryos. We find that *has* mutants display epithelial defects in organs where we have previously described morphogenetic defects, such as the heart and certain digestive organs. In

collaboration with Salim Abdelilah-Seyfried and Juh-Nung Jan we also describe epithelial defects within the *has* mutant retina. Our data indicate that aPKCλ regulates the clustering and maintenance of apical adherens junctions and that *has* is required for the formation of the zonula adherens, as opposed to the zonula occludens, during early epithelial development in vertebrates.

Results

Epithelial defects in the myocardium of *has* mutants

When we first reported that the *has* mutation disrupts the tilting of the cardiac cone, we believed that the structure of the myocardium was essentially normal and that the defect was specific to the tilting morphogenesis. Differences seen in cone structure were attributed to variations in the time of fusion of the myocardial precursors within a given clutch of embryos. Identification of the *has* genetic lesion has enabled us to unambiguously identify homozygous mutant embryos through PCR genotyping. It is now clear that the epithelial structure of the cardiac cone is abnormal in *has* mutants prior to the stage when tilting occurs. Figure 4.1 shows dorsal views of three wild-type cones and three mutant cones stained for *cardiac myosin light chain 2* expression at the 22 somite stage. In general, *has* cones tend to be wider, have a ragged appearance and occasionally show incomplete fusion of the myocardial precursors at the midline. In wild-type embryos, myocardial cell shape is fairly regular, whereas in *has* mutants there is much more variability in cell morphology (Fig. 4.1a). Over time, the myocardium begins to show defects that are consistent with a defect in cell adhesion. Figure 4.1g shows that strings of myocardial cells appear to dissociate from a stalled cardiac cone in mutant embryos at 32 hpf. These data indicate that the myocardium in *has* mutants exhibits epithelial phenotypes prior to the defect in tilting morphogenesis and that myocardial cell adhesion is appears to be strongly affected later in development.

Epithelial defects in the digestive organs of *has* mutants

Identifying a potential epithelial defect that coincides with the morphogenetic defect in *has* mutant hearts prompted us to examine whether there are epithelial defects in

the digestive organs as well. To better visualize cell and organ morphologies, we stained transverse sections through the digestive organs with rhodamine-phalloidin. In addition to labeling the cortical actin in each cell, phalloidin also marks the apical actin belt at the zonula adherens, providing general information about epithelial polarity within these organs. Figure 4.2a shows a cross section through a wild-type embryo at 48 hpf. The endodermal portion of the esophagus is near the midline, surrounded by a thick layer of mesodermal mesenchyme, and the liver projects to the left of the esophagus. By contrast, the liver in *has* mutants is a single, elongated structure ventral to the esophagus (Figure 4.2b).

In a more posterior section through wild-type (Figure 4.2c), the swimbladder appears as a large, round structure near the midline. The bulk of this organ primordium is composed of mesodermal mesenchyme, but there is also a thin endodermal lining, which forms a polarized epithelium (note the strong apical localization of actin). The intestine is to the left of the swimbladder and the pancreas lies ventral and to the right. In *has* mutants, the endodermal lining of the swimbladder is morphologically indistinguishable from the surrounding mesenchyme, as it fails to form a polarized epithelium, and the intestine is in the midline (Figure 4.2d). These data indicate that aPKCλ plays a critical role in digestive organ morphogenesis as well as in the formation of a polarized epithelium in the swimbladder.

Localization of aPKC isoforms within the digestive organs

To help elucidate the role of aPKCλ during epithelial formation and endodermal organ morphogenesis, we employed a polyclonal antibody that recognizes both vertebrate aPKC proteins, λ and ξ, to examine the distribution of aPKC isoforms in these tissues.

Since this antibody was generated against the C-terminal 20 amino acids of the protein, it does not recognize the truncated proteins encoded by *has*^{m129} and *has*^{m567}. By comparing wild-type and mutant embryos, the staining domains of the two family members can be distinguished. Staining that is present exclusively in wild-type embryos likely corresponds to aPKCλ. Any immunoreactivity observed in *has* mutants must be due to aPKCξ and/or residual levels of full-length aPKCλ.

We find that aPKCλ is the only aPKC expressed in the endodermal components of the liver, pancreas, and swimbladder. There is strong, patchy staining in the liver (Figure 4.2e) and pancreas (Figure 4.2g), which may correspond to the formation of ductal structures within these organs. There is also diffuse staining throughout the liver. In addition, aPKCλ shows strong apical localization within the endodermal epithelium of the swimbladder (Figure 4.2g). These staining patterns are not observed in *has* mutants (Figures 4.2f, h).

In addition to aPKC immunoreactivity within the endodermal component of these organs, there is also staining throughout the digestive tract mesoderm. This staining is most apparent in the mesenchyme surrounding the esophagus (Figure 4.2e) and in the mesodermal component of the swimbladder (Figure 4.2g). Once again, this immunoreactivity appears to be exclusive to aPKCλ, as it is missing in *has* mutants (Figures 4.2f, h).

Finally, we observed three expression domains that are likely to include aPKCξ. The pronephric ducts are epithelial tubules, which are part of the primitive zebrafish kidney. These are not endodermally derived structures, but we do observe clear apical localization of aPKC proteins within them (Figure 4.2e). Because *has* mutants have a

significant amount of staining in these structures and no apparent pronephric defects (Figures 4.2e, g), it appears that aPKCξ is strongly expressed in these tubules. There is also apical localization of aPKCs in the polarized epithelium lining the esophagus (Figure 4.2e). This staining is present but reduced in *has* mutants, suggesting that both λ and ξ are expressed in this tissue (Figure 4.2f). Finally, there is strong apical localization of aPKCs in the polarized epithelium of the intestine (Figure 4.2g). aPKCξ is clearly present, as there is strong staining in *has* mutants (Figure 4.2h). However, subtle polarity defects in the intestinal epithelium, discussed below, point to a role for aPKCλ in this tissue as well.

aPKCλ directs the apical clustering of adherens junctions during intestinal lumen formation

The intestinal epithelium in *has* mutants typically forms well along most of its length. However, when wider parts of the *has* intestine are viewed in cross section at 60 hpf, the structure may have two or even three lumens (Figure 4.3g). On first inspection, the apico-basal polarity of these cells appears normal, as most cells surrounding the lumens have a columnar shape with strong apical localization of actin (Figure 4.3g), aPKCξ, and ZO-1 (data not shown).

To address how these multiple lumens arise, we examined a time course of rhodamine phalloidin staining during gut tube formation. In wild-type zebrafish, endodermal cells migrate to the midline and initially form a multicellular rod with no visible lumen. With time, these cells rearrange in space, polarize and produce a lumen in the center. Because phalloidin strongly labels the actin associated with adherens junctions, we were able to follow the clustering and apical targeting of these structures

during lumen formation. We find that small foci of adherens junctions form locally between a few cells at a time within the rod (Figure 4.3a). These foci appear to move toward the center and merge with one another, until there is a single focus of adherens junctions in the middle of the rod (Figure 4.3b). At this time the cells display apico-basal polarity, but the apical domain appears to be very small. Finally, a lumen forms within this central spot (Figure 4.3c). It is unclear how lumen formation occurs, but we speculate that it could be due to expansion of the apical membrane domain. In the case of *has* mutants, this central clustering of adherens junctions appears to be delayed and generally less efficient than in wild-type (Figure 4.3e). Multiple lumens result when lumen formation begins before the clusters of adherens junctions have converged to the center of the rod (Figure 4.3f). These observations suggest that aPKCλ regulates the apical clustering of adherens junctions during initial polarization of intestinal epithelial cells.

The zonula adherens is not maintained in *has* mutant neural retinae

One of the original defects reported in *has* mutants was retinal degeneration. To investigate whether an epithelial defect might be responsible for this phenotype, we examined this tissue in *has* mutants. Prior to neuronal differentiation and lamination, the neural retina exists as a single sheet of pseudostratified epithelial cells, with its apical (ventricular) surface facing the RPE and its basal (vitreal) domain apposed to the lens. Immunohistochemistry shows distinct apical localization of aPKC proteins within the wild-type retinal neuroepithelium at 32 hpf (Figure 4.4a). This staining is slightly apical to and partially overlapping with staining for the junctional protein ZO-1 (Figure 4.4b). We believe that these two proteins localize to the zonula adherens, as this domain also

overlaps with apical actin (data not shown). It appears that aPKCλ is the predominant aPKC expressed in this tissue at this stage, as immunoreactivity is greatly reduced in *has* mutants. Despite the low level of aPKC protein, apical adherens junctions form in *has* mutants. Localization of ZO-1 (Figure 4.4c) and junctional actin (data not shown) are both normal, and mutant cells show the same elongated morphology as in wild-type (data not shown).

Between 30 and 60 hpf, the bulk of the various neuronal and non-neuronal cell types in the retina exit the cell cycle, differentiate, and organize into functional laminae [9]. Throughout this process, there continues to be a clear clustering of adherens junctions at the ventricular surface of the neural retina in wild-type embryos, and aPKCs continue to co-localize at these junctions with ZO-1 and β-catenin (Figures 4.4d, e). Over this same time period, apical adherens junctions are progressively lost from *has* mutant retinae. At 60 hpf, there is a complete lack of ZO-1 and β-catenin positive junctions at the ventricular surface in *has* mutants (Figure 4.4f). Finally, at 70 hpf wild-type retinae have a columnar layer of epithelial cells at the ventricular surface, whereas mutant retinae only have round, disorganized cells in this location (Figures 4.4g, h). Apical adherens junctions are also progressively lost from the ventricular surface of the neural tube during the same stages (data not shown). These data indicate that aPKCλ is not only required for the formation of the zonula adherens, as seen in the digestive tract, but for its maintenance as well.

Discussion

We have previously shown that the zebrafish *has* gene encodes aPKCλ. *has* represents the first mutation identified in the highly conserved Par-3/Par-6/aPKC complex in a vertebrate organism. Previous work in mammals has suggested that localization of this complex to the tight junction is required for proper apico-basal polarity in epithelial cells [7, 8]. Here we provide genetic evidence that aPKCλ is required for the formation and maintenance of the zonula adherens during early stages of epithelial morphogenesis. It is possible that localization to tight junctions may correspond to a later role for this protein in mature epithelia.

While our results from Chapter 3 strongly suggest that has^{m129} and has^{m567} encode kinase-inactive versions of aPKCλ, some aPKC activity is provided by aPKCζ and maternal aPKCλ in *has* mutants. The partial functional overlap of these aPKCs helped reveal discrete aspects of aPKCλ's role in establishing epithelial polarity. Zygotic aPKCλ appears to be the only aPKC expressed within the endodermal epithelium of the swimbladder. Consequently, these cells do not form a clear epithelium in *has* mutants. In the intestine, where aPKCξ is also expressed, a polarized epithelium forms, but some aspects of zonula adherens formation are abnormal in *has* mutants. Our results show that adherens junctions cluster less efficiently during initial cell polarization and lumen formation in this organ. In *Drosophila,* Par-3 (Bazooka) directs the apical clustering of spot adherens junctions to form the zonula adherens during gastrulation [3], which suggests that this particular function of the Par-3/Par-6/aPKC complex may be conserved between flies and vertebrates. Finally, the progressive loss of apical adherens junctions in the neural retina of *has* mutants demonstrates a requirement for aPKCλ in the

maintenance of the zonula adherens. It is probable that maternal aPKCλ is sufficient to establish the zonula adherens in these tissues and that the junctions gradually degrade when there is no functional zygotic protein to replace maternal stores.

Although there is considerable evidence that aPKCs play a role in the formation and maintenance of polarized epithelia, no role has yet been described for aPKCs in mesenchymal tissues during development. It is interesting to speculate that loss of aPKCλ from the mesenchyme surrounding the digestive tract is responsible for the defects in gut looping and organ budding in *has* mutants. Indeed, there is extensive communication between the mesoderm and endoderm during digestive tract formation [10]. In addition, we have found that the genetic reduction of digestive tract mesoderm leads to defects in gut looping and endodermal organ morphogenesis that are extremely similar to those seen in *has* mutants (unpublished observations). It will be important to determine whether proteins such as Par-3 and Par-6 interact with aPKCλ within this mesenchymal tissue or if this phenotype represents a role for this protein in an entirely different pathway.

In addition to the cell polarity defects we have observed in the intestine, swimbladder and retina, we have observed other cell adhesion defects in *has* mutants. Following the morphogenetic defect in heart tube assembly, cardiomyocytes appear to dissociate from the stalled cardiac cone. This phenotype is reminiscent of the cardiac defect in *N-cadherin* (-/-) mice, in which clusters of cardiomyocytes dissociate from the primitive heart tube but remain loosely aggregated with one another [11]. Since cadherins are major components of adherens junctions, this phenotype may also point to a role for aPKCλ in regulating these structures in the myocardium, a tissue that does not

appear to form a classical polarized epithelium. Furthermore, the patchy appearance of the retinal pigmented epithelium [12], one of the first phenotypes described in *has*, is also likely due to defects in cell adhesion (data not shown).

Materials and Methods

In situ hybridizations

In situ hybridizations were performed as previously described [13]. Embryos older than 24hpf were raised in 0.003% 1-phenyl-2-thiourea (PTU, Sigma) in egg water to inhibit production of pigment. The probe was *cmlc2* [13].

Antibody and phalloidin staining

For most antibody stainings, embryos were fixed for 1 hr at RT in 4% PFA in PBS. After several rinses, embryos were embedded in 5% bactoagar or 4% SeaPlaque agarose (BioWhittaker Molecular Applications) and 200 μm sections were cut with a Leica VT1000S vibratome. Incubations and washes for antibody stainings were performed on floating sections in a solution of 0.1% tween, 1% DMSO and 5% normal goat serum in PBS. Phalloidin stainings followed a similar protocol, excluding the goat serum.

We used the following antibodies: rat polyclonal anti-PKCξ (C-20) at 1:1000 (Santa Cruz Biotechnology), mouse monoclonal anti-ZO-1 [14] at 1:25 (gift of S. Tsukita), and rabbit polyclonal anti-β-catenin [15] at 1:500 (gift of P. Hausen). We used secondary antibodies conjugated to Rhodamine or Cy2 (Molecular Probes) at 1:400. To visualize actin, embryos were incubated in phalloidin conjugated with either rhodamine or Alexa-568 at 1:100 (Molecular Probes).

Fluorescence images were produced using either a Leica TCS NT confocal microscope or a Nikon TE 300 inverted microscope equipped with a BioRad Confocal Laser (BioRad MRC) and BioRad Laser Sharp version 3.2 software.

Figure 4.1 Epithelial defects in the myocardium of *has* mutants

(a-g) Wholemount in situ hybridization for *cmlc2*; dorsal views, anterior to the top. **(a,c,e)** Abnormal morphology of the cardiac cone in *has* mutant embryos at 22 somites (20 hpf). The cones are generally wider, have a more ragged appearance and can have patches of cells with abnormal morphology (arrow in a). **(b,d,f)** Cardiac cones of wild-type siblings at 22 somites. **(g)** Morphology of the stalled cardiac cone in a *has* mutant at 32 hpf. Strings of cardiomyocytes appear to have dissociated from the bulk of the organ suggesting a defect in cell adhesion.

Figure 4.1

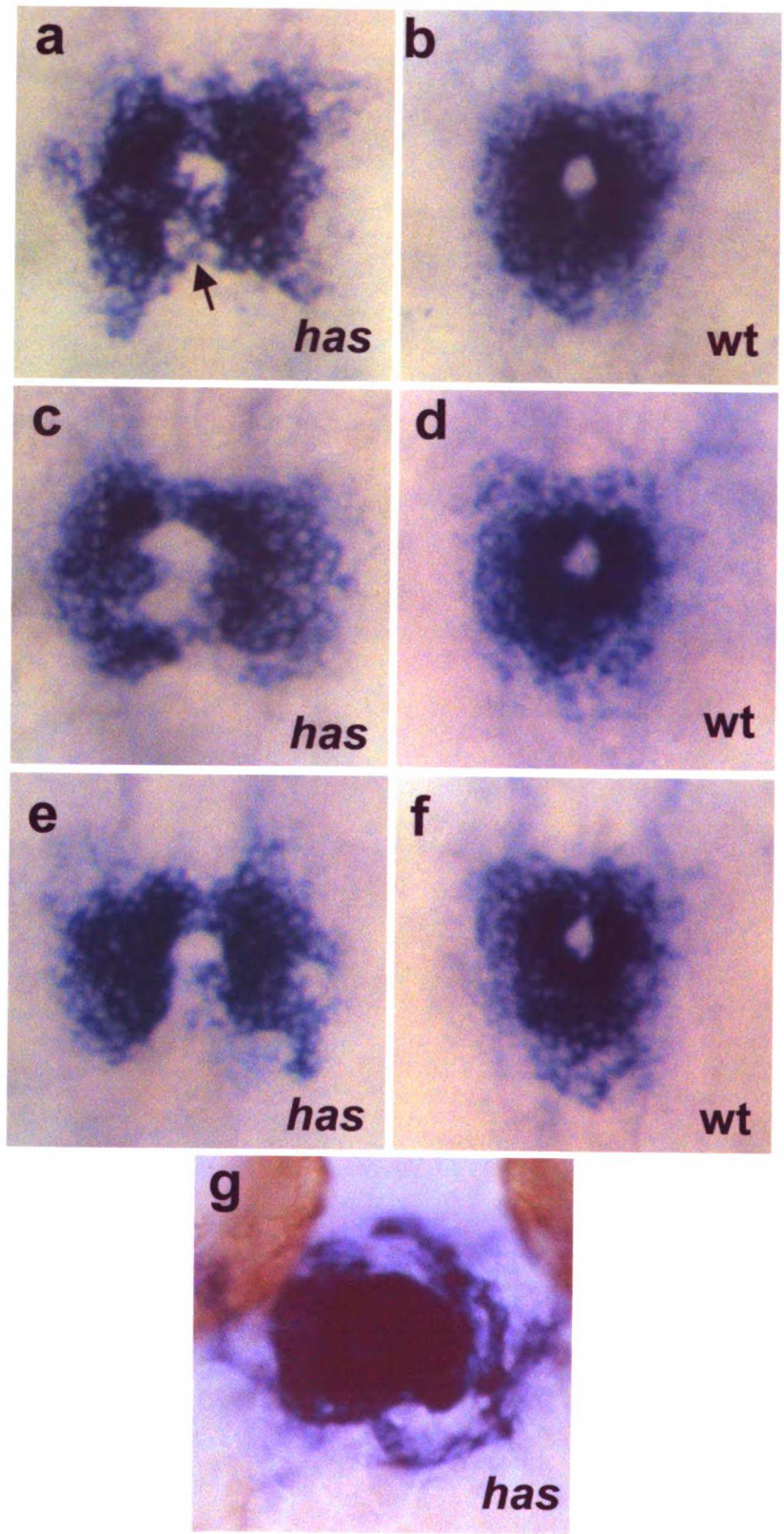

Figure 4.2 Epithelial Defects in the digestive organs of *has* mutants

(a-d) Transverse sections stained with rhodamine-phalloidin, dorsal to the top. **(a)** In wild-type embryos, the esophagus lies near the midline and the liver is on the left. **(b)** In *has* mutants, the liver is ventral to the esophagus. The phalloidin strongly stains the apical actin belt in the esophageal endoderm **(a,b)**. **(c)** There is strong apical actin staining in the endodermal linings of the swimbladder and the intestine in wild-type embryos. **(d)** In *has* mutants, the endodermal lining of the swimbladder does not form a polarized epithelium and the intestine is in the midline. We have not yet identified the pancreas in cross section at these stages. **(e-h)** Transverse sections stained with an antibody that recognizes the C-terminus of both aPKCλ and aPKCζ. Because the *m129* and *m567* alleles of *has* lack the C-terminus, they are not recognized by this antibody. In wild-type, there is strong apical staining in the polarized epithelia of the esophagus and pronephric ducts **(e)** as well as in the endodermal lining of the swimbladder and intestine **(g)**. Patchy staining is observed in the liver **(e)** and pancreas **(g)**. Finally, aPKCλ is found throughout the mesodermal mesenchyme surrounding the digestive organs **(e,g)**. *has* mutants lack much of this staining, indicating that aPKCλ is the predominant aPKC in these regions. However, there is immunoreactivity in the pronephric ducts and intestine **(h)**. There is also weak staining in the esophagus **(f)**. This staining observed in *has* mutants may be due to the presence of aPKCζ or residual full-length aPKCλ. Throughout the figure, the embryos are 48 hpf. L, liver; S, swimbladder; P, pancreas; E, esophagus; I, intestine; PD, pronephric duct.

Figure 4.2

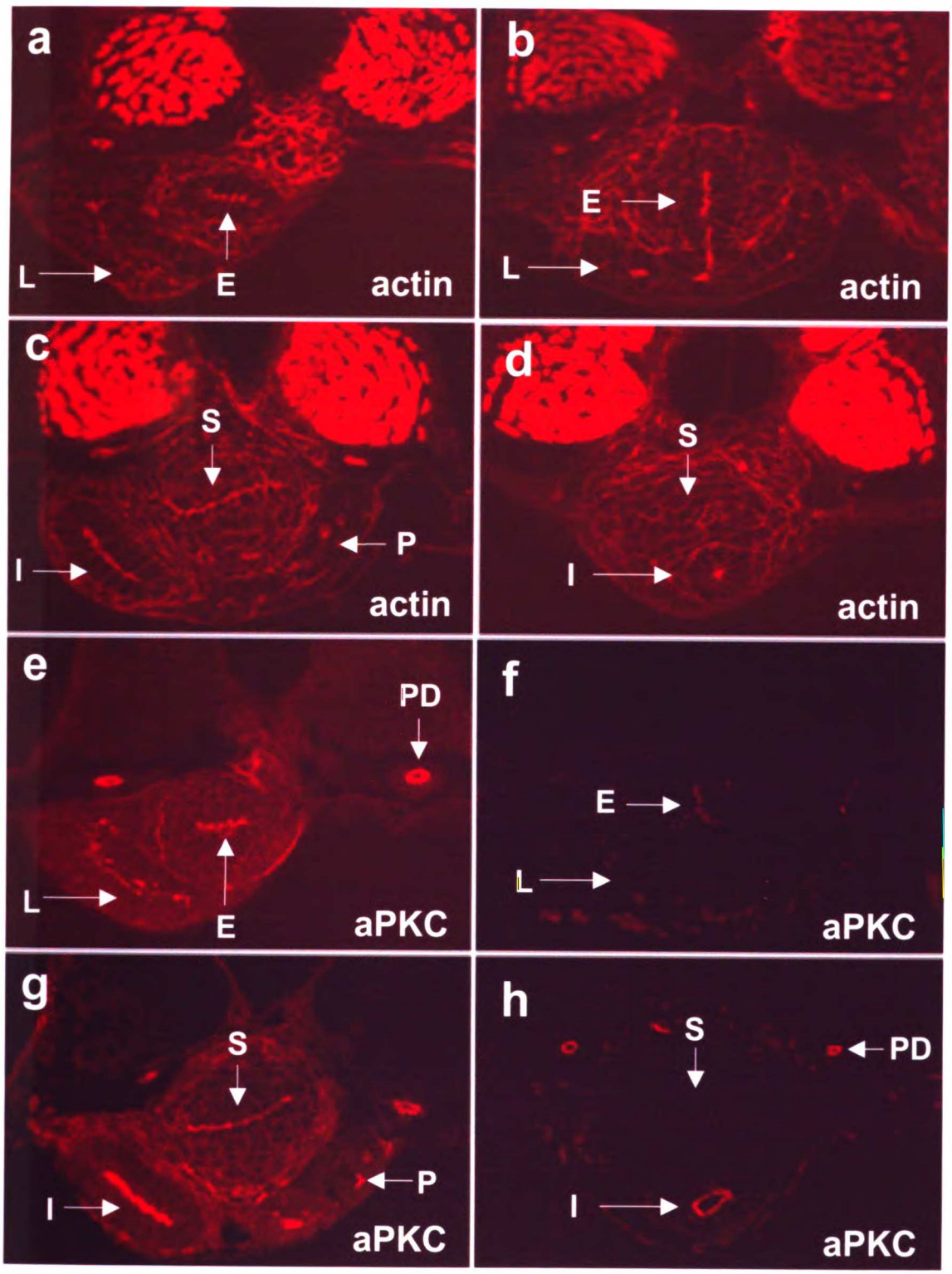
a
L
E
actin
b
E
L
actin
c
S
P
I
actin
d
S
I
actin
e
PD
L
E
aPKC
f
E
L
aPKC
g
S
P
I
aPKC
h
S
PD
I
aPKC

Figure 4.3 Loss of aPKCλ disrupts the apical clustering of adherens junctions during lumen formation in the intestine

(a-g) Photographs show transverse sections through the intestine stained with rhodamine phalloidin. In the diagrams, red spots correspond to foci of adherens junctions. **(a-d)** Formation of the intestinal lumen in wild-type embryos. **(a,b)** 36 hpf. Initially small foci of adherens junctions form locally between a few cells at a time within the rod of gut endoderm **(a)**. These foci appear to move toward the apical side of the cells, merging with one another, until there is a single focus of adherens junctions in the center of the rod **(b)**. (c) 42 hpf. Eventually, a lumen opens within the central spot of adherens junctions. **(d)** At 60 hpf the wild-type intestine has a large, single lumen. **(e-g)** Apical clustering of adherens junctions is disrupted in *has* mutants. **(e)** 42 hpf. Clustering of adherens junctions occurs in *has* mutants but is far less efficient. **(f)** 48 hpf. Multiple lumens result when lumens open before all the foci of adherens junctions have made it to the center of the rod. **(g)** At 60 hpf in *has* mutants, much of the intestine has a single lumen, but occasional regions with multiple lumens are found. In each image, dorsal is to the top.

Figure 4.3

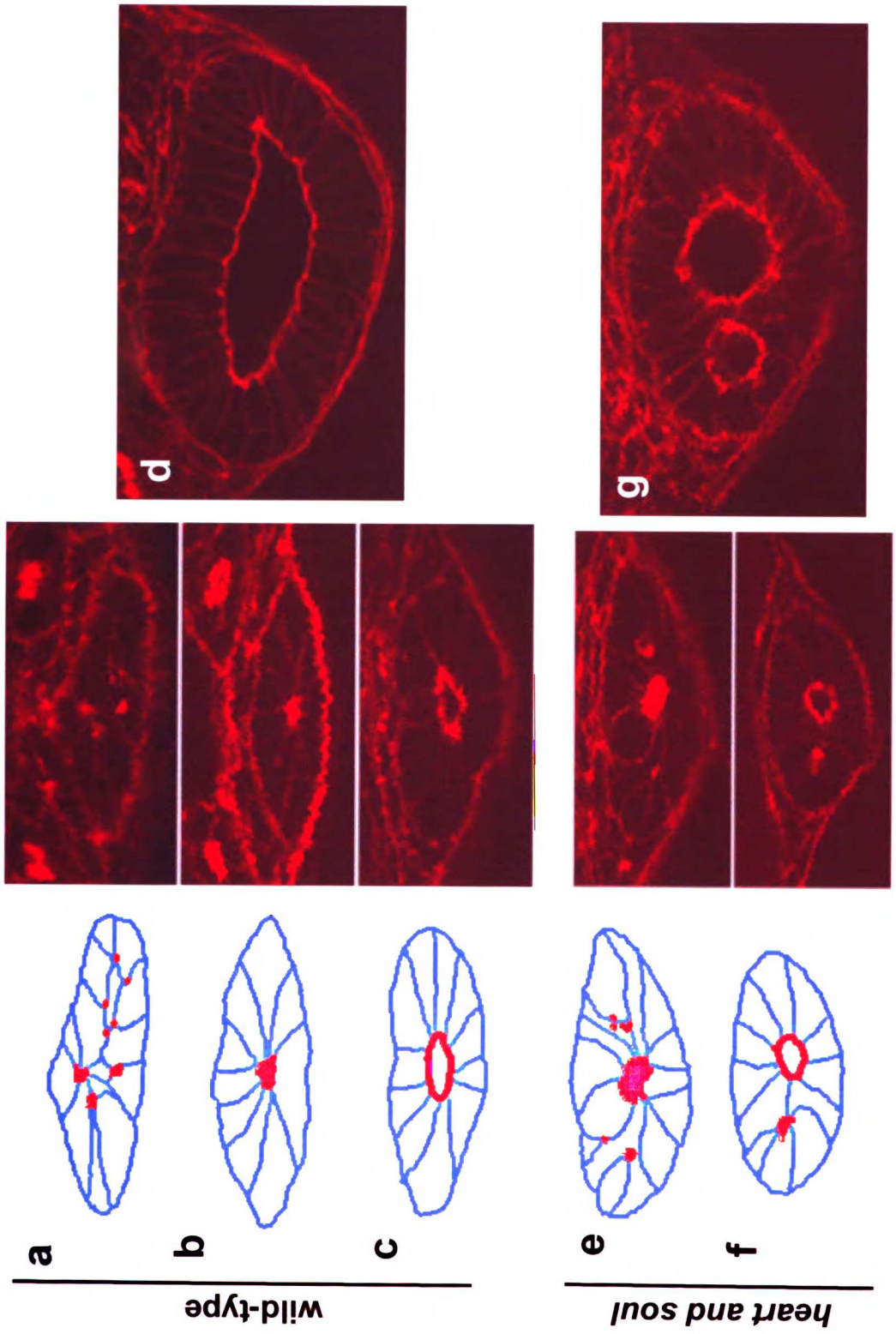

Figure 4.4 The zonula adherens is not maintained in *has* mutant neural retinae

(a-c) Subcellular localization of aPKCλ (red) and ZO-1 (green) in the pseudostratified retinal neuroepithelium at 32 hpf. **(a)** aPKCλ localizes to the ventricular surface in the neural retina. **(b)** aPKCλ is slightly apical to and partially overlapping with with ZO-1 at apical adherens junctions in wild-type embryos. **(c)** In *has* mutants, aPKCλ shows similar localization with respect to ZO-1, but the amount of aPKCλ protein is greatly reduced. **(d-f)** 60 hpf. **(d)** aPKCλ (red) continues to localize near ZO-1 (green) at the ventricular surface of the neural retina in wild-type embryos. **(e)** ZO-1 (green) co-localizes with β-catenin (red), indicating that aPKCλ likely localizes to adherens junctions. **(f)** There are no ZO-1 or β-catenin positive junctions at the ventricular surface in *has* mutants, indicating that apical adherens junctions are missing by 60 hpf. **(g,h)** Alexa568-conjugated phalloidin staining (in grayscale) of the neural retina at 70 hpf. **(g)** In wild-type, a columnar epithelium of photoreceptor cells is present at the ventricular surface of the neural retina. **(h)** In *has* mutants, a disorganized layer of rounded cells is observed at the ventricular surface. With the exception of (a), the apical or ventricular side is to the top.

Figure 4.4

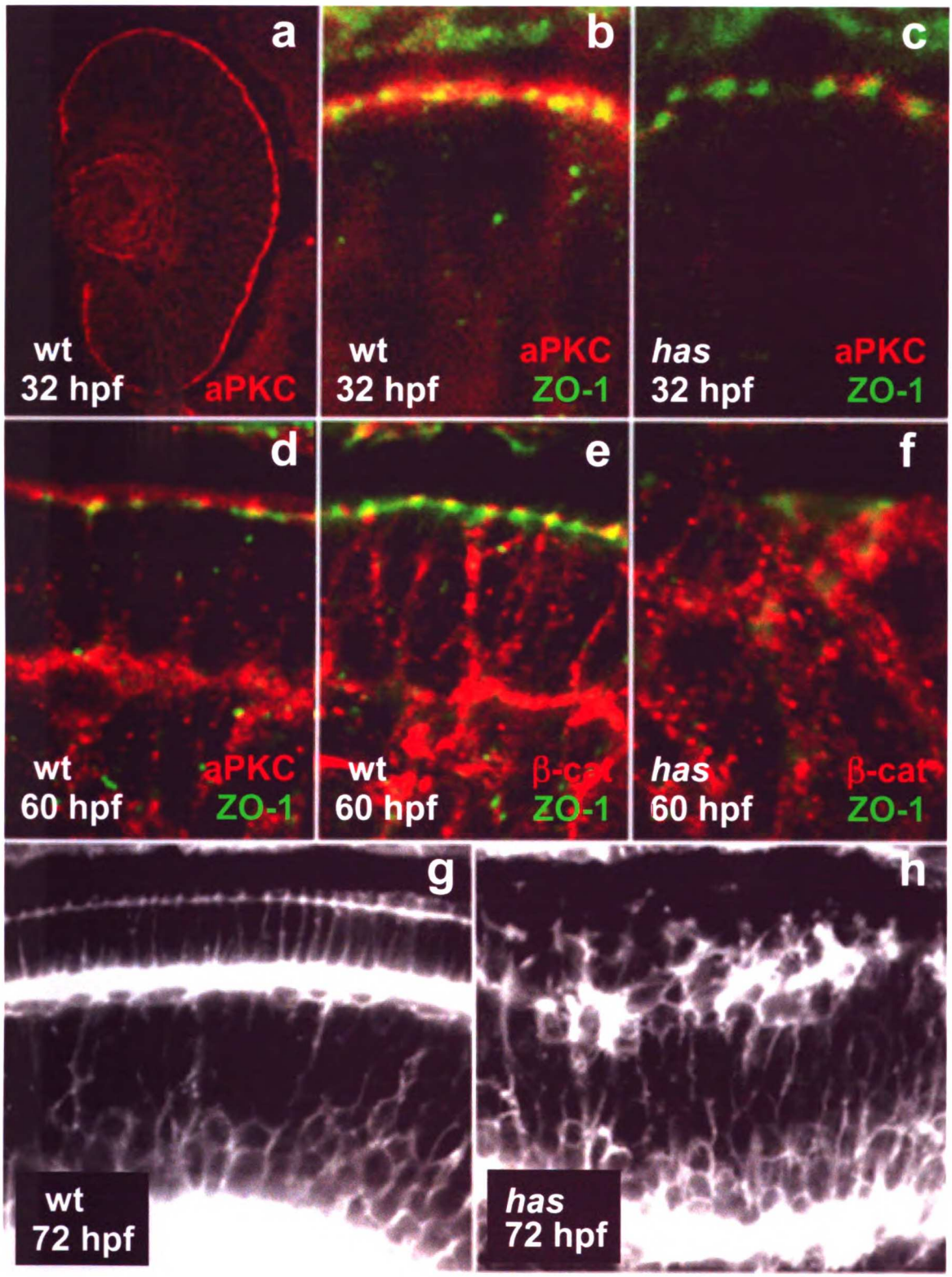
a
wt
32 hpf
aPKC
b
wt
32 hpf
aPKC
ZO-1
c
has
32 hpf
aPKC
ZO-1
d
wt
60 hpf
aPKC
ZO-1
e
wt
60 hpf
β-cat
ZO-1
f
has
60 hpf
β-cat
ZO-1
g
wt
72 hpf
h
has
72 hpf

References

1. Yap, A.S., Brieher, W.M., and Gumbiner, B.M. (1997). Molecular and functional analysis of cadherin-based adherens junctions. Annu Rev Cell Dev Biol *13*, 119-146.

2. Stevenson, B.R., Anderson, J.M., and Bullivant, S. (1988). The epithelial tight junction: structure, function and preliminary biochemical characterization. Mol Cell Biochem *83*, 129-145.

3. Muller, H.A., and Wieschaus, E. (1996). armadillo, bazooka, and stardust are critical for early stages in formation of the zonula adherens and maintenance of the polarized blastoderm epithelium in Drosophila. J Cell Biol *134*, 149-163.

4. Kuchinke, U., Grawe, F., and Knust, E. (1998). Control of spindle orientation in Drosophila by the Par-3-related PDZ- domain protein Bazooka. Curr Biol *8*, 1357-1365.

5. Petronczki, M., and Knoblich, J.A. (2001). DmPAR-6 directs epithelial polarity and asymmetric cell division of neuroblasts in Drosophila. Nat Cell Biol *3*, 43-49.

6. Wodarz, A., Ramrath, A., Grimm, A., and Knust, E. (2000). Drosophila atypical protein kinase C associates with Bazooka and controls polarity of epithelia and neuroblasts. J Cell Biol *150*, 1361-1374.

7. Izumi, Y., Hirose, T., Tamai, Y., Hirai, S., Nagashima, Y., Fujimoto, T., Tabuse, Y., Kemphues, K.J., and Ohno, S. (1998). An atypical PKC directly associates and colocalizes at the epithelial tight junction with ASIP, a mammalian homologue of Caenorhabditis elegans polarity protein PAR-3. J Cell Biol *143*, 95-106.

8. Suzuki, A., Yamanaka, T., Hirose, T., Manabe, N., Mizuno, K., Shimizu, M., Akimoto, K., Izumi, Y., Ohnishi, T., and Ohno, S. (2001). Atypical protein kinase C is involved in the evolutionarily conserved par protein complex and plays a critical role in establishing epithelia- specific junctional structures. J Cell Biol *152*, 1183-1196.

9. Hu, M., and Easter, S.S. (1999). Retinal neurogenesis: the formation of the initial central patch of postmitotic cells. Dev Biol *207*, 309-321.

10. Roberts, D.J. (2000). Molecular mechanisms of development of the gastrointestinal tract. Dev Dyn *219*, 109-120.

11. Radice, G.L., Rayburn, H., Matsunami, H., Knudsen, K.A., Takeichi, M., and Hynes, R.O. (1997). Developmental defects in mouse embryos lacking N-cadherin. Dev Biol *181*, 64-78.

12. Malicki, J., Neuhauss, S.C., Schier, A.F., Solnica-Krezel, L., Stemple, D.L., Stainier, D.Y., Abdelilah, S., Zwartkruis, F., Rangini, Z., and Driever, W. (1996). Mutations affecting development of the zebrafish retina. Development *123*, 263-273.

13. Yelon, D., Horne, S.A., and Stainier, D.Y. (1999). Restricted expression of cardiac myosin genes reveals regulated aspects of heart tube assembly in zebrafish. Dev Biol *214*, 23-37.

14. Itoh, M., Yonemura, S., Nagafuchi, A., and Tsukita, S. (1991). A 220-kD undercoat-constitutive protein: its specific localization at cadherin-based cell-cell adhesion sites. J Cell Biol *115*, 1449-1462.

15. Schneider, S., Steinbeisser, H., Warga, R.M., and Hausen, P. (1996). Beta-catenin translocation into nuclei demarcates the dorsalizing centers in frog and fish embryos. Mech Dev *57*, 191-198.

Asymmetric migration of the lateral plate mesoderm drives gut looping in zebrafish

While many vertebrate organs adopt asymmetric positions with respect to the midline, little is known about the cellular changes and tissue movements that occur downstream of left-right (L-R) gene expression to produce this asymmetry. Some of the most dramatic examples of asymmetric organ morphogenesis in response to left-right (L-R) positional cues [1-3] occur in the digestive system, where the liver and pancreas occupy asymmetric positions with respect to the midline, and the intestine bends and folds in a complex pattern for proper packing into the abdominal cavity. In zebrafish, the first leftward bend in the developing intestine arises through a morphogenetic process known as gut looping. All of the digestive organs in zebrafish originate from a solid rod of endodermal cells that forms at the ventral midline during mid to late somitogenesis [4]. Looping occurs between 26 and 30 hours post fertilization (hpf), when the region of the endodermal rod that will give rise to the esophagus, intestinal bulb, and liver curves to the left (Fig. 1a, b).

The *heart and soul* (*has*) mutation causes striking defects in asymmetric organ morphogenesis, in which gut looping fails to occur and the liver and pancreas are both symmetrical with respect to the midline [5]. *has* encodes an atypical protein kinase C, aPKCλ[5, 6], which localizes to the apical junctional complex in epithelial cells and has

been shown to be required for the establishment of epithelial polarity [7]. Consistent with this function, *has* mutants show defects in the formation and maintenance of several embryonic epithelia [5]. These observations led us to hypothesize that an epithelial tissue plays a critical role in gut looping.

In this chapter we provide evidence that the looping of the zebrafish gut results from the asymmetric migration of the neighboring lateral plate mesoderm (LPM). Mutations that disrupt the epithelial structure of the LPM perturb this asymmetric migration and inhibit gut looping. Furthermore, asymmetric LPM migration can still occur when endoderm is genetically ablated from the gut looping region, showing that the LPM can autonomously provide a motive force for gut displacement. Finally, reducing left-sided Nodal activity randomizes the pattern of LPM migration and gut looping. This work reveals a cellular framework for the regulation of organ laterality by asymmetrically expressed genes.

Results

The LPM forms a columnar epithelium in the gut looping region.

To determine which epithelial tissue might affect visceral L-R morphogenesis, we examined the localization of aPKCs λ and ζ in the gut looping region at 30 hpf. We found that the endoderm at this stage is a compact mass of cells with little to no polarization and weak expression of aPKCs (Figure 5.1g, h). In contrast, the lateral plate mesoderm (LPM) forms a highly polarized epithelium with strong expression and apical localization of aPKCs (Figure 5.1g, h). The left and right LPM epithelia each have a U-shaped structure in which the apical side of the epithelium corresponds to the inside of the U and each arm of the U is comprised of either columnar or squamous cells (Figure 5.1g, h, g′, h′). The most striking feature of the LPM epithelia, however, is that the left and right sides show a distinct asymmetry in their morphology and position. The left LPM is dorsal to the endoderm with its columnar cells on the ventral arm of the U while the right LPM is ventro-lateral to the endoderm, with its columnar cells on the dorsal arm of the U (Figure 5.1g, h).

The LPM is a structure that spans the entire anterior-posterior (A-P) extent of the trunk in vertebrate embryos. Intriguingly, we only observe these columnar cells and the asymmetric placement of the left and right sides of the LPM in the A-P region of the embryo where gut looping occurs (Figure 5.1g, h). Posterior to the looping region, the LPM cells still express aPKCs but the cells appear squamous and both sides of the LPM lie dorsal to the endoderm (Figure 5.1i). These data show that the two sides of the LPM form columnar epithelia with morphological L-R asymmetry specifically in the A-P region where gut looping occurs.

Asymmetric migration of the LPM

To further investigate this process, we examined the structure and position of the LPM at earlier times in development. Prior to looping, the endodermal rod lies in the midline and both sides of the LPM are symmetrical and at approximately the same dorso-ventral level as the endodermal rod (Figure 5.1e). During looping, however, the LPM undergoes an unexpected asymmetric migration: both sides of the LPM migrate medially, but the left side moves dorsal to the endoderm, while the right side undergoes a ventro-lateral migration directly abutting the endodermal rod (Figure 5.1 f-h). Intriguingly, the morphology of the LPM is markedly asymmetric before the endoderm is displaced from the midline (Figure 5.1f). The early morphological asymmetry in the LPM combined with the close apposition of the right LPM to the endoderm throughout its migration past the midline (Figure 5.1h) suggest that the LPM may push the developing intestine to the left.

Gut looping defects in *has* and *nok* mutants

To test the hypothesis that the asymmetric migration of the LPM is required for gut looping, we examined this process in *has* and *nagie oko* (*nok*) mutants. *nok*, which encodes a membrane associated guanylate kinase (MAGUK), is required, like *has/aPKCλ*, for the establishment of epithelial polarity [8]. We examined endodermal morphogenesis in *nok* mutants and found that, as in *has* mutants, the gut does not loop (Figure 5.2a-c). To assess whether the non-looping phenotype in these mutants is due to a defect in L-R gene expression, we examined two genes that are asymmetrically expressed within the left LPM of the gut looping region, the *Nodal* gene *southpaw (spaw)*[9] and the transcription factor gene *pitx2*[10]. In both *has* and *nok* mutants, *spaw*

and *pitx2* expression appears normal (Table 5.1), indicating that the failure of their guts to loop is unlikely to be due to a defect in L-R gene expression.

Since L-R gene expression appears to be unaffected in *has* and *nok* mutants, the failure of the gut to loop is likely to be due to a defect in the morphogenetic process itself. Examination of transverse sections through the gut looping region in *has* and *nok* mutants revealed that the epithelial structure of the LPM is severely disrupted, and that the ventro-lateral migration of the right LPM is perturbed (Figure 5.2d, e). Although some cells from the right LPM move in the direction of the ventro-lateral migration, the majority migrates dorsal to the endoderm (Figure 5.2d, e), similar to what is seen in non-looping regions of the intestine (Figure 5.1i). Together with the high expression of Has and Nok (Figure 5.2f) proteins in the LPM during looping stages, the mutant phenotypes suggest that a defect in the LPM is responsible for the non-looping gut phenotype observed in *has* and *nok* mutants, and that the asymmetric migration of the LPM provides the motive force for gut looping.

Asymmetric LPM migration can occur in the absence of endoderm

If the LPM provides the motive force to displace the endoderm to the left, ablation of the looping endoderm should not affect the asymmetric migration of this tissue. Mutants that completely lack endoderm, like *casanova*, have numerous defects in the migration of mesodermal tissues toward the midline [11]. *bonnie and clyde* (*bon*) mutants have a reduced number of endodermal cells [12] and correspondingly fewer defects in mesodermal migration (data not shown). We examined a single transverse section through the gut looping region of 44 randomly selected *bon* mutants at 30 hpf, and found that 35 (80%) showed clear asymmetric migration of the LPM past the midline

(Figure 5.3e, f). Out of these 35 sections, 23 (66%) completely lacked endoderm (Figure 5.3f), and in the rest the amount of endoderm was significantly reduced (Figure 5.3e). Furthermore, the left LPM was dorsal to the right LPM in 97% of the sections showing asymmetric LPM migration (Figure 5.3e, f). These data show that asymmetric migration of the LPM can occur in the absence of endoderm and suggest that the force for gut displacement is autonomous to the LPM.

Reducing *spaw* function randomizes LPM migration

To investigate whether the asymmetric migration of the LPM is dependent on normal L-R positional cues, we injected embryos with a morpholino antisense oligo (MO)[13, 14] targeted against the *Nodal* gene *southpaw* (*spaw*). MO-knockdown of *spaw* abolishes left-specific gene expression in the LPM in 80-100% of injected embryos, yet, unlike the reported zebrafish mutations that affect L-R gene expression, the *spaw*-MO does not appear to disrupt developmental processes other than L-R asymmetry [9]. Whole mount in situ hybridization with *foxA3* revealed that gut looping is randomized in *spaw-MO* injected embryos (data not shown). More importantly, we found that injection of the *spaw-MO* randomizes LPM migration. Out of 60 injected embryos, 22 (37%) showed the normal pattern of LPM migration (Figure 5.4a), 25 (41%) showed a reversed pattern of LPM migration (Figure 5.4b), 7 (11%) showed bilateral dorsal migrations (Figure 5.4c), and 6 (10%) showed bilateral ventro-lateral migrations (Figure 5.4d). The epithelial structure of the LPM appears normal in *spaw*-MO injected embryos (Figure 5.4a-d), indicating that it is unlikely that *has* and *nok* act as morphogenetic effectors downstream of the Nodal pathway. These data show that the pattern of LPM migration and gut looping is regulated by L-R gene expression.

Discussion

Previous work on vertebrate L-R asymmetry has largely focused on signaling events that establish and pattern the L-R axis. Little is known, however, about how these L-R signals ultimately affect cell and tissue behavior to generate organ asymmetry. Our data suggest that the LPM undergoes a dynamic asymmetric migration that in turn causes the initial leftward bend in the developing intestine in zebrafish. An alternative model is that the endoderm autonomously loops to the left and the LPM follows. However, both wild-type and mutant analyses strongly suggest that the LPM provides the motive force for looping. For example, the LPM displays marked morphological asymmetry prior to the leftward displacement of the endoderm in wild-type embryos (Figure 5.1f). Furthermore, studies with *has* and *nok* mutants show that the gut fails to loop when asymmetric migration of the LPM is perturbed, and studies with *bon* mutants show that asymmetric LPM migration can occur in the absence of endoderm. In the future, it will be important to investigate the cellular mechanisms that drive asymmetric LPM morphogenesis. It is possible that the LPM epithelia are actively migratory; alternatively the medial movement could result from concerted cell shape changes or proliferation within the plane of the epithelium. It will also be of great interest to understand how asymmetric gene expression within the LPM regulates the pattern of migration of this tissue.

Materials and Methods

Zebrafish strains

Confocal studies were performed on wild-type, *has*^{m567}, and *nok*^{m520} embryos carrying the gut GFP transgene [15]. For studies involving genetic ablation of the endoderm, embryos were obtained from *bon*^{s9} heterozygous females crossed to *bon*^{m425} homozygous males (gift of Le Trinh). *bon*^{m425} homozygous males were created by injecting wild-type *bon* mRNA into homozygous mutant embryos at the 1 to 4 cell stage to rescue embryonic defects.

Antibody and phalloidin staining

Embryos were fixed for 1 hour at RT in 4% Paraformaldehyde in phosphate buffered saline (PBS) and embedded in 4% SeaPlaque agarose (BioWhittaker Molecular Applications). 200 or 300 μm sections were cut with a Leica VT1000S vibratome. Staining and washes were performed on floating sections in a solution of 0.1% tween, 1% DMSO and 5% goat serum in PBS. We used the following antibodies: anti-PKCζ (C-20) (Santa Cruz Biotechnology), which recognizes zebrafish aPKC λ and ζ, at 1:1000, anti-Nok[8] at 1:800 and a goat anti-rabbit secondary antibody conjugated to rhodamine red-X (Molecular Probes) at 1:200. To visualize actin, embryos were incubated in Alexa-488 phalloidin (Molecular Probes) at 1:50. Fluorescence images were produced using either a Leica TCS NT confocal microscope or a Zeiss LSM5 Pascal confocal microscope.

In situ hybridization

In situ hybridizations were performed as previously described[16]. Embryos older than 24 hpf were raised in 0.003% 1-phenyl-2-thiourea (PTU, Sigma) in egg water to inhibit pigment production.

Analysis of L-R gene expression

We performed wholemount in situ hybridizations with *spaw*[9] and *pitx2*[10] (probe recognizes both a and c isoforms) on 20-24 somite embryos from *has*^{m567} and *nok*^{m520} heterozygous crosses in addition to wild-type crosses. All embryos were raised at ≥ 25°C. *has*^{m567} embryos were genotyped as described [5]. To detect *nok*^{m520}, we designed primers (5'-GGACAGGTTTGCTGGACCT-3', 5'-CGTTTGCCTCAGCGTCAC-3') to amplify the mutant lesion. We digested the PCR products with SalI (NEB), which selectively cleaves the wild-type allele, and resolved the bands on a 3.5% agarose gel.

Morpholino knockdown of *spaw*

The morpholino oligo is targeted against the putative translational start site of the *spaw* gene, and has been previously designated *spaw*-MO1[9]. We injected approximately 6 ng of MO in a volume of 4.6 nl into the yolks of embryos at the 1-4 cell stage.

Figure 5.1 The LPM undergoes asymmetric migration in the gut looping region. **(a-b)** Whole mount *in situ* hybridization with *foxA3* reveals endodermal morphology prior to **(a)** and immediately following **(b)** looping morphogenesis. The looping region (brackets) lies between the caudal border of the pharyngeal endoderm and the pancreatic islet. Dorsal views, anterior to the top. **(c)** Diagram of the looped gut at 30 hpf. Blue lines indicate position of sections in **(g-i)**. **(d)** Key for the diagrams in **(e'-i')**. **(e-i)** Transverse sections through the endoderm and LPM. aPKCs (red) show weak expression in the endoderm but are highly expressed and apically localized in the LPM epithelium. Most cells are outlined with cortical actin (green) and endodermal cells have weak cytoplasmic GFP. Dorsal to the top. **(e)** At 20 hpf the endodermal rod lies in the midline and both sides of the LPM are at the same dorso-ventral level as the endodermal rod. **(f)** At 26 hpf both sides of the LPM have migrated medially. The left LPM is dorsal to the endoderm and the right LPM is beginning to migrate ventro-laterally. Although the LPM is markedly asymmetric at this stage, the developing intestine is still in the midline. Asymmetry seen within the endoderm is due to leftward budding of the liver, which can be genetically uncoupled from gut looping [15]. **(g-h)** At 30 hpf the migration is complete. The developing intestine has shifted to the left and the position of the left versus the right LPM is highly asymmetric. **(i)** Posterior to the looping region, the LPM cells appear squamous and both sides of the LPM are dorsal to the endoderm. **(e'-i')** Diagrams of the relative positions of the LPM and endoderm in confocal images **(e-i)**.

Figure 5.1

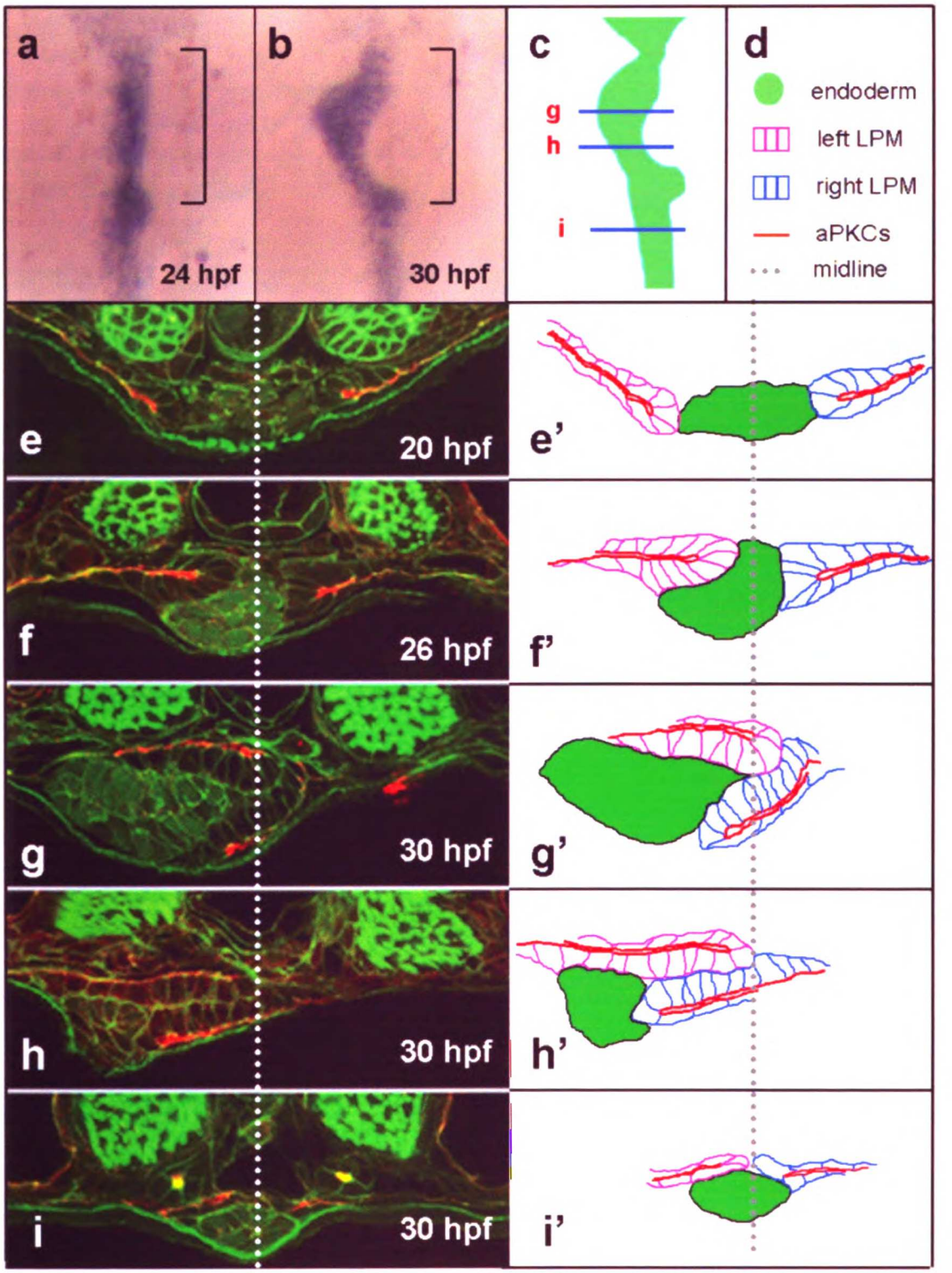
a
24 hpf
b
30 hpf
c
g
h
i
d
endoderm
left LPM
right LPM
aPKCs
midline
e
20 hpf
e'
f
26 hpf
f'
g
30 hpf
g'
h
30 hpf
h'
i
30 hpf
i'

Figure 5.2 Gut looping defects in *has* and *nok* mutants.

(a-c) Whole mount *in situ* hybridization with *foxA3* reveals endodermal morphology. Dorsal views, anterior to the top. In wild-type **(a)** the gut loops to the left, whereas in *has* **(b)** and *nok* **(c)** mutants it remains medial. Brackets denote the looping region. **(d-f)** Transverse sections through the gut looping region, dorsal to the top. Most cells are outlined with cortical actin (green) and endodermal cells contain weak cytoplasmic GFP. In *has* **(d)** and *nok* **(e)** mutants, the epithelial structure of the LPM is severely disrupted and the right LPM fails to undergo the ventro-lateral migration seen in wild-type. aPKCs are in red **(d-e)**. Red staining is low in *has* mutants **(d)** as the aPKC antibody does not recognize the truncated protein encoded by $has^{m567;4}$. **(f)** Nok (red) is weakly expressed in the endoderm but strongly expressed and apically localized in the LPM. All images at 30 hpf.

Figure 5.2

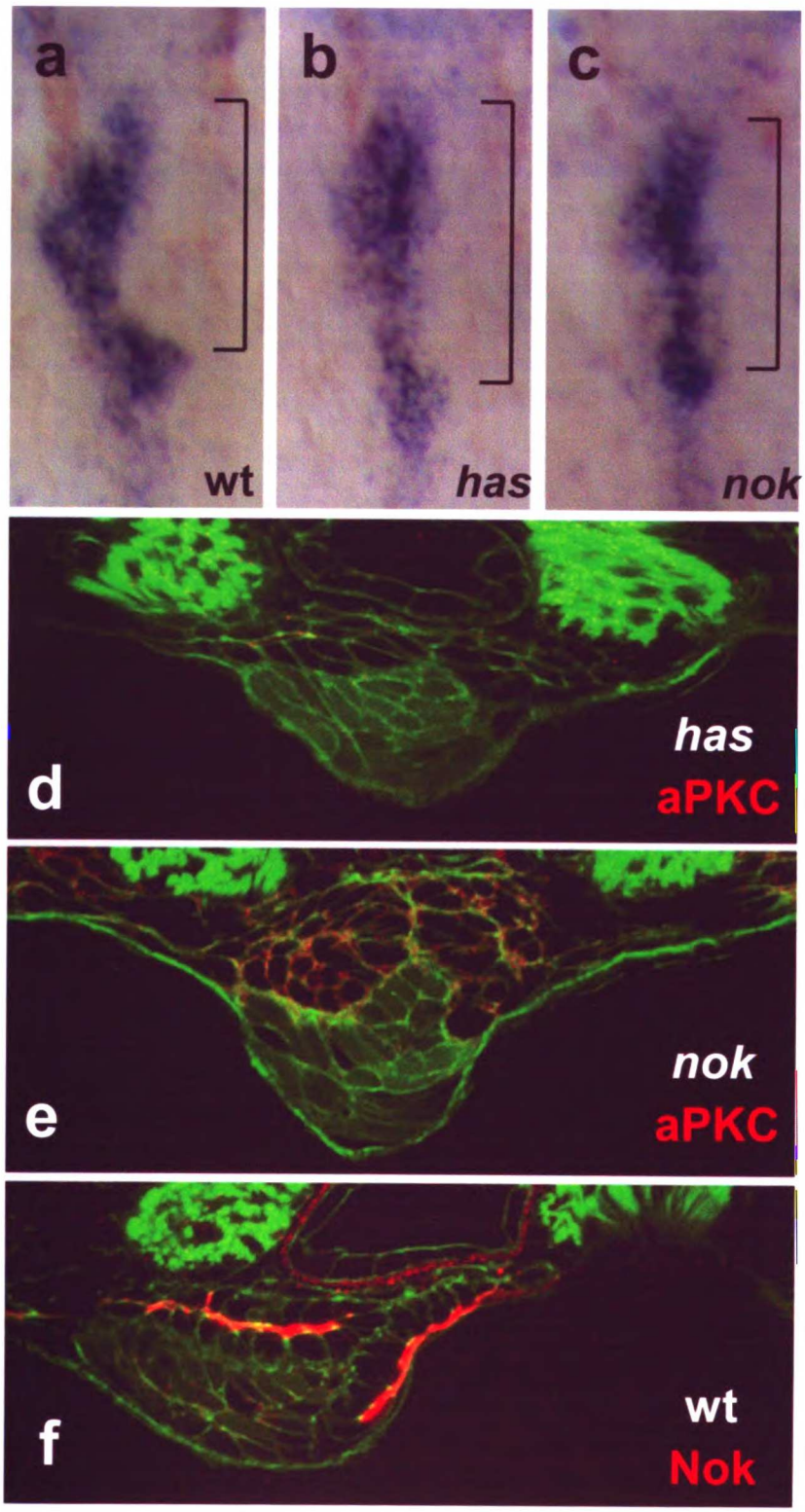

Table 5.1. L-R gene expression in the LPM appears to be normal in *has* and *nok* mutants. The table shows the percentage of embryos that had L-R gene expression either in the left LPM, the right LPM, bilaterally in the LPM, or absent from the LPM. PCR genotyping of a subset of the embryos from the *has* and *nok* crosses showed that aberrant expression of *spaw* or *pitx2* did not segregate with either mutation (data not shown).

		Total	Left (%)	Right (%)	Bilateral (%)	Absent (%)
wt	*spaw*	462	96.97	0.65	1.95	0.43
	pitx2	368	92.66	3.53	2.45	1.36
has	*spaw*	471	96.6	0.64	2.34	0.42
	pitx2	417	95.2	0.96	1.92	1.92
nok	*spaw*	439	92.03	2.05	4.78	1.14
	pitx2	417	91.96	3.35	2.90	1.79

Figure 5.3 Asymmetric LPM migration can occur in the absence of endoderm. **(a-d)** Whole mount *in situ* hybridization with *foxA3*. Brackets denote the gut looping region. Dorsal views, anterior to the top. **(a)** wild-type. **(b-d)** Endoderm is greatly reduced in *bon* mutants. The 74 mutants scored fell into three classes: **(b)** those with a reduced, but continuous stretch of endoderm in the gut looping region (14%), **(c)** those with small, discontinuous, patches of endoderm (red arrowhead) in the gut looping region (8%), **(d)** and those with a complete absence of endoderm in the gut looping region (78%). **(e-f)** Transverse sections through the gut looping region of *bon* mutants, dorsal to the top. actin (green), aPKCs (red). We examined a single transverse section in 44 randomly selected *bon* mutants and found that 35 (80%) showed clear asymmetric migration of the LPM past the midline **(e-f)**. Out of these 35 sections, 12 (34%) contained endoderm, but the amount was significantly reduced **(e)**; 23 (66%) showed asymmetric LPM migration in the complete absence of endoderm **(f)**. In 34 out of the 35 sections that showed asymmetric LPM migration the left LPM had migrated dorsal to the right LPM **(e'-f')** Diagrams of the relative positions of the LPM and endoderm in confocal images **(e-f)**. All images at 30 hpf. Dotted lines mark the midline.

Figure 5.3

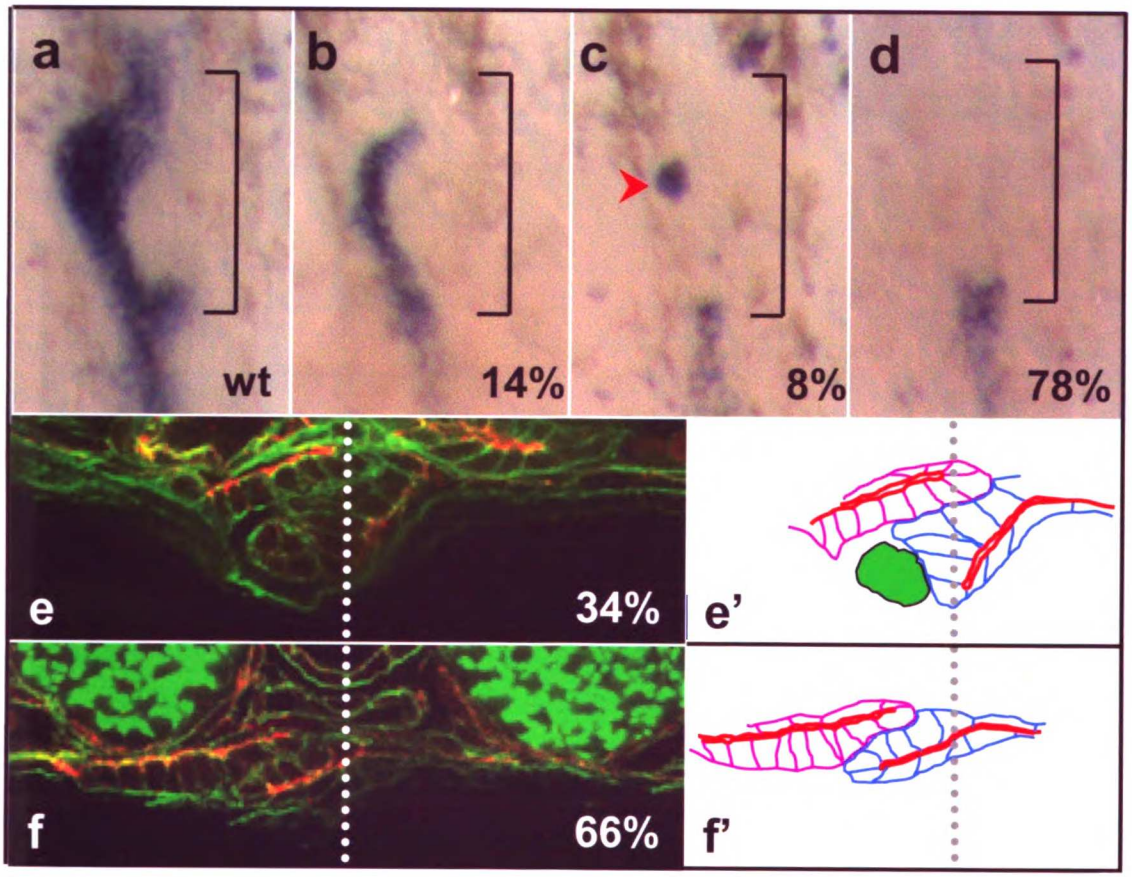

Figure 5.4 Reducing *spaw* function randomizes LPM migration.

(a-d) Transverse sections through the gut looping region at 30 hpf, dorsal to the top. Sections are stained as in Fig. 5.1. Out of 60 injected embryos, 22 showed the normal pattern of LPM migration: left dorsal, right ventro-lateral **(a)** 25 showed a reversed pattern of LPM migration: right dorsal, left ventro-lateral **(b)** 7 had both sides of the LPM migrate dorsally **(c)** and 6 had both sides of the LPM migrate ventro-laterally **(d)**.

Figure 5.4

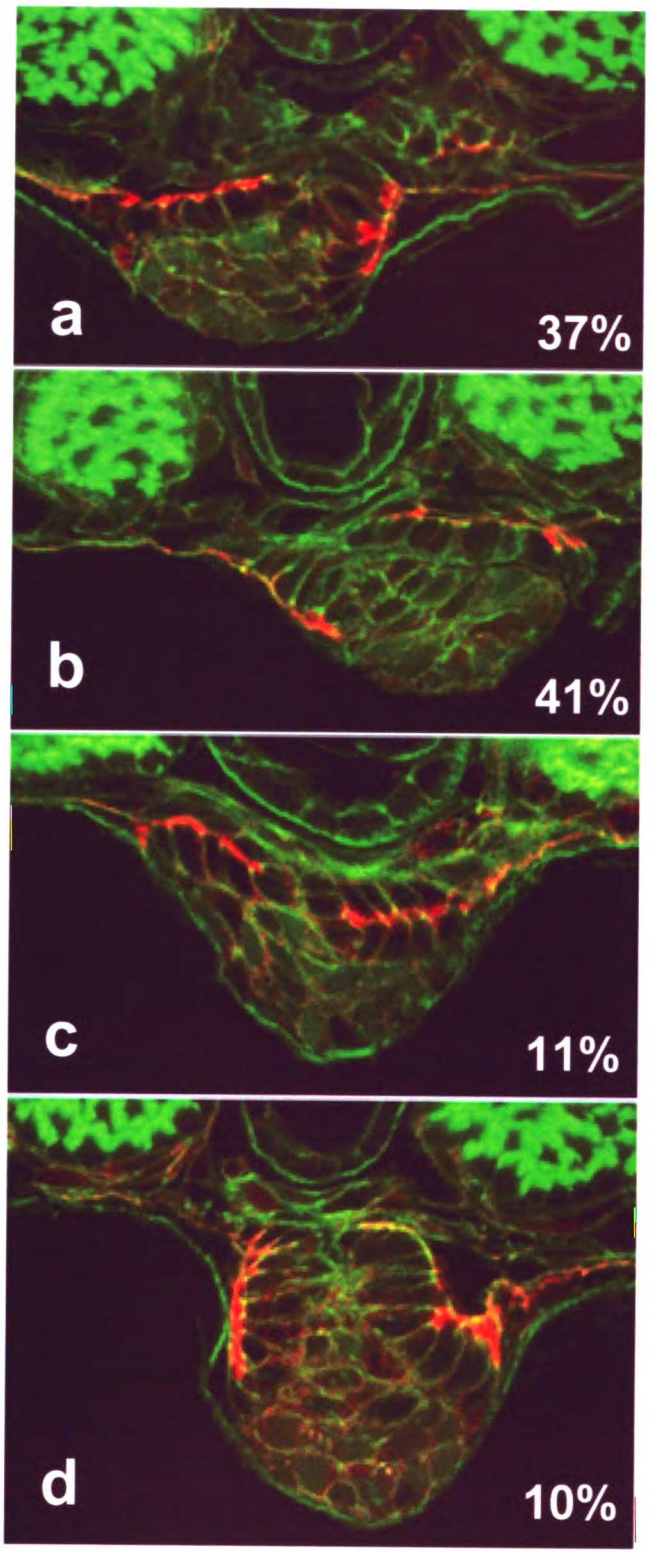

References

1. Burdine RD, Schier AF: Conserved and divergent mechanisms in left-right axis formation. *Genes Dev* 2000; 14:763-776.

2. Mercola M, Levin M: Left-right asymmetry determination in vertebrates. *Annu Rev Cell Dev Biol* 2001; 17:779-805.

3. Tabin CJ, Vogan KJ: A two-cilia model for vertebrate left-right axis specification. *Genes Dev* 2003; 17:1-6.

4. Ober EA, Field HA, Stainier DY: From endoderm formation to liver and pancreas development in zebrafish. *Mech Dev* 2003; 120:5-18.

5. Horne-Badovinac S, Lin D, Waldron S, Schwarz M, Mbamalu G, Pawson T, Jan Y, Stainier DY, Abdelilah-Seyfried S: Positional cloning of *heart and soul* reveals multiple roles for PKC lambda in zebrafish organogenesis. *Curr Biol* 2001; 11:1492-1502.

6. Peterson RT, Mably JD, Chen JN, Fishman MC: Convergence of distinct pathways to heart patterning revealed by the small molecule concentramide and the mutation *heart-and-soul*. *Curr Biol* 2001; 11:1481-1491.

7. Ohno S: Intercellular junctions and cellular polarity: the PAR-aPKC complex, a conserved core cassette playing fundamental roles in cell polarity. *Curr Opin Cell Biol* 2001; 13:641-648.

8. Wei X, Malicki J: *nagie oko*, encoding a MAGUK-family protein, is essential for cellular patterning of the retina. *Nat Genet* 2002; 31:150-157.

9. Long S, Ahmad N, Rebagliati M: The zebrafish nodal-related gene southpaw is required for visceral and diencephalic left-right asymmetry. *Development* 2003; 130:2303-2316.

10. Campione M, Steinbeisser H, Schweickert A, Deissler K, van Bebber F, Lowe LA, Nowotschin S, Viebahn C, Haffter P, Kuehn MR, Blum M: The homeobox gene Pitx2: mediator of asymmetric left-right signaling in vertebrate heart and gut looping. *Development* 1999; 126:1225-1234.

11. Alexander J, Rothenberg M, Henry GL, Stainier DY: casanova plays an early and essential role in endoderm formation in zebrafish. *Dev Biol* 1999; 215:343-357.

12. Kikuchi Y, Trinh LA, Reiter JF, Alexander J, Yelon D, Stainier DY: The zebrafish bonnie and clyde gene encodes a Mix family homeodomain protein that regulates the generation of endodermal precursors. *Genes Dev* 2000; 14:1279-1289.

13. Heasman J, Kofron M, Wylie C: Beta-catenin signaling activity dissected in the early Xenopus embryo: a novel antisense approach. *Dev Biol* 2000; 222:124-134.

14. Nasevicius A, Ekker SC: Effective targeted gene 'knockdown' in zebrafish. *Nat Genet* 2000; 26:216-220.

15. Field H, Ober EA, Roeser T, Stainier DY: Formation of the digestive system in zebrafish: I. Liver morphogenesis. *Dev Biol* 2003; 253:279-290.

16. Yelon D, Horne SA, Stainier DY: Restricted expression of cardiac myosin genes reveals regulated aspects of heart tube assembly in zebrafish. *Dev Biol* 1999; 214:23-37.

A two step model for leftward budding of the liver

Many vertebrate organs display morphological asymmetry with respect to the L-R axis. Among different organs and organ systems, this asymmetry can take many forms. For instance, discrete organs such as the liver and pancreas can adopt positions on one side of the midline. Organs that have a tube-like structure such as the heart and intestine undergo directional looping or coiling. Bilaterally paired structures such as the lungs or habenular nuclei of the brain can show morphological differences on the left vs. the right and in the case of some blood vessels, there can be selective degeneration on one side of the embryo [1].

The development of the L-R axis has been described as a three-step process: (1) initial break in symmetry; (2) establishment of asymmetric gene expression; and (3) transfer of positional information to developing organs [2]. The majority of what we understand about L-R asymmetry falls under the first two steps. The initial break in symmetry appears to involve the rotation of localized monocillia, which eventually leads to the asymmetric expression of Nodal pathway genes in the left lateral plate mesoderm (LPM) [1, 3]. Little is known, however, about the mechanisms that underlie the transfer of positional information from the LPM to the developing organs.

Given the variety of ways in which organs display L-R asymmetry, a variety of mechanisms may be used to impart L-R positional information to individual organs. In

chapter 5, we showed that gut looping in zebrafish results from a dynamic asymmetric migration of the LPM that displaces the gut endoderm to the left. In zebrafish, all of the digestive organs originate from a solid rod of endodermal cells that forms at the ventral midline during mid to late somitogenesis [4]. Prior to gut looping, the U-shaped epithelia of the LPM lie on either side of the endodermal rod (Figure 6.1a). During looping, however, both sides of the LPM migrate medially, but the left side moves dorsal to the endoderm, while the right side undergoes a ventro-lateral migration directly abutting the endoderm (Figure 6.1b). In the case of gut looping, L-R positional information within the LPM (i.e. asymmetric gene expression) is transferred to the gut endoderm indirectly through the asymmetric morphogenesis of the LPM itself.

It is likely, however, that a different mechanism is used to impart L-R positional information during liver morphogenesis. As the gut is looping, the anterior two thirds of the endoderm in the looping region appears thicker than more posterior regions of the developing intestine. This aggregation of cells marks the origin of the liver, which buds from the ventral side of the intestinal rod toward the left side of the embryo [5]. Although gut looping and liver budding occur with close temporal and spatial proximity, studies employing morpholino-knockdown of the *no tail* (*ntl*) gene have shown that these morphogenetic processes can be genetically uncoupled [5]. This result, in turn, suggests that the liver and gut may receive L-R positional information in different ways.

In this chapter we describe a two-step model for L-R morphogenesis of the liver in zebrafish. We show that the leftward budding of hepatocytes from the endodermal rod appears to be the first occurrence of L-R asymmetry in the gut and that this occurs prior to any morphological asymmetry in the neighboring LPM. We further show that the

asymmetric migration of the LPM then reinforces the leftward position of the liver by inducing a clockwise rotation in the endoderm and creating a physical barrier with the right LPM. This model appears to explain the complex laterality phenotypes observed in the digestive organs of several zebrafish mutants. Furthermore, this model points to at least two strategies for transferring positional information from the LPM to the endodermal organs. Genes expressed asymmetrically within the LPM first act non-cell autonomously to provide a signal for the initial budding of hepatocytes then act autonomously within the LPM to drive gut looping and reinforce the leftward position of the liver.

Results

Relationship between liver budding and gut looping

In zebrafish, the relative positions and timing of liver budding and gut looping are very similar, and yet genetic manipulations have suggested that these two events can be uncoupled [5]. To further investigate the relationship between these morphogenetic processes, we examined transverse sections through the liver region at 24 hpf. These sections revealed that the liver buds to the left prior to the appearance of morphological asymmetry in the LPM. Figure 6.1a shows that, while the intestinal primordium is still in the midline and the LPM is symmetrical, presumptive hepatocytes appear to grow out in close apposition to the basal side of the left LPM epithelium. This observation suggests that the leftward budding of the liver is the first break in morphological L-R symmetry in the digestive system and supports the prior assertion that liver position is independent of gut looping.

Although LPM migration does not appear to be required for the initial leftward budding of the liver, the relative positions of the LPM and endoderm later in development suggest that LPM migration may play a role in reinforcing the leftward position of the liver. By comparing transverse sections through the liver region at 24 and 30 hpf, we observed that the endoderm appears to undergo a clockwise rotation concurrent with the leftward displacement of gut looping. At 24 hpf a right angle (dotted line) can been superimposed over the future alimentary canal and liver (Figure 6.1a). The same right angle can be drawn over these structures at 30 hpf, but now the angle is rotated by approximately 45 degrees (Figure 6.1b). These data suggest that the asymmetric migration of the LPM may rotate the endoderm as it is being displaced to the

left. This rotation would, in turn, shift the hepatocytes from a position predominantly ventral to the developing intestine (Figure 6.1a) to a position predominantly to the left of this structure (Figure 6.1b).

The morphology of the right LPM in the liver region following its asymmetric migration suggests that the LPM may also play a second role in reinforcing the leftward position of the liver. The ventro-lateral migration path of the right LPM varies at different A-P levels (data not shown) within the looping region. Adjacent to the liver, the migration path of the right LPM is more ventral than lateral (Figure 6.1b) and the resulting morphology of the right LPM appears to create a physical barrier that could help to maintain the liver on the left as it grows (compare liver size in Figure 6.1 a and b).

The comparison of LPM and liver morphologies between 24 and 30 hpf suggests a two-step model for the leftward positioning of the liver (Figure 6.2). In the first step, asymmetric expression of the Nodal pathway genes within the left LPM first acts non-cell autonomously to provide a signal for the initial leftward budding of the hepatocytes. In the second step, these same signals act cell autonomously within the LPM to direct its asymmetric migration. The asymmetric LPM migration rotates the endoderm, such that the hepatocytes shift from the ventral to the left side of the developing intestine, and the ventral migration of the right LPM creates a physical barrier that helps restrict the liver to the left as it grows.

Initial hepatocyte budding is normal in *has* and *nok* mutants

To investigate the validity of the two-step model for L-R liver morphogenesis, we have characterized several mutants with defects in liver laterality. *heart and soul* (*has*) and *nagie oko* (*nok*) are two mutations that are known to disrupt epithelial polarity in

zebrafish [6, 7]. *has* and *nok* both have symmetrical livers and unlooped guts at 48 hpf ([6]; Figure 6.3b, c and Table 6.1). In these mutants L-R gene expression appears to be normal; the gut fails to loop because a defect in the epithelial structure of the LPM causes both sides to migrate dorsal to the endoderm (Chapter 5).

Since L-R gene expression appears to be unaffected in *has* and *nok*, our model predicts that initial leftward liver budding should be normal in these mutants. We expect that transverse sections through the liver of a *has* or *nok* mutants at 24 hpf would be indistinguishable from wild-type (Figure 6.1a), however, this experiment has not yet been done (see future directions). We have, however, used wholemount in situ hybridization with *foxA3* to examine endodermal morphology between 30 and 32 hpf. We were unable to score the liver using this method in 27% of the mutants examined (see future directions), but in ≥ 70% of the mutants with scorable livers, there was a distinct leftward bias to the liver (Figure 6.3e, f and Table 6.1). We have observed a similar leftward bias to the liver in transverse sections of *has* and *nok* mutants at 30 hpf (Figure 5.3d, e and data not shown). These data suggest that the initial leftward budding of the liver is normal in the majority of *has* and *nok* mutants.

To determine how the liver becomes bilateral in *has* and *nok* mutants by 48 hpf, we next examined the aspects of liver laterality that appear to depend on asymmetric LPM migration. As we have previously reported, transverse sections through the liver region in *has* and *nok* mutants at 30 hpf show a strong disruption in the epithelial structure of the LPM that results in both sides migrating dorsal to the endoderm. We have reexamined these sections to assess the affect of bilateral dorsal migrations on gut rotation and have found that endodermal rotation occurs in *has* and *nok* mutants but is

reduced compared to wild-type (data not shown). These data indicate that the dorsal migration of the left LPM, which is relatively unaffected in *has* and *nok* mutants, still induces some endodermal rotation. It is likely, therefore, that the bilateral livers observed in these mutants at 48 hpf result from the loss of the barrier function normally provided by the ventro-lateral migration of the right LPM.

Early liver budding is bilateral in *ntl* mutants

The observation that early leftward liver budding is typically normal in *has* and *nok* mutants strengthens our hypothesis that asymmetric gene expression within the LPM acts non-cell autonomously to provide the early directional cue for liver budding. To further investigate the relationship between L-R gene expression and liver morphogenesis, we examined this process in *no tail* (*ntl*) mutants. The *ntl* mutation, which disrupts the zebrafish homologue of *Brachyury* [8], causes defects in notochord differentiation that lead to bilateral LPM expression of Nodal pathway genes such as *spaw* [9] and *pitx2* [10, 11]. Similar to *has* and *nok* mutants, the liver is symmetrical in *ntl* mutants by 48 hpf, however, gut looping occurs, but is randomized ([5]; Figure 6.4b and Table 6.1).

If the initital direction of liver budding is directly controlled by signals from the adjacent LPM, early hepatocytes should bud bilaterally in *ntl* mutants. Ideally we would like to examine transverse sections through the liver of *ntl* mutants at 24 hpf, as we expect that this would clearly show bilateral outgrowth, however, this experiment has not yet been done (see future directions). We have, however, examined liver budding in *ntl* mutants using wholemount in situ hybridization with *foxA3* between 30 and 32 hpf. Among the 46 mutant embryos examined, 89% showed bilateral livers at this stage

(Figure 6.4e,f and Table 6.1), indicating that the initial direction of liver budding correlates with the bilateral pattern of L-R gene expression in *ntl* mutants.

To gain a better understanding of the effect of asymmetric LPM migration on gut and liver laterality in *ntl* mutants, we next examined transverse sections through the liver region at 30 hpf. Consistent with the previous observation that gut looping is randomized when Ntl function is reduced [5], this experiment revealed that the *ntl* mutation randomizes the pattern of LPM migration. Out of 17 mutant embryos, 6 showed the normal pattern of LPM migration (Fig. 6.4g), 6 showed a reversed pattern of migration (Fig. 6.4h), 3 showed bilateral dorsal migrations, and 2 showed bilateral ventro-lateral migrations (data not shown). Although asymmetric LPM migration does occur in *ntl* mutants, the early bilateral outgrowth of hepatocytes partially blocks the ventro-lateral migration of the LPM, overriding its proposed barrier function and often leading to a rounded morphology in this structure (Figure 6.4g, h). Furthermore, the partial block in LPM migration appears to reduce the amount of endodermal rotation in *ntl* mutants as compared to wild-type (Figure 6.4g, h).

Liver and gut laterality are coordinated in *sur* mutants

Our studies of the *has*, *nok* and *ntl* mutants have shown that the initial pattern of hepatocyte outgrowth appears to correlate with the pattern of L-R gene expression in the adjacent LPM. We next wanted to investigate L-R liver morphogenesis in the absence of L-R gene expression in the LPM. The *schmalspur* (*sur*) mutation disrupts the *fast1/foxH1* gene, which acts as a transcription factor in the Nodal signaling pathway [12, 13]. Similar to injection of the *spaw*-MO [9], the *sur* mutation abolishes all known L-R gene expression within the LPM [11]. We examined endodermal morphology in *sur*

mutants at 48 hpf (n=26) and found that gut looping is randomized (Figure 6.5 a-d). Intriguingly, the position of the liver correlated with the position of the gut in all cases (Figure 6.5 a-d). These data indicate that there is coordination between the L-R morphogenesis of the liver and gut in the absence of L-R gene expression in the LPM.

Our model predicts that there should be no directionality to the initial budding of the liver in the absence of L-R gene expression in the LPM. In fact, we think that it is likely that the hepatocytes simply bud ventrally from the endodermal rod, however, transverse sections at 24 hpf will be required to test this hypothesis (see future directions). Previous work with the *spaw*-MO indicates that asymmetric LPM migration occurs in the absence of L-R gene expression, but is randomized (Chapter 5). Therefore, later aspects of liver laterality that depend on asymmetric LPM migration likely do occur in *sur* mutants and could override the lack of direction found in the initial stage of liver morphogenesis. The complete dependence of both liver and gut laterality on asymmetric LPM migration would then explain the coordination between these organs observed in *sur* mutants.

Discussion

We have used wild-type and mutant analyses to investigate L-R liver morphogenesis in zebrafish. Our results indicate that the leftward positioning of the liver in zebrafish is a two-step process. The first step appears to be independent of asymmetric LPM migration, as initial leftward liver budding occurs when the LPM is still symmetric. In the second step, the asymmetric migration of the LPM reinforces leftward liver budding by rotating the gut endoderm and providing a physical barrier that may restrict the liver to the left as it grows. This two step model appears to explain the complex laterality phenotypes observed in the digestive organs of several zebrafish mutants (Figure 6.6). Furthermore, when combined with our previous work showing that asymmetric LPM migration induces the first leftward bend in the developing intestine, these studies show that a variety of mechanisms are used to transmit L-R positional information from the LPM to individual organs undergoing L-R morphogenesis.

L-R positional information can be transferred to endodermal organs through signaling from the LPM

We have shown that, in wild-type embryos, the initial leftward budding of the hepatocytes from the endodermal rod occurs prior to any morphological asymmetry in the LPM. This result indicates that asymmetric gene expression within the left LPM likely controls a signal from the LPM to the endoderm that regulates the initial direction of liver outgrowth. This hypothesis is supported by our observation that, in three different mutants that show bilateral livers at 48 hpf, the initial direction of liver outgrowth correlated with the pattern of L-R gene expression. In *has* and *nok* mutants, L-R gene expression appears unaffected and the liver initially shows normal leftward budding in

the majority of mutants examined. In *ntl* mutants, however, the L-R genes are expressed bilaterally and the early hepatocytes bud to both sides. Although we do not yet have direct evidence, we speculate that in the absence of L-R gene expression in the LPM, the early hepatocytes will show no direction and will simply bud ventrally from the endodermal rod.

The close apposition of the hepatocytes to the basal surface of the left LPM during early budding may tell us something about the nature of the signal from the LPM. It is possible that expression of Nodal pathway genes within the left LPM leads to the deposition of a guidance cue in the basal lamina of this columnar epithelium. As the earliest hepatocytes emerge from the ventral side of the endodermal rod, they would recognize this guidance cue and begin to migrate along the basal surface of the epithelium that presented it. Alternatively, there could be a diffusible signal from the left LPM, perhaps even Nodal itself, which regulates the direction of liver budding. The Stainier lab has recently completed a screen for mutations affecting liver morphogenesis and it will be of great interest to see if any of these mutants reveal the molecular nature of the signal from the LPM to the liver.

L-R positional information can be transferred to endodermal organs through LPM morphogenesis

The L-R genes also appear to act cell autonomously within the LPM to regulate the asymmetric migration and morphogenesis of this tissue. We have previously shown that the asymmetric migration of the LPM appears to provide the motive force to displace the developing intestine to the left during gut looping (Chapter 5). In this report, we describe a second role for asymmetric LPM migration - reinforcing the leftward position

of the liver. In both cases L-R positional information contained within the LPM in the form of asymmetrically expressed genes is transferred to the endoderm indirectly through morphogenesis of the LPM.

In addition to driving the L-R morphogenesis of the gut and liver, the asymmetric migration of the LPM may also contribute to the lateral morphogenesis of the pancreas. In zebrafish the pancreas arises from the fusion of two buds from the gut endoderm [14]. The posterior bud, which corresponds to the pancreatic islet, sits on the dorsal aspect of the endodermal rod prior to gut looping, but is found on the right immediately following looping morphogenesis [14]. We have shown that asymmetric migration of the LPM induces a clockwise rotation in the endoderm that shifts the position of the early liver from a position predominantly ventral to the developing intestine to a position predominantly to the left of the developing intestine. It is likely that this endodermal rotation likewise shifts the position of the posterior pancreatic bud from the dorsal side of the gut endoderm to the right. This model is consistent with what is seen in mammals where early leftward bending and rotation of the duodenum brings the two pancreatic buds together and places the pancreas on the right [15].

The liver and LPM respond differently to L-R positional information

In this report we have used wild-type and mutant analyses to described two strategies for transmitting L-R positional information from the LPM to the endoderm. Importantly, these data have also revealed that the LPM and liver respond to L-R positional information in different ways. The liver appears to respond to the presence of Nodal activity within the LPM. If the Nodal pathway is active on the left, the liver buds to the left; if it is active on both sides, the liver buds bilaterally; and if Nodal activity is

missing from the LPM, we speculate that the liver buds ventrally. These data suggest that Nodal activity within the LPM provides an instructive cue for the directional budding of the hepatocytes.

The LPM, however, appears to respond to a difference in Nodal signaling between the left and right sides. When Nodal expression is restricted to the left, asymmetric LPM migration is biased such that the left LPM migrates dorsal to the endoderm, while the right LPM migrates ventro-laterally. However, if Nodal activity is the same on both sides (either bilateral or absent), the pattern of LPM migration is randomized. It will be of great interest in the future to investigate the cellular mechanisms that underlie these distinct modes employed by different tissues to interpret L-R positional information.

Asymmetric gene expression and heart morphogenesis

The hypothesis that asymmetric gene expression within the LPM acts cell autonomously within this tissue to regulate its morphogenesis is likely to also be important when thinking about L-R morphogenesis of the heart. The heart is the first organ to display morphological asymmetry in vertebrates. In all vertebrates, the primitive heart tube loops to the right, but in zebrafish there is also an earlier asymmetry, termed cardiac tilting [16] or jogging [17], in which heart tube elongation occurs with a distinct leftward bias. The heart is a derivative of the anterior LPM and, just prior to cardiac jogging, the myocardial precursors reside within U-shaped epithelial structures that are remarkably similar to those observed in the LPM of the gut looping region (S. H-B and Le Trinh unpublished observations). Like the LPM adjacent to the gut, the U-shaped epithelia that contribute to the heart undergo a medial migration and show asymmetric

expression of Nodal pathway genes. It will be of great interest, therefore, to further investigate the level of similarity between the asymmetric LPM morphogenesis that drives gut looping and the LPM morphogenesis that underlies cardiac tilting/jogging.

Future Directions

This work on L-R liver morphogenesis in zebrafish is preliminary and will require a number of experiments before it can be submitted for publication. A new graduate student in the lab, Chantilly Munson, plans to complete the experiments detailed below so that a paper can be submitted sometime within the next year.

The first and most important thing that will need to be done is to examine transverse sections of *has*, *nok*, *ntl*, and *spaw*-MO injected embryos (*sur*), at 24 hpf to determine the direction of initial liver budding in these mutants. Ideally, we would like to have a liver-specific marker to label the hepatocytes at this stage, but we currently do not have one available. It is fairly easy to identify hepatocytes by position and morphology, however. I have gleaned some preliminary information from some of these mutants by examining wholemount embryos stained with *foxA3* at 30-32 hpf, but these experiments have many caveats. Much of the liver is ventral to the developing intestine, even after looping/rotation, therefore it is often difficult to score the direction of liver budding when the entire gut endoderm is stained. Put simply, I do not believe that one can rigorously score liver position under these conditions and may remove these data prior to publication. These experiments were also performed at a relatively late stage when asymmetric LPM migration was complete, which complicates our analysis given that asymmetric LPM migration also plays a role in positioning the liver on the left.

Transverse sections through the liver region of *has* and *nok* mutants at 24 hpf may also provide evidence to support our hypothesis that a guidance cue for liver budding is deposited in the basal lamina of the left LPM. During my examination of embryos stained with *foxa3* at 30-32 hpf, I found that I was not able to see any directional liver

outgrowth in 27% of the *has* and *nok* mutants examined. This phenomenon could be due to a delay in liver morphogenesis in these mutants. Alternatively, it could indicate that the liver had budded ventrally and was being obscured from view by the overlying intestine. The epithelial polarity defect in the LPM of *has* and *nok* mutants is highly variable and can range from a relatively normal looking epithelium, to an disorganized array of rounded-up cells. When examining transverse sections at 24 hpf, it will be most interesting to determine whether initial leftward budding of the liver in these mutants occurs only when the left LPM epithelium is relatively intact. If there is a guidance cue on the basal surface of the left LPM, it is likely that proper apico-basal polarity is required for the directed secretion of this signal. In cases where the polarity of the left LPM is severely disrupted, there may be no localized guidance cue and the liver could bud ventrally.

Within this chapter, I have used the *sur* mutation to examine liver morphogenesis in the absence of L-R gene expression in the LPM. Unfortunately, it is nearly impossible to identify *sur* mutants before 48 hpf, making the experiments involving transverse sections at 24 hpf quite difficult. For the paper, it would be best to use the *spaw*-MO to eliminate L-R gene expression in the LPM. In general, I have always believed that it is better to use mutants over morpholinos because it is very difficult to determine the developmental age of an injected embryo. However, the difficulty in scoring *sur* mutants makes this case exceptional.

Finally, there are a few cases in the current data set where we might want to increase the numbers of embryos scored. In particular, we may wish to examine more transverse sections at 30 hpf of *has*, *nok* and *ntl* mutants.

Materials and Methods

Zebrafish strains

Confocal studies were performed on wild-type, *has*^{m567}, *nok*^{m520}, and *ntl*^{m550} embryos carrying the gut GFP transgene. Studies with the *sur* mutant used the m768 allele.

Antibody and phalloidin staining

Embryos were fixed for 1 hour at RT in 4% Paraformaldehyde in phosphate buffered saline (PBS) and embedded in 4% SeaPlaque agarose (BioWhittaker Molecular Applications). 200 or 300 μm sections were cut with a Leica VT1000S vibratome. Staining and washes were performed on floating sections in a solution of 0.1% tween, 1% DMSO and 5% goat serum in PBS. We used the following antibodies: anti-PKCζ (C-20) (Santa Cruz Biotechnology), which recognizes zebrafish aPKC λ and ζ, at 1:1000 and a goat anti-rabbit secondary antibody conjugated to rhodamine red-X (Molecular Probes) at 1:200. To visualize actin, embryos were incubated in Alexa-488 phalloidin (Molecular Probes) at 1:50. Fluorescence images were produced using a Leica TCS NT confocal microscope.

In situ hybridization

In situ hybridizations were performed as previously described. Embryos older than 24 hpf were raised in 0.003% 1-phenyl-2-thiourea (PTU, Sigma) in egg water to inhibit pigment production.

Figure 6.1 The relationship between liver budding and gut looping

(a-b) Transverse sections through the liver region. The LPM shows apical localization of aPKCs (red). Most cells are outlined with cortical actin (green) and endodermal cells have weak cytoplasmic GFP. Dorsal to the top. **(a)** At 24 hpf hepatocytes can be seen budding from the ventral side of the future alimentary canal along the basal side of the left LPM epithelium. **(b)** By 30 hpf the endoderm has rotated, such that the hepatocytes are now predominantly to the left of the future alimentary canal. Compare dotted lines in (a) and (b). **(a'-b')** Diagrams of the sections in (a) and (b). **(c)** Key for the diagrams in (a') and (b').

Figure 6.1

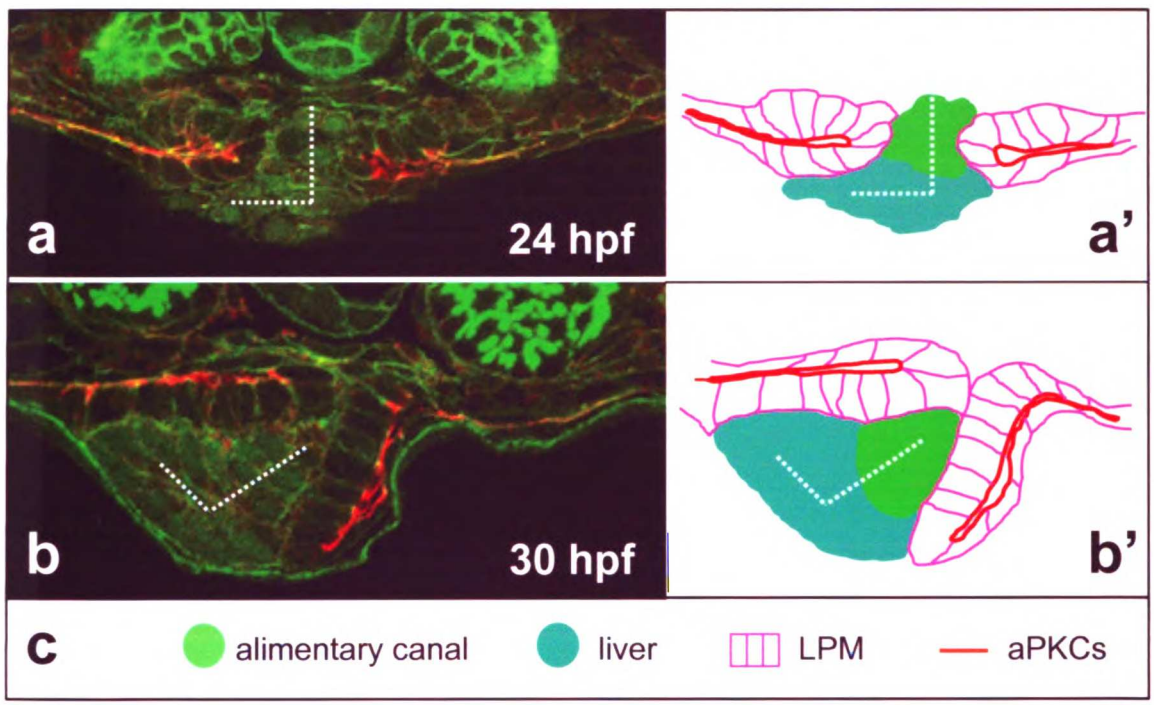

Figure 6.2

A two step model for leftward liver budding
asymmetric gene expression
early leftward liver budding
reinforcement of liver laterality by LPM migration
LPM
gut endoderm
spaw + pitx2 expression
direction of liver outgrowth

Figure 6.3 Liver position in *has* and *nok* mutants

Wholemount in situ hybridization with *foxA3*. **(a-c)** Endodermal morphology at 48 hpf. In wild-type embryos the liver is on the left and the intestine loops to the left (a). In *has* (b) and *nok* (c) mutants the liver is symmetrical and the intestine is in the midline. **(d-f)** Endodermal morphology at 30-32 hpf. Black arrowheads mark position of the liver. In wild-type embryos the liver and developing intestine are both on the left (d). In ≥ 70% of *has* (e) and *nok* (f) mutants, the liver has budded to the left even though the gut has not looped (e). All images are dorsal views, anterior to the top.

Figure 6.3

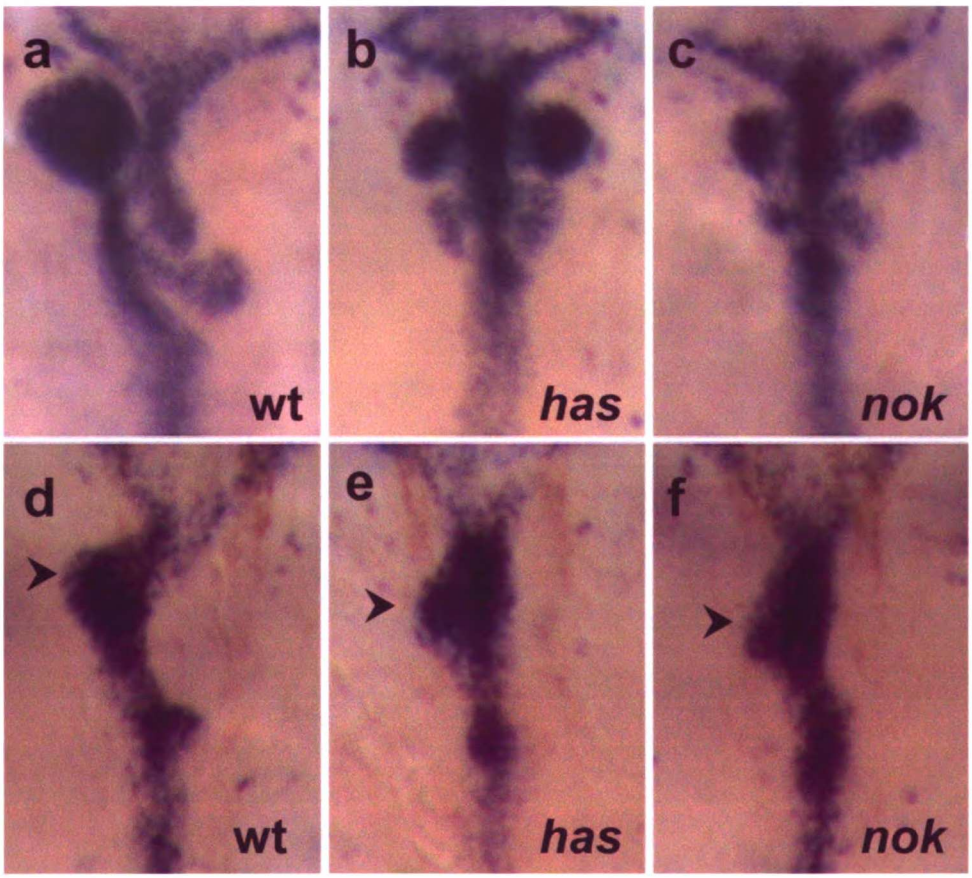

Figure 6.4 Liver position in *ntl* mutants

(a-f) Wholemount in situ hybridization with *foxA3*. Dorsal views, anterior to the top. **(a-c)** Endodermal morphology at 48 hpf. In wild-type embryos the liver is on the left and the intestine loops to the left (a). In *ntl* mutants the liver is symmetrical and gut looping is randomized (b-c). **(d-f)** Endodermal morphology at 30-32 hpf. Black arrowheads mark position of the liver. In wild-type embryos the liver and developing intestine are both on the left (d). In 89% of *ntl* mutants, initial liver budding was bilateral (e-f). In (e) the gut is looped to the left and in (f) the gut is looped to the right. **(g-h)** Transverse sections through the liver region of *ntl* mutants at 30 hpf. The LPM shows apical localization of aPKCs (red). Most cells are outlined with cortical actin (green) and endodermal cells have weak cytoplasmic GFP. Dorsal to the top. In *ntl* mutants, the early bilateral outgrowth of the liver partially impedes the ventro-lateral LPM migration, blocking its proposed barrier function and resulting in reduced endoderm rotation. (g) *ntl* mutant with normal LPM migration pattern – left dorsal, right ventro-lateral. (h) *ntl* mutant with reversed LPM migration pattern – right dorsal, left ventro-lateral. **(g'-h')** Diagrams of the sections in (g) and (h).

Figure 6.4

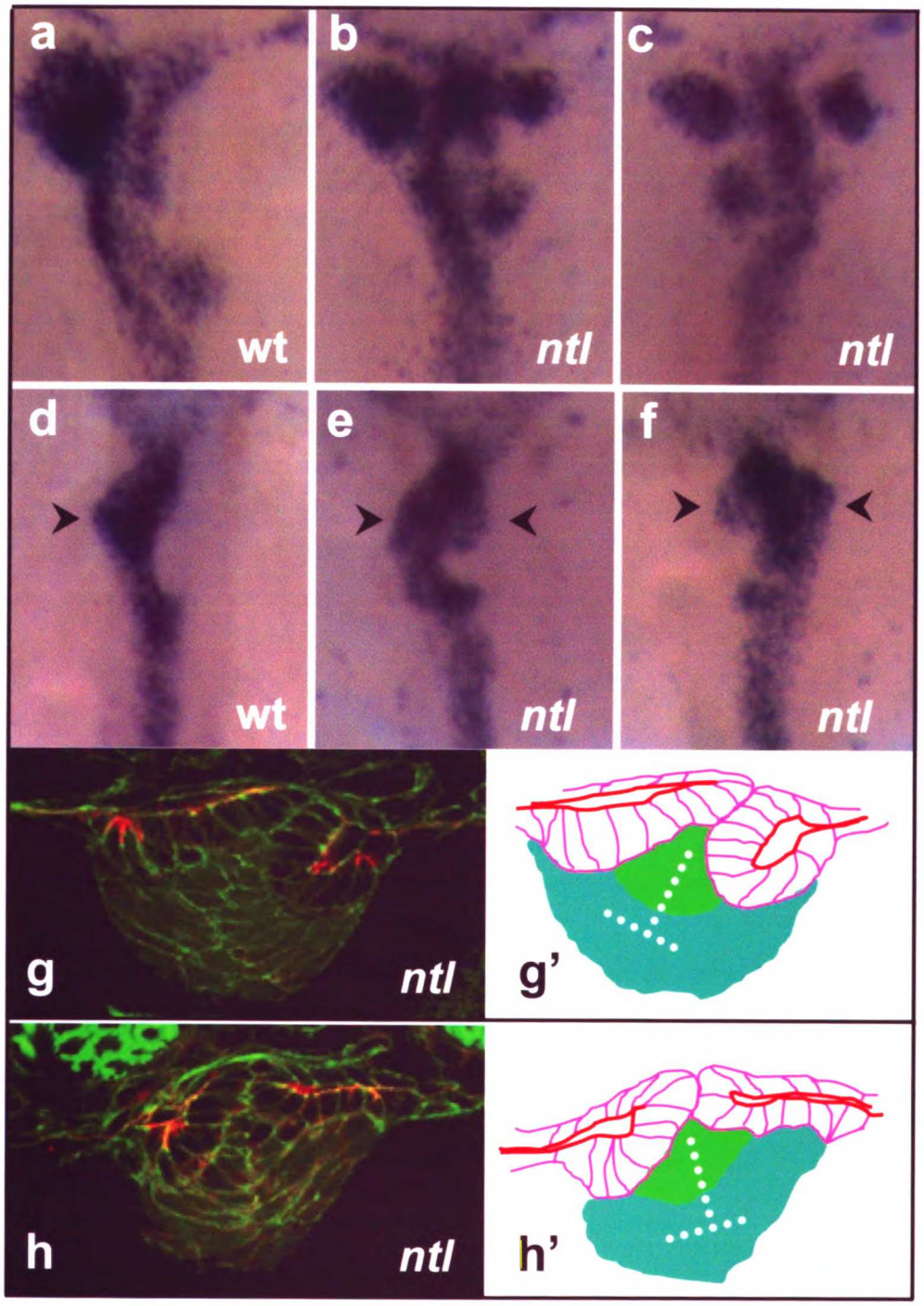

Table 6.1 Liver position in *has*, *nok* and *ntl* mutants.

			Total	Left (%)	Bilateral (%)	Right (%)
has	30-32 hpf	mut	46	72	28	0
		wt	61	95	2	3
	48 hpf	mut	54	2	96	2
		wt	48	96	2	2
nok	30-32 hpf	mut	48	70	28	0
		wt	74	91	0	9
	48 hpf	mut	59	13	83	4
		wt	65	85	5	10
ntl	30-32 hpf	mut	46	0	89	11
		wt	56	82	0	18
	48 hpf	mut	52	0	98	2
		wt	48	98	2	0

Note: could not score a liver in 27% of 30-32 hpf *has* and *nok* mutants examined.

Figure 6.5 Liver position in *sur* mutants

(a-d) Wholemount in situ hybridization with *foxA3* reveals endodermal morphology at 48hpf. Dorsal views, anterior to the top. **(a)** In wild-type embryos the liver is on the left and the intestine loops to the left. **(b-d)** In *sur* mutants, the gut can loop to the left **(b)**, loop to the right **(d)**, or remain in the midline **(c)**.

Figure 6.5

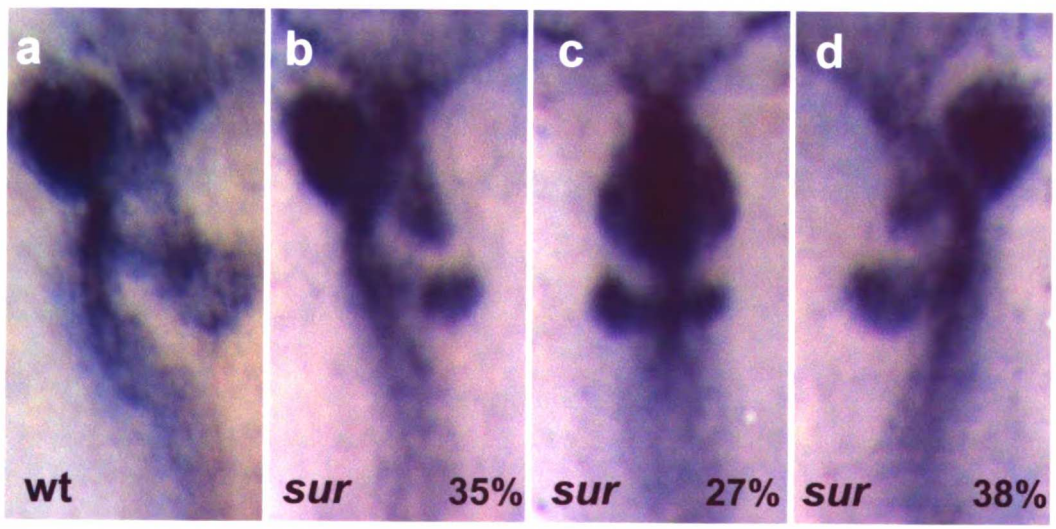

Figure 6.6 Summary of mutant phenotypes

(a) In wild-type embryos, genes such as *spaw* and *pitx2* are asymmetrically expressed in the left LPM. The liver buds to the left prior to any morphological asymmetry in the LPM and then asymmetric LPM morphogenesis reinforces the leftward position of the liver. **(b)** In *has* and *nok* mutants asymmetric gene expression and initial liver budding both appear to be normal. However, a defect in the epithelial structure of the LPM perturbs its asymmetric morphogenesis and abolishes the presumed barrier function of the right LPM, allowing the liver to spread to both sides as it grows. **(c)** In *ntl* mutants, *spaw* and *pitx2* are expressed bilaterally and the liver initially buds to both sides. Although asymmetric LPM morphogenesis does occur the early budding of hepatocytes to both sides appears to override the presumed barrier function of the right LPM, leading to a symmetrical liver at 48 hpf. **(d)** In *sur* mutants and *spaw*-MO injected embryos, expression of *spaw* and *pitx2* is missing from the LPM. We presume that the hepatocytes bud ventrally under these circumstances, but this is not yet known. Later aspects of liver laterality that depend on asymmetric LPM morphogenesis then override the initial lack of liver direction, leading to the coordination of liver and intestinal position at 48 hpf.

Figure 6.6

Summary of Mutant Phenotypes
asymmetric
early liver
reinforcement of ver-
a
b
c
d
?
* Pattern of LPM migration is randomized

References

1. Hamada, H., Meno, C., Watanabe, D., and Saijoh, Y. (2002). Establishment of vertebrate left-right asymmetry. Nat Rev Genet *3*, 103-113.
2. Burdine, R.D., and Schier, A.F. (2000). Conserved and divergent mechanisms in left-right axis formation. Genes Dev *14*, 763-776.
3. Tabin, C.J., and Vogan, K.J. (2003). A two-cilia model for vertebrate left-right axis specification. Genes Dev *17*, 1-6.
4. Ober, E.A., Field, H.A., and Stainier, D.Y. (2003). From endoderm formation to liver and pancreas development in zebrafish. Mech Dev *120*, 5-18.
5. Field, H., Ober, E.A., Roeser, T., and Stainier, D.Y. (2003). Formation of the digestive system in zebrafish: I. Liver morphogenesis. Dev Biol *253*, 279-290.
6. Horne-Badovinac, S., Lin, D., Waldron, S., Schwarz, M., Mbamalu, G., Pawson, T., Jan, Y., Stainier, D.Y., and Abdelilah-Seyfried, S. (2001). Positional cloning of *heart and soul* reveals multiple roles for PKC lambda in zebrafish organogenesis. Curr Biol *11*, 1492-1502.
7. Wei, X., and Malicki, J. (2002). *nagie oko*, encoding a MAGUK-family protein, is essential for cellular patterning of the retina. Nat Genet *31*, 150-157.
8. Schulte-Merker, S., van Eeden, F.J., Halpern, M.E., Kimmel, C.B., and Nusslein-Volhard, C. (1994). no tail (ntl) is the zebrafish homologue of the mouse T (Brachyury) gene. Development *120*, 1009-1015.
9. Long, S., Ahmad, N., and Rebagliati, M. (2003). The zebrafish nodal-related gene *southpaw* is required for visceral and diencephalic left-right asymmetry. Development *130*, 2303-2316.

10. Chin, A.J., Tsang, M., and Weinberg, E.S. (2000). Heart and gut chiralities are controlled independently from initial heart position in the developing zebrafish. Dev Biol *227*, 403-421.

11. Bisgrove, B.W., Essner, J.J., and Yost, H.J. (2000). Multiple pathways in the midline regulate concordant brain, heart and gut left-right asymmetry. Development *127*, 3567-3579.

12. Pogoda, H.M., Solnica-Krezel, L., Driever, W., and Meyer, D. (2000). The zebrafish forkhead transcription factor FoxH1/Fast1 is a modulator of nodal signaling required for organizer formation. Curr Biol *10*, 1041-1049.

13. Sirotkin, H.I., Gates, M.A., Kelly, P.D., Schier, A.F., and Talbot, W.S. (2000). Fast1 is required for the development of dorsal axial structures in zebrafish. Curr Biol *10*, 1051-1054.

14. Field, H.A., Si Dong, P.D., Beis, D., and Stainier, D.Y. (2003). Formation of the digestive system in zebrafish: II. Pancreas morphogenesis. Dev Biol *261*, 197-208.

15. Moore, K.L., and Persaud, T.V.N. (1998). The Developing Human. W. B. Saunders Company, Philadelphia, London, New York, St. Louis, Sydney, Toronto.

16. Yelon, D. (2001). Cardiac patterning and morphogenesis in zebrafish. Dev Dyn *222*, 552-563.

17. Chen, J.N., van Eeden, F.J., Warren, K.S., Chin, A., Nusslein-Volhard, C., Haffter, P., and Fishman, M.C. (1997). Left-right pattern of cardiac BMP4 may drive asymmetry of the heart in zebrafish. Development *124*, 4373-4382.

L-R morphogenetic defects in the digestive organs of *hands off* mutants

Tissue recombination experiments in chick and mouse have suggested that the cardiac mesoderm plays an inductive role in liver formation [1]. Elke Ober decided to test this hypothesis in zebrafish by examining liver formation in *hands off* (*han*) mutants. *han* encodes the bHLH transcription factor *hand2*, and the mutation leads to defects in the differentiation, patterning and morphogenesis of the anterior lateral plate mesoderm (LPM), including the cardiac precursors [2]. When Elke examined liver formation in *han* mutants, she found no defect in liver induction, but rather observed defects in the L-R morphogenesis of the digestive organs. It is likely that this laterality phenotype is due to defects within the LPM of the gut looping region, as *hand2* is expressed throughout the LPM during somitogenesis stages and is never expressed in the endoderm ([2] and unpublished observations).

In this appendix, I provide a more detailed description of the laterality defects in *han* mutants, which include: unlooped guts, randomized liver position and the reduction or absence of L-R gene expression in the LPM. This particular combination of organ laterality and gene expression defects is unique among the L-R asymmetry mutants we have investigated to date. We further show that the pattern of LPM migration appears to vary at different anterior-posterior (A-P) levels within the gut looping region in *han* mutants. LPM migration is randomized adjacent to the liver, however, posterior to the liver region, both sides of the LPM migrate dorsal to the endoderm. These preliminary

data suggest that the *han* mutation may perturb asymmetric organ formation in two ways: by disrupting L-R gene expression in the LPM and by affecting LPM morphogenesis downstream of L-R gene expression.

Results

han mutants have defects in L-R organ morphogenesis

To further characterize the defect in L-R organ morphogenesis that Elke observed in *han* mutants, we have used wholemount in situ hybridization to examine endodermal morphology in *han* mutants at 48 hpf. In *han* mutants, the intestine is always in the midline, but liver position appears to be randomized. Out of 24 mutants examined, 10 (42%) showed symmetrical livers (Figure A1.1a), 6 (25%) had the liver on the left (Figure A1.1b), 5 (21%) had the liver on the right (Figure A1.1c), and 3 (12%) showed a "restricted liver" phenotype (Figure A1.1d), where the liver remains close to the gut tube. As is typical when the gut fails to loop, the pancreatic islet in *han* mutants remains dorsal to the intestine and the anterior bud is duplicated.

han mutants have defects in L-R gene expression

The observation that *han* mutants have midline gut tubes and randomized liver position makes *han* unique among previously described laterality mutants in zebrafish. Therefore, we next wanted to investigate whether *han* also causes defects in asymmetric gene expression in the LPM. We examined two genes that are asymmetrically expressed within the left LPM of the gut looping region, the *Nodal* gene *southpaw (spaw)* [3] and the transcription factor gene *pitx2* [4]. We found that the expression of both genes was missing from the LPM in approximately 25% of embryos derived from parents heterozygous for *han* (Table A1.1). These data suggested that *han* mutants may lack L-R gene expression in the LPM.

To further investigate whether *han* mutants lack asymmetric gene expression in the LPM, we performed additional experiments on some of the *pitx2*-stained embryos

described above. We PCR genotyped one of the *han* clutches. This experiment did not work well, but of the 19 embryos that appeared to be *han* mutants by PCR genotyping, 12 lacked *pitx2* expression (data not shown). Another clutch was stained both with *pitx2* and *cmlc2*. The presence of *cmlc2* revealed the cardiac defect in *han* mutants and allowed the mutant embryos to be unambiguously sorted from their wild-type siblings. Of the 37 *han* mutants examined, 73% had a complete absence of *pitx2* expression in the LPM and 24% showed reduced left-sided expression of *pitx2* (data not shown). Together these data indicate that there is some variability in the L-R gene expression defect in *han* mutants; it appears that L-R gene expression can be either absent or reduced.

han mutants show A-P differences in the pattern of LPM migration

Given that the asymmetric migration of the LPM is required both for gut looping and the left-sided position of the liver, we next wanted to investigate the pattern of LPM migration in *han* mutants. We examined a single transverse section through the gut looping region in 18 *han* mutants at 30 hpf. In 11 of these mutants, the transverse sections occurred at the level of the liver and the pattern of LPM migration appeared to be randomized; 4 of the sections showed asymmetric LPM migrations (Figure A1.1e), 1 showed bilateral ventro-lateral migrations (data not shown), and 4 showed bilateral dorsal migrations (Figure A1.1f). The remaining 7 sections cut through more posterior levels of the looping region, where the endoderm predominantly contributes to the intestinal bulb. In all of these sections the LPM showed bilateral dorsal migrations (Figure A1.1g). These data suggest that the pattern of LPM migration varies at different anterior-posterior (A-P) levels within the gut looping region.

Discussion

A-P regionalization within the LPM of the gut looping region

Our preliminary studies of *han* mutants indicate that the *han* mutation causes variations in the pattern of LPM migration at different A-P levels within the gut looping region[1]. The ability of this mutation to affect discrete regions of the asymmetrically migrating LPM in different ways may reflect inherent A-P regionalization in wild-type embryos. In general there is a high degree of A-P regionalization within the LPM that is evidenced by differences in gene expression and/or cell morphology. We have previously shown that the LPM in the gut looping region is distinguishable from the surrounding LPM by its ability to form columnar cells that undergo asymmetric medial migration. These new data suggest that there may be further subdivisions within this already distinct population of LPM cells.

The hypothesis that there may be subpopulations of LPM cells within the looping region is consistent with unpublished observations we have made of LPM morphology in transverse sections of wild-type embryos at 30 hpf. Conceptually, the endoderm in the looping region can be broken down into two regions: an anterior region that gives rise to liver and intestinal bulb and a more posterior region that contributes almost exclusively to the intestinal bulb. It is predominantly the behavior of the right LPM that varies between these two regions. Adjacent to the liver, the medial migration of the right LPM is more ventral than lateral and the dorsal side of the right LPM is predominantly contacts the endoderm over the length of its migratory path (Figures 5.1g and 6.1a). In contrast, the medial migration of the right LPM in more posterior regions is more lateral than ventral

and the dorsal side of the LPM predominantly contacts the left LPM over the length of its migratory path (Figure 5.1h).

These differences in morphology of the right LPM between the liver region and the intestinal region may, in turn, correspond to the two roles that we have described for asymmetric LPM migration during L-R morphogenesis of the endodermal organs. Within the liver region, there is very little lateral displacement of the endoderm that will give rise to the alimentary canal (Figures 5.1g and 6.1a), indicating that the deep ventral migration of the right LPM in this region may predominantly function to reinforce leftward liver budding. It is in the more posterior region that we observe the most significant displacement of the future alimentary canal from the midline (Figure 5.1h). Therefore, we hypothesize that it is the lateral migration of the right LPM in this more posterior region that is predominantly responsible for gut looping.

In fact, the phenotypes observed in the digestive organs of *han* mutants support this model for different A-P functions of the LPM in the looping region. The gut fails to loop in 100% of *han* mutants examined. Importantly, all *han* mutants also show bilateral dorsal LPM migrations in the posterior portion of the looping region. Bilateral dorsal migrations have also been associated with midline gut tubes in *has* and *nok* mutants. Asymmetric LPM migration does occur in the liver region of some mutants, yet this is clearly not sufficient to displace the gut endoderm to the left. It is likely that the mutants that show asymmetric migration in the liver region correspond to the mutants that have livers on the left or right side at 48 hpf.

han disrupts asymmetric gene expression in the LPM

We have shown that the majority of *han* mutants fail to express *spaw* (as well as its downstream effector *pitx2*) in the LPM adjacent to the gut looping region. Zebrafish mutants that show defects in L-R gene expression tend to fall into one or more of three categories: mutations that disrupt Kuppfer's vesicle (presumed location of the monocilia involved in the establishment of L-R asymmetry in zebrafish), mutations that disrupt the midline, and mutations that disrupt components of the *nodal* signaling pathway [3, 5, 6]. Given that *han* expression has only been reported in derivatives of the LPM and neural crest [2], we find it highly unlikely that *han* falls into either of the first two categories. However, it is reasonable to speculate that *han* function may be required to facilitate *nodal* signaling within the LPM.

How might a transcription factor that is expressed bilaterally within the LPM regulate asymmetric gene expression? Two components of the *nodal* signaling pathway, *one eyed pinhead* (*oep*) [7] and *schmalspur* (*sur*)/*foxh1* [8], show bilateral expression in the LPM prior to the onset of left-sided *spaw* expression [3]. Mutation of either *oep* or *sur* abolishes L-R gene expression in the LPM, likely due to the requirement for a positive feedback loop to establish a stable domain of *nodal* expression. It will be most interesting, therefore, to determine whether *han* is required for the bilateral expression of *oep* and/or *sur*.

han disrupts LPM morphogenesis downstream of L-R gene expression

Previous experiments, with embryos that had reduced function of *spaw* or *sur*, have shown that the pattern of LPM migration is randomized in the absence of *nodal* signaling in the LPM (Chapters 5 and 6). Therefore, the absence of asymmetric gene

expression in the LPM is sufficient to explain the randomization of LPM migration in the liver region of *han* mutants. However, the loss of asymmetric gene expression does not seem to explain the bilateral dorsal migrations seen more posteriorly. Our results show that some *han* mutants retain *pitx2* expression within the LPM, and yet 100% of *han* mutants show defects in gut looping. These data suggest that the *han* mutation may also disrupts another aspect of LPM morphogenesis downstream of L-R gene expression.

Future Directions

As has been previously stated in the text, this work on the laterality defects in *han* mutants is preliminary. The conclusions I have drawn from these data are based on very low numbers and, therefore, all of the experiments detailed in this appendix will need to be repeated. In particular, more genotyping will need to be done on clutches stained with *spaw* and *pitx2* to better determine the extent of the defect in L-R gene expression in *han* mutants. Furthermore, during the experiment where I examined transverse sections of *han* mutants at 30 hpf, I failed to keep track of the left and right sides of the embryos. Based on the randomization of liver position at 48 hpf, I assume that the asymmetric LPM migration observed in the liver region is also randomized, but this will have to be confirmed in future experiments.

As was mentioned in the discussion, it would be interesting to investigate the basis for the L-R gene expression defect in *han* mutants. One obvious experiment is to use wholemount in situ hybridization to examine the expression of *oep* and *sur* in *han* mutants. It will also be interesting to investigate the defects in LPM morphogenesis that appear to occur downstream of L-R gene expression.

Materials and Methods

Zebrafish strains

Confocal studies were performed on *han*^{s6} embryos carrying the gut GFP transgene.

Antibody and phalloidin staining

Embryos were fixed for 1 hour at RT in 4% Paraformaldehyde in phosphate buffered saline (PBS) and embedded in 4% SeaPlaque agarose (BioWhittaker Molecular Applications). 200 or 300 μm sections were cut with a Leica VT1000S vibratome. Staining and washes were performed on floating sections in a solution of 0.1% tween, 1% DMSO and 5% goat serum in PBS. We used the following antibodies: anti-PKCζ (C-20) (Santa Cruz Biotechnology), which recognizes zebrafish aPKC λ and ζ, at 1:1000 and a goat anti-rabbit secondary antibody conjugated to rhodamine red-X (Molecular Probes) at 1:200. To visualize actin, embryos were incubated in Alexa-488 phalloidin (Molecular Probes) at 1:50. Fluorescence images were produced using a Leica TCS NT confocal microscope.

In situ hybridization

In situ hybridizations were performed as previously described. Embryos older than 24 hpf were raised in 0.003% 1-phenyl-2-thiourea (PTU, Sigma) in egg water to inhibit pigment production. L-R gene expression was examined between 20 and 24 somites.

Genotyping *han* mutants

PCR genotyping of *han* mutant embryos was performed as described [2], using the following primers: 5'-AATTTCCCACTACGGACATTGGA-3' and 5'-AGAGACAGAAATAGATAATGAACGT-3'.

Figure A1.1 L-R morphogenetic defects in the digestive organs of *han* mutants

(a-d) Wholemount in situ hybridization with *foxA3* reveals endodermal morphology in *han* mutants at 48 hpf. Dorsal views, anterior to the top. In *han* mutants the intestine is always in the midline, but liver position appears to be randomized. Out of 24 mutants examined 10 (42%) had symmetrical livers **(a)**, 6 (25%) had livers on the left **(b)**, 5 (21%) had livers on the right **(c)**, and 3 (12%) had restricted livers **(d)**. **(e-g)** Transverse sections through the gut looping region of *han* mutants at 30 hpf. The LPM shows apical localization of aPKCs (red). Most cells are outlined with cortical actin (green) and endodermal cells have weak cytoplasmic GFP. Dorsal to the top. In *han* mutants, the apico-basal polarity of the cells is relatively normal, but the pattern of LPM migration appears to vary at different A-P levels within the gut looping region. In the liver region, LPM migration appears to be randomized. **(e)** Shows an example of asymmetric LPM migration in the liver region and **(f)** shows an example of bilateral dorsal migrations. In more posterior regions, both sides of the LPM migrate dorsal to the developing intestine **(g)**.

Figure A1.1

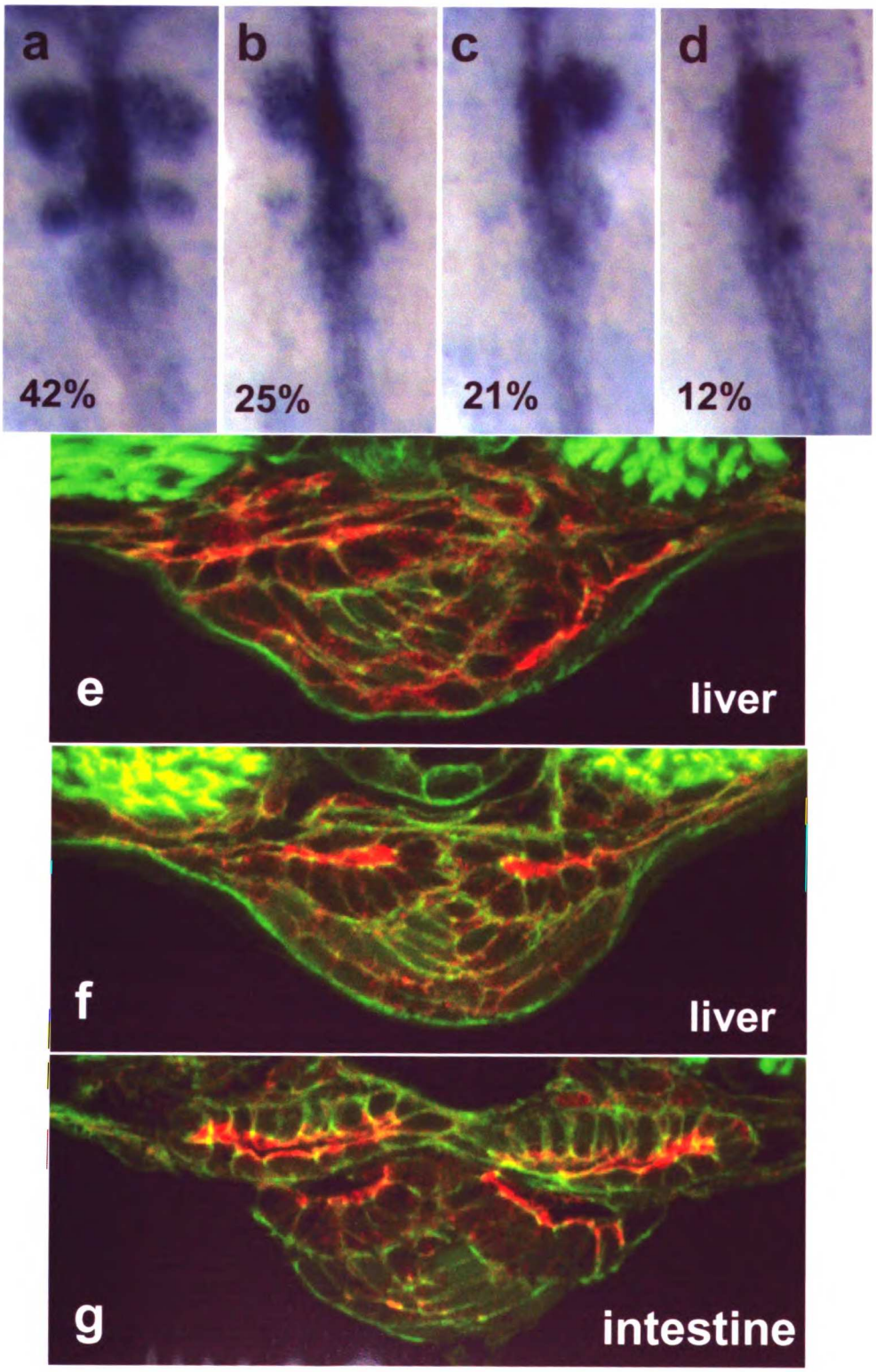

Table A1.1 L-R gene expression is often missing from the LPM of *han* mutants.

		Total	Left (%)	Right (%)	Bilateral (%)	Absent (%)
han	*spaw*	38	76	0	3	21
	pitx2	179	67	2	7	24

References

1. Zaret, K.S. (2002). Regulatory phases of early liver development: paradigms of organogenesis. Nat Rev Genet *3*, 499-512.

2. Yelon, D., Ticho, B., Halpern, M.E., Ruvinsky, I., Ho, R.K., Silver, L.M., and Stainier, D.Y. (2000). The bHLH transcription factor hand2 plays parallel roles in zebrafish heart and pectoral fin development. Development *127*, 2573-2582.

3. Long, S., Ahmad, N., and Rebagliati, M. (2003). The zebrafish nodal-related gene *southpaw* is required for visceral and diencephalic left-right asymmetry. Development *130*, 2303-2316.

4. Campione, M., Steinbeisser, H., Schweickert, A., Deissler, K., van Bebber, F., Lowe, L.A., Nowotschin, S., Viebahn, C., Haffter, P., Kuehn, M.R., and Blum, M. (1999). The homeobox gene Pitx2: mediator of asymmetric left-right signaling in vertebrate heart and gut looping. Development *126*, 1225-1234.

5. Burdine, R.D., and Schier, A.F. (2000). Conserved and divergent mechanisms in left-right axis formation. Genes Dev *14*, 763-776.

6. Bisgrove, B.W., Essner, J.J., and Yost, H.J. (2000). Multiple pathways in the midline regulate concordant brain, heart and gut left-right asymmetry. Development *127*, 3567-3579.

7. Yan, Y.T., Gritsman, K., Ding, J., Burdine, R.D., Corrales, J.D., Price, S.M., Talbot, W.S., Schier, A.F., and Shen, M.M. (1999). Conserved requirement for EGF-CFC genes in vertebrate left-right axis formation. Genes Dev *13*, 2527-2537.

8. Pogoda, H.M., Solnica-Krezel, L., Driever, W., and Meyer, D. (2000). The zebrafish forkhead transcription factor FoxH1/Fast1 is a modulator of nodal signaling required for organizer formation. Curr Biol *10*, 1041-1049.

Future directions for the study of cardiac tilting

When I first joined the Stainier Lab I intended to study early L-R morphogenesis in the heart. Specifically, I wanted to investigate the cellular mechanisms that drive tilting morphogenesis and describe the role of *heart and soul* (*has*) in this process. However, as is so often the case in science, I became distracted by other projects and did not have a chance to pursue these studies. In this appendix, I will present some of my thoughts on tilting morphogenesis, which could provide the basis for future experimentation.

Epithelial integrity and tilting morphogenesis

I have shown that *has* mutants have defects in the epithelial integrity of the LPM that is associated with the heart (Chapter 4) and the looping region of the gut (Chapter 5). My data indicate that epithelial defects in the LPM of the gut looping region disrupt the asymmetric morphogenesis of this tissue. However, the epithelial defects in the myocardium of the heart cone may not be sufficient to explain the tilting defect observed in *has* mutants. I have examined heart morphology in two other mutants that have epithelial defects similar to *has*, *nagie oko* (*nok*) [1] and *oko meduzy* (*ome*) [2]. The morphology of the cardiac cone in *nok* and *ome* mutants is remarkably similar to the morphology of the cone in *has* mutants (Figure 4.1), however, the cones in *nok* and *ome* mutants do tilt and go on to form heart tubes. Heart morphogenesis is far from normal in *nok* and *ome* mutants – heart tube assembly is delayed and circulation is weak - but it

does progress much further than in *has* mutants. This is quite intriguing because the other epithelial defects shared by these three mutants appear to be much more severe in *nok* and *ome* mutants than they are in *has* mutants. These data suggest that aPKCλ may play a specific role in tilting morphogenesis that is at least partially independent of its role in establishing and maintaining epithelial polarity.

Studies with the small molecule concentramide may help to elucidate the role of aPKCλ in tilting morphogenesis. Treating wild-type zebrafish embryos with concentramide leads to a block in tilting morphogenesis that is very similar to the defect observed in *has* mutants [3]. Although the identity of the protein that is pharmacologically inhibited by concentramide is not yet known, two things can be said about the action of this small molecule. First, concentramide does not appear to inhibit aPKCλ, as the only phenotype shared by concentramide-treated embryos and *has* mutants is the cardiac defect. Second, concentramide does not appear to affect epithelial integrity in the heart ([3] and Le Trinh, personal communication). It is possible that the protein targeted by concentramide works together with aPKCλ to drive tilting morphogenesis in the heart. Therefore, it will be of great interest to identify the protein targeted by concentramide as this information may shed light on the biochemical pathway in which aPKCλ participates to regulate cardiac morphogenesis.

Comparison of asymmetric LPM morphogenesis during cardiac tilting and gut looping

Many parallels can be drawn between the asymmetric LPM morphogenesis that occurs in the gut looping region and the asymmetric LPM morphogenesis that occurs during cardiac tilting. In both cases, bilaterally situated, U-shaped epithelia undergo

medial migration and begin asymmetric morphogenesis shortly after reaching the midline. Some aspects of the morphogenesis itself can even look quite similar. Le Trinh recently showed me a striking transverse section through the lumen of a tilted cone, in which the endocardial precursors sat in the midline with the left LPM dorsal to the endocardium and the right LPM ventro-lateral to the endocardium. Furthermore, the LPM in both the heart and gut regions also show A-P restricted expression of *pitx2* in the left LPM that is participating in the asymmetric behavior.

Although there are many similarities between gut looping and cardiac tilting, it is likely that the morphogenetic events that drive tilting are far more complicated than those that drive gut looping. In the case of gut looping, the direction of the morphogenesis is to the left and is therefore easily explained by migration of the right LPM past the midline. During cardiac tilting, the direction of morphogenesis is diagonal to the midline - toward the left-anterior. Furthermore, the two sides of the LPM are fused just anterior to and posterior to the central lumen of the cone. These aspects of cardiac morphogenesis suggest that tilting requires a much more complex rearrangement of the LPM than is required for gut looping.

The apparent complexity of tilting morphogenesis may explain the large number of genes that show asymmetric expression in the cardiac cone. There have been 5 genes reported to show left sided expression specifically in the cardiac cone (*pitx2*, *cyclops*, *lefty2*, *bmp4* and *nkx2.5*) as opposed to one gene that has been reported for the gut looping region (*pitx2*). Brent Bisgrove has created a beautiful diagram detailing the complex and partially overlapping pattern of the five genes expressed in the cardiac region [4]. The gene that shows the most interesting pattern of expression in the cardiac

cone, however, is *pitx2*. *pitx2* is expressed bilaterally in an anterior region of the cone, but the expression extends a little more posteriorly on the left side. The result is that the portion of *pitx2* expression that is asymmetric in the cone is situated in the left-anterior, highly indicative of the direction of cardiac tilting. This very specific localization of *pitx2* in the cone combined with the localization of this gene in the gut looping region may indicate that *pitx2* is the primary regulator or asymmetric morphogenesis in both regions. It will be of great interest therefore to investigate the downstream targets of *pitx2*, as they are likely to represent direct regulators of asymmetric LPM morphogenesis.

References

1. Wei, X., and Malicki, J. (2002). *nagie oko*, encoding a MAGUK-family protein, is essential for cellular patterning of the retina. Nat Genet *31*, 150-157.

2. Malicki, J., and Driever, W. (1999). oko meduzy mutations affect neuronal patterning in the zebrafish retina and reveal cell-cell interactions of the retinal neuroepithelial sheet. Development *126*, 1235-1246.

3. Peterson, R.T., Mably, J.D., Chen, J.N., and Fishman, M.C. (2001). Convergence of distinct pathways to heart patterning revealed by the small molecule concentramide and the mutation *heart-and-soul*. Curr Biol *11*, 1481-1491.

4. Bisgrove, B.W., Essner, J.J., and Yost, H.J. (2000). Multiple pathways in the midline regulate concordant brain, heart and gut left-right asymmetry. Development *127*, 3567-3579.